



University Mohamed Khider of Biskra
Faculty of Exact Sciences and Nature and Life
Department of Matter Sciences

Final Dissertation in Master

Matter Sciences
Physics
Energy Physics and Renewable Energies

Ref.:

Presented by:

Saad manal

Thursday, June 27, 2019

Optimization of Cuprous Oxide (Cu_2O) Heterojunction Solar Cells Using Silvaco TCAD

Jury:

Pr.	Meftah Afak	Professor	University of Biskra	President
Dr.	Boumaraf Rami	M.C. « B »	University of Biskra	<i>Reporter</i>
Dr.	Tibermacine Tawfik	M.C. « A »	University of Biskra	<i>Examiner</i>

Academic Year: 2018-2019

Acknowledgements

First and foremost, I owe profound thanks and deepest gratitude to Almighty **ALLAH**, Creator of the universe, and worthy of all praises, who blessed me with the potential, ability and determination to complete this research work. “*Alhamdulillah*”.

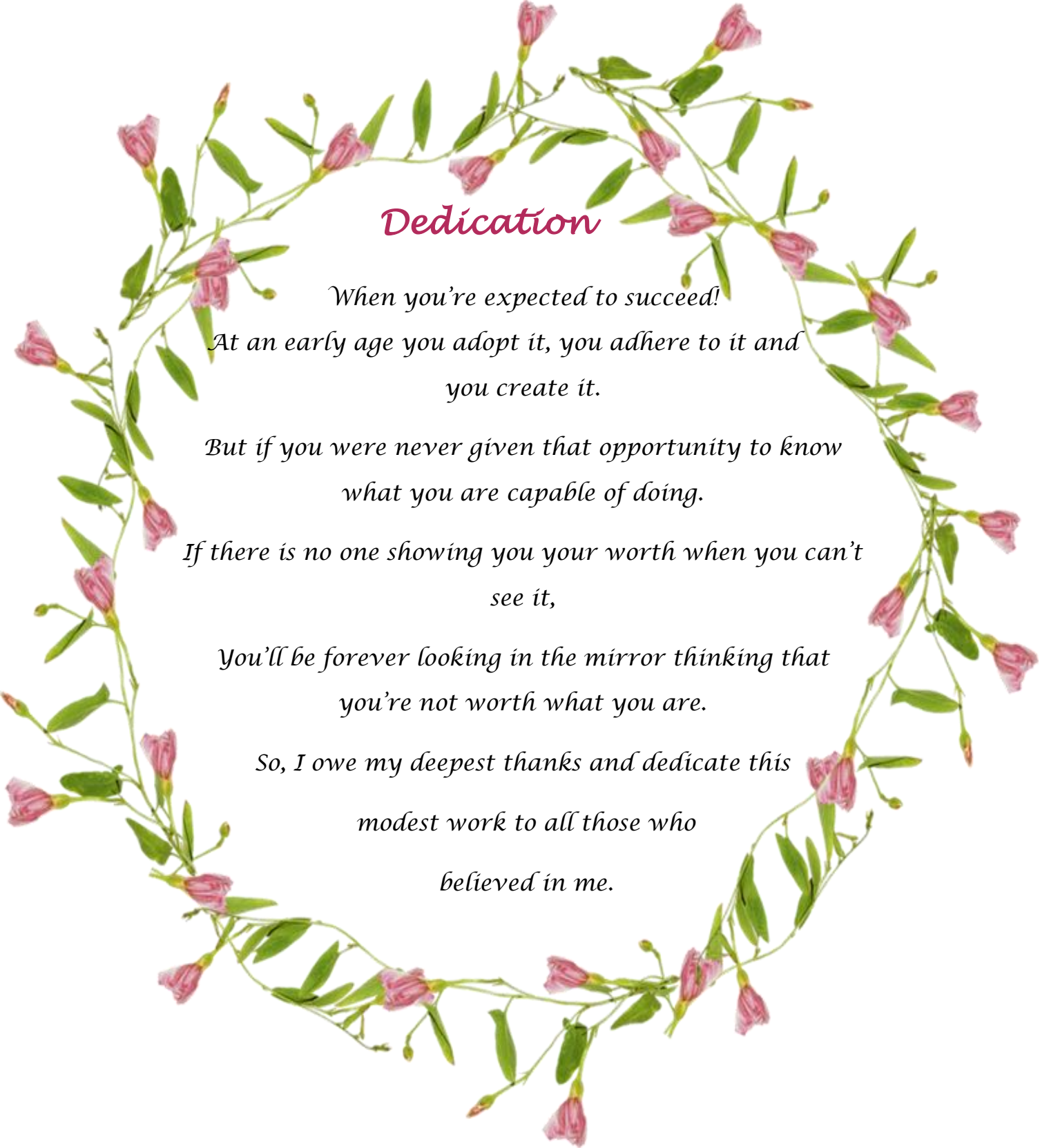
I wish to express my heartfelt thanks and respect to my supervisor **Dr. Boumaraf Rami**. I am very grateful and I express my deep gratitude to him, he supported me on every occasion and he always knew how to guide me and direct me in the work. During this period, he shared with me his scientific and educational knowledge. I was happy to the ideas he gave me, to the solicitude with which he guided me, and to the wise advices that allowed me to carry out this work.

My gratitude also goes to the members of the jury who accepted to examine and evaluate my work. My thanks to **Pr. Tibermacine Toufik** for having honored me by his presence on the jury as an examiner and I thank heartily **Pr. Meftah Afak** who accepted to preside the jury.

A special thanks to my family: my parents my brothers and sisters for trusting and supporting me spiritually throughout writing this thesis, words cannot express how grateful I am to my father **Mr. Med. Saad and** mother **Mrs. H. Saad** for all of the sacrifices that they have made on my behalf, their prayer for me was what sustained me thus far, that have made the hard times so much easier, for being a great support for me all throughout my research and my life and pushed me to strive towards my goal, thank you both for giving me life and strength. Last but not the least; I would also like to thank all my friends for their love and support.

This acknowledgment will be incomplete if I do not thank all my fellow students who gave me the guidelines, courage and support, especially student Attafi Djemaa. I would also like to thank the professors of the Laboratory of Semiconductor that help me by answering my questions.





Dedication

When you're expected to succeed!

*At an early age you adopt it, you adhere to it and
you create it.*

*But if you were never given that opportunity to know
what you are capable of doing.*

*If there is no one showing you your worth when you can't
see it,*

*You'll be forever looking in the mirror thinking that
you're not worth what you are.*

*So, I owe my deepest thanks and dedicate this
modest work to all those who
believed in me.*

List of Figures

Figure I.1: Visualization of electron diffusion.....	19
Figure I.2: Visualization of bandgap-to-bandgap (a) generation, and (b) recombination processes using the bonding model and the energy band diagram.....	20
Figure I.3: (a) Dangling bonds (surface defects) on a semiconductor surface. (b) The trap states within the bandgap created by the surface defects.....	26
Figure I.4: Two-step recombination processes.....	27
Figure I.5: Equivalent-circuit model for Solar cells.....	28
Figure I.6: Typical I-V and power curves for a PV module operating at 1,000 W/m ² ...	29
Figure I.7: Comparison of energy losses from narrow bandgap materials (left) and wide bandgap materials (right).....	33
Figure I.8: The structure of ARC layers on semiconductor material and rear reflector	34
Figure I.9: Textured interfaces (a) compared to a flat interface (b).....	35
Figure II.1: Unit cell of bulk Cu ₂ O; small red and larger white spheres denote O and Cu atoms, respectively.....	38
Figure II.2: Cause of that cuprous oxide of p-type not n-type is acceptor.....	39
Figure II.3: Carrier concentrations and Specific resistance as a function of the oxygen flow.....	42
Figure II.4: Transmittance of Cu ₂ O deposited at different pH values.....	43
Figure II.5: Schematic of the p–n homojunction Cu ₂ O solar cell.....	45
Figure II.6: (a) This cross-section is structure of heterojunction cell; shows material 1 and material 2. The anode is the left-side contact (ET) and the cathode is the right-side contact (HT), (b) band diagram of heterojunction cell from p–n absorber-window structure with light entering	46
Figure II.7: Band diagram of a Cu ₂ O/ZnO heterojunction.....	46
Figure II.8: J–V characteristics of the Cu ₂ O /ZnO TFSCs for various thicknesses (2.2-4.5 μm) of the absorber under light.....	48
Figure II.9: The absorption spectra of the samples.....	49

Figure II.10: Recombination current prefactor J_{0p^+} as a function of the total dopant dose for Gaussian p^+ back surface regions with a varying depth or a varying surface dopant concentration.....	51
Figure III.1: Schematic diagram of studied device from TonyPlot.....	55
Figure III.2: Curve I-V of the studied device from TonyPlot.....	55
Figure III.3: DeckBuild window interface.....	56
Figure III.4: Mesh of the studied device structure.....	58
Figure III.5: Regions with defined materials of the simulated structure.	59
Figure III.6: Electrodes of the simulated structure.....	60
Figure III.7: Doping concentration is specific by colors of simulated structure.....	61
Figure III.8: (a) Structure and (b) band diagram of simulated structure.....	63
Figure III.9: The effect of ZnO thickness on the J-V characteristics.....	66
Figure III.10: η , V_{oc} , J_{sc} and FF as functions of the ZnO thin-film layer thickness...	67
Figure III.11: The effect of Cu ₂ O thickness on the J-V characteristics.....	68
Figure III.12: η , V_{oc} , J_{sc} and FF as functions of the Cu ₂ O thin-film layer thickness....	69
Figure III.13: The effect of ZnO doping concentration on the J-V characteristics.....	71
Figure III.14: η , V_{oc} , J_{sc} and FF as functions of doping concentration of the ZnO layer	71
Figure III.15: (a) The electrons and holes concentration distribution, and (b) the recombination rate as function of structure depth for doping concentration in the ZnO layer at $1 \times 10^{17} \text{ cm}^{-3}$	73
Figure III.16: (a) The electrons and holes concentration distribution, and (b) the recombination rate as function of structure depth for doping concentration in the ZnO layer at $1 \times 10^{21} \text{ cm}^{-3}$	73
Figure III.17: The effect of Cu ₂ O doping concentration on the J-V characteristics.....	74
Figure III.18: η , V_{oc} , J_{sc} and FF as functions of the doping concentration of the Cu ₂ O layer.	75
Figure III.19: (a) Effect of the doping concentration of the p^+ layer on the J-V characteristics and (b) η , V_{oc} , J_{sc} and FF output parameters.	77
Figure III.20: (a) Thickness effect of the p^+ layer on the J-V characteristics and (b) η , V_{oc} , J_{sc} and FF output parameters.	78

List of Tables

Table II.1: Crystallographic properties of Cu ₂ O.....	38
Table II.2: The resistivity ρ , mobility μ and carrier concentration p of the samples.....	49
Table II.3: Literature review of <i>Cu₂O</i> solar cells.....	52
Table III.1: Properties of the used materials for the simulation	64
Table III.2: ZnO Thickness effect on the output parameters of Cu ₂ O based heterojunction solar cell	66
Table III.3: Cu ₂ O Thickness effect on the output parameters of Cu ₂ O based heterojunction solar cell, when the ZnO layer has a thickness of 0.041 μm	68
Table III.4: Doping concentration effect of ZnO layer on the output parameters of Cu ₂ O based heterojunction solar cell	70
Table III.5: Doping concentration effect of Cu ₂ O layer on the output parameters of Cu ₂ O heterojunction cell	74
Table III.6: Doping concentration effect of p ⁺ layer on the output parameters of Cu ₂ O based heterojunction solar cell.....	76
Table III.7: Thickness effect of p ⁺ layer on the output parameters of Cu ₂ O based heterojunction solar cell.....	77

Abstract

In recent years, Cuprous oxide (Cu_2O) has become an interesting research topic, well suited to work in thin film photovoltaic applications due to its low-cost fabrication, abundance in the Earth's crust, non-toxic and for their interesting properties such as good conductivity, direct band gap about of **2.1eV** and high absorption coefficient ($\sim 10^5 \text{cm}^{-1}$). In this work, the simulation software Silvaco (TCAD) was used to study the effect of several parameters (such as Thickness of both ZnO and Cu_2O layers and their doping concentration and effect of inserting heavily doped layer p^+) on the AZO/n-ZnO/p- Cu_2O heterojunction solar cell in order to improve their performance. The performance of Cu_2O cell was determined at the ideal values for the following parameters: ZnO thickness, Cu_2O thickness, doping concentration of ZnO transparent layer and doping concentration of Cu_2O absorbent layer which are: **0.041 μm , 6.6 μm , $3 \times 10^{20} \text{cm}^{-3}$ and $6 \times 10^{15} \text{cm}^{-3}$** , respectively. As follows :The J_{sc} , V_{oc} , FF and η , which were: **8.487mA/cm², 0.753V, 78.374% and 5.015%**, respectively. Also, when doping concentration and thickness of p^+ layer at **$4 \times 10^{20} \text{cm}^{-3}$ and 0.6 μm** , we found $\eta = 5.017\%$ and **5.017%**, respectively.

Key words: Numerical simulation, Silvaco Atlas, Heterojunction solar cell, Cuprous oxide Cu_2O .

المخلص

في السنوات الأخير، أصبح أكسيد النحاس (Cu_2O) موضوع بحث مثير للإهتمام، مناسب تمامًا للعمل في التطبيقات الكهروضوئية ذات الطبقات الرقيقة نظرًا لتكافته تصنيعه المنخفضة، وفرته في الأرض، كونه غير سام ولخصائصه المثيرة للإهتمام مثل التوصيل الجيد، فجوة نطاق مباشر حوالي **2.1eV** و معامل إمتصاص عالي ($\sim 10^5 \text{cm}^{-1}$). في هذا العمل، تمت دراسة تأثير عدة قيم على الخلية الشمسية غير المتجانسة AZO/n-ZnO/p- Cu_2O ، وهي: سمك كل من الطبقتين ZnO و Cu_2O وتركيز التطعيم بهما، من خلال محاكاة باستخدام برنامج (TCAD) Silvaco، لتحسين أدائها. تم تحديد أداء خلية أكسيد النحاس (Cu_2O) عند القيم المثالية للمعاملات التالية: سمك ZnO، سمك Cu_2O ، ركيز تطعيم الطبقة Cu_2O الماصة و تركيز تطعيم طبقة ZnO الشفافة التي هي: **0.041 μm ، 6.6 μm ، $3 \times 10^{20} \text{cm}^{-3}$ و $6 \times 10^{15} \text{cm}^{-3}$** كالتالي: J_{sc} ، V_{oc} ، FF و η ، التي بلغت **8.487mA/cm²، 0.753V، 78.374% و 5.015%**، على التوالي. أيضًا عند تركيز تطعيم وسمك الطبقة p^+ عند **$4 \times 10^{20} \text{cm}^{-3}$ و 0.6 μm** وجدنا $\eta = 5.017\%$ و **5.017%**، على التوالي.

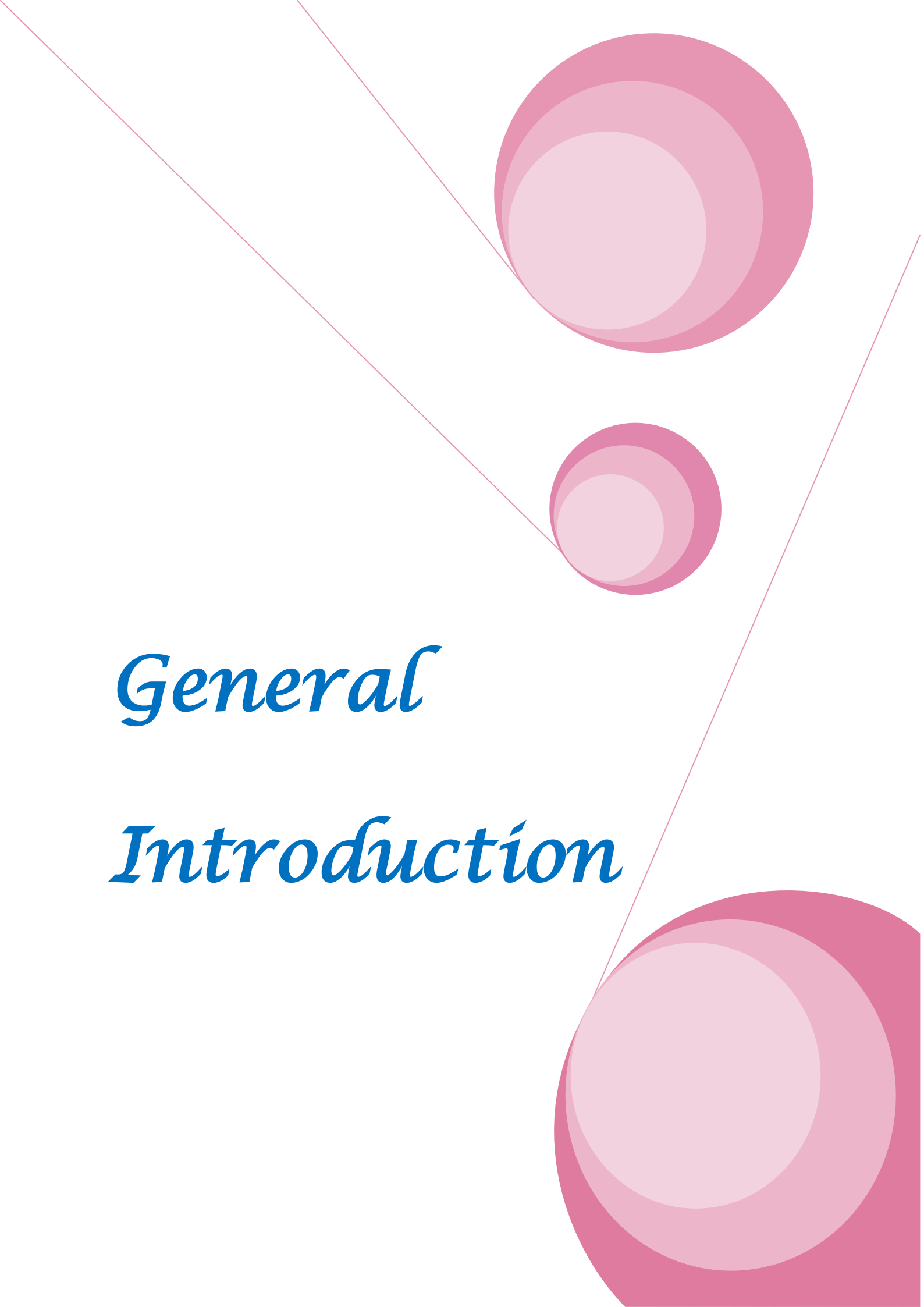
الكلمات المفتاحية: نمذجة رقمية، برنامج المحاكاة Silvaco Atlas، خلية شمسية غير متجانسة، أكسيد النحاس (Cu_2O).

Table of Contents

Acknowledgements	III
Dedication	IV
List of Figures	V
List of Tables.....	VII
Abstract	VIII
المخلص	VIII
General introduction.....	XII
Chapter I Overview of The Principles of Solar Cells.....	15
I.1 Introduction	16
I.2 Energy solar	16
I.3 PN-Junction of solar cell	16
I.3.1 Transport properties	17
I.3.1.1 Drift.....	17
I.3.1.2 Diffusion	18
I.3.2 Conductivity	19
I.3.3 Carrier generation and recombination.....	20
I.3.3.1 Generation.....	20
I.3.3.2 Recombination	21
I.3.3.2.1 Direct recombination	21
I.3.3.2.2 Shockley–Read–Hall recombination	23
I.3.3.2.3 Auger recombination	25
I.3.3.2.4 Surface recombination	25
I.3.3.2.5 Trap-state recombination	27
I.4 Equivalent circuit of solar cell.....	27
I.5 PV Electrical characteristics of solar cell	29
I.5.1 Short circuit current <i>I_{sc}</i>	29
I.5.2 Open circuit voltage <i>V_{oc}</i>	29
I.5.3 Fill factor	30
I.5.4 Efficiency	30
I.5.5 External quantum efficiency	30
I.6 Types of solar cells and application.....	30
I.7 Reasons for low efficiency and improvements.....	31
I.7.1 Series and shunt resistance losses	32
I.7.2 Non-absorption.....	32
I.7.3 Recombination	33

I.7.4 Reflection	33
I.7.4.1 Double layer antireflection coating.....	33
I.7.4.2 Textured interfaces.....	34
I.8 Conclusion	35
Chapter II Solar Cell Based on Cuprous Oxide (Cu ₂ O) and Their Properties	36
II.1 Introduction	37
II.2 Cuprous Oxide Thin Film (Cu₂O).....	37
II.2.1 History cuprous oxide material (Cu₂O).....	37
II.2.2 Cuprous Oxide material (Cu₂O)	37
II.2.3 Cuprous oxide (Cu₂O) Doping	39
II.2.3.1 P-Type	39
II.2.3.2 N-type	39
II.2.4 Defects and interface states in Cu₂O	40
II.2.4.1 Defects in Cu₂O	40
II.2.4.2 Interface states IST in Cu₂O	41
II.2.5 Electrical and optical properties.....	41
II.2.5.1 Electrical properties	41
II.2.5.2 Optical properties	42
II.3 Methods of manufacturing cuprous oxide material.....	43
II.3.1 Thermal Oxidation	43
II.3.2 Electro-deposition	44
II.3.3 Sputtering	44
II.4 Homojunction and Heterojunction Solar Cells	44
II.4.1 Homojunction Solar Cells.....	44
II.4.2 Heterojunction solar cells	45
II.5 ZnO as a solar cell material	46
II.6 Effect of some parameters on solar cell properties	47
II.6.1 Effect thickness of Cu₂O and ZnO layers.....	47
II.6.1.1 Electrical properties	47
II.6.1.2 Optical properties	48
II.6.2 Effect doping of Cu₂O material.....	48
II.6.3 Effect of passivation types	50
II.7 Literature review of Cu₂O based heterojunction solar cells	51
II.8 Conclusion.....	52
Chapter III Results and discussions	53
III.1 Introduction.....	54
III.2 Silvaco TCAD.....	54

III.2.1 Numerical Methods	54
III.2.2 Tools	54
III.2.3 Statements.....	57
III.2.3.1 Mesh	57
III.2.3.2 Region	58
III.2.3.3 Electrode.....	59
III.2.3.4 Material	60
III.2.3.5 Doping.....	61
III.2.3.6 Defects.....	61
III.2.3.7 Models.....	62
III.2.3.8 Beam.....	62
III.2.3.9 Solve.....	62
III.2.3.10 Extract	62
III.3 Description of simulated structure of heterojunction solar cell based on Cuprous oxide (Cu ₂ O)	63
III.4 Results and discussions.....	65
III.4.1 Thickness effect of the ZnO layer	65
III.4.2 Thickness effect of the Cu ₂ O layer	68
III.4.3 Doping effect of the ZnO layer.....	70
III.4.4 Doping effect of the Cu ₂ O layer	73
III.4.5 Passivation effect on the solar cell characteristics.....	76
III.4.5.1 Doping and thickness effect of the p ⁺ layer	76
III.5 Conclusion	78
General conclusion and perspectives	81
Bibliography.....	83

The background features a decorative graphic consisting of three overlapping pink circles of varying sizes, arranged in a diagonal line from the top right to the bottom right. Two thin, light pink lines intersect at the top left and extend diagonally across the page, framing the circles and text.

General

Introduction

General introduction

Solar energy is considered as the most promising alternative energy source to replace environmentally distractive fossil fuel. But it is a challenging task, especially the development of solar energy converting devices using low cost techniques and environmentally friendly materials. Photovoltaics solar cell is the elementary building of the photovoltaic technology and research related to the devices which directly convert sunlight into electricity. Which are made of light-sensitive semiconductor materials. One of the properties of semiconductors that makes them most useful is that their conductivity may easily be modified by introducing impurities into their crystal lattice. The fabrication of solar cells has passed through a large number of improvement steps from one generation to another. In order to choose the right solar cell, we should understand the fundamental mechanisms and functions of several solar technologies that are widely studied. Increasing the efficiency of real devices is possible by minimizing energy losses as a result of optimizing their design and improving the properties of the layers.

The studied device in this work based on cuprous oxide material which is considered an attractive material for photovoltaic applications. It's a naturally p-type conducting semiconductor material and a promising for thin-film photovoltaic applications due to its elemental abundance in the Earth's crust and non-toxic. A lot of studies have been intensively pursued about cuprous oxide material in the recent years not only because of their low cost but also for their interesting properties such as good conductivity, direct band gap (about of 2.1 eV), high absorption coefficient ($\sim 10^5 \text{ cm}^{-1}$) [1]. Various methods have been developed for their preparation such as: Electro-deposition, sputtering, Thermal Oxidation methods, etc.[2]. To achieve a heterojunction structure, another layer of n-type as a buffer layer must be present. In our study, the ZnO material is considered attractive candidate for low-cost photovoltaic applications. They are abundant, non-toxic and relatively stable [3]. The highest conversion efficiency currently achieved experimentally for the n-ZnO/p-Cu₂O heterojunction solar cell is only 8.1% [4], while the theoretical conversion efficiency limit is about 20% [1]. It is clear that further improvements of Cu₂O based solar cells is required in order to realize their full potential in photovoltaic applications. For this purpose, it's better to use simulation, which provides a strong tool for understanding the fundamental physical mechanisms and designing efficient solar cell by avoid material losses and time.

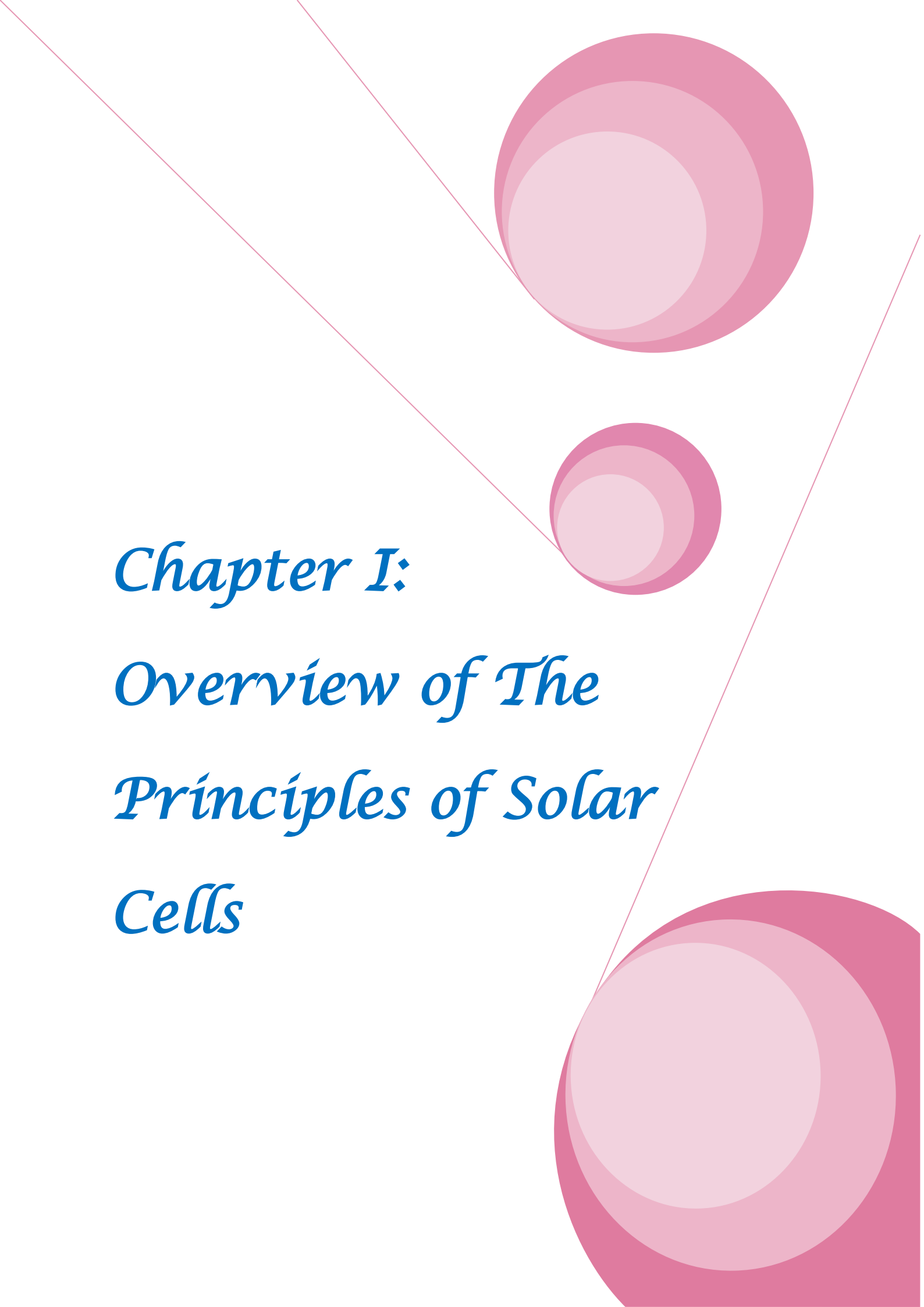
The main objective of this thesis is to investigate the optimum parameters that improve the performance of (AZO/n-ZnO/p-Cu₂O) solar cells and raise their conversion efficiency. Therefore, we divided our study to three main parts. At first, we will change thickness of both the Cu₂O and ZnO layers. The second step, we will change doping concentration of both the Cu₂O and ZnO layers. While the third part, we will add a heavily doped layer with change each of thickness and doping concentration to this layer. This process called passivation which in turn creates a back-surface field (BSF).

To implement this study, we organized this thesis as follows:

chapter I: Presents the essential principles of a solar cell, the main concepts, electrical characteristics, reasons for low efficiency in PV cells and how to reduce or overcome these losses will be explicated.

Chapter II: Describes solar cells on the basis of cuprous oxide absorber layer (Cu₂O), and their structure, optical and electrical properties, their Methods of manufacturing, definition of ZnO as a solar cell material, effect of some parameters on ZnO/Cu₂O heterojunction solar cell characteristics, finally, literature review of the Cu₂O based heterojunction solar cells.

Chapter III comprises three parts: The first part, describes some definitions about the Silvaco TCAD simulation with all the simulation steps of our cell. The second part, describes the solar cell that is simulated in two dimensions and the most properties of the used materials for the simulation. In the last part, the simulation results and their discussions will be presented.

The background features a decorative graphic consisting of three overlapping circles in shades of pink and red, arranged in a vertical line. Two thin, light red diagonal lines cross the page, one from the top-left to the bottom-right, and another from the top-right to the bottom-left, intersecting the circles.

*Chapter I:
Overview of The
Principles of Solar
Cells*

Chapter I: Overview of The Principles of solar cells

I.1 Introduction

The solar cell is the smallest practical element for the photovoltaic effect. Light shining on the solar cell create an electrical current in material which generate electric power.

Key factors of this process are the intensity of radiation, light absorption materials, design of the external circuit and PV electrical characteristics that are satisfy the requirements for photovoltaic energy conversion.

However, for efficient photovoltaic energy conversion; semiconductor materials in the form of a p-n junction are essential.

I.2 Energy solar

Solar energy comes to earth in the form of radiation or sunlight with spectral components mostly in the visible near infrared and near ultraviolet.

The total power density of solar is 1.366 Kw/m^2 just outside the atmosphere, where AM spectrum that means air mass for a path length through the atmosphere, and solar radiation incident at angle to the normal to earth's surface, matches well with the blackbody radiation spectrum at 5800 K, diluted by the distance from the Sun to earth [5].

On the surface of earth the total power density is 1.0kw/m^2 , AM1.5 that means air mass corresponds to a solar zenith angle of $48,19^\circ$ [6]. The solar spectrum is standardized on the surface of earth, for performance evaluation of solar cells.

I.3 PN-Junction of solar cell

Power generation is achieved with the use of a p-n junction in many photovoltaic devices. A p-n junction consists of two layers of the same material (Homojunction) or different materials (Heterojunction) the p-type layer will have a greater density of holes compared to electrons, whilst the n-type layer will have a greater density of electrons than holes. When a p-type semiconductor and an n-type semiconductor are brought together, a *built-in potential* is established. Because the Fermi level of a p-type semiconductor is close to the top of the valence band and the Fermi-level of an n-type semiconductor is close to the bottom of the conduction band, there is a difference between the Fermi levels of the two sides. When the two pieces are combined to form a single system, the Fermi levels must be aligned. As a result, the energy levels of the two sides must undergo a shift with a potential V_0 . Letting E_{cp} be the energy level

Chapter I: Overview of The Principles of solar cells

of the bottom of the conduction band for the p -type semiconductor versus the Fermi level and E_{cn} that for the n -type semiconductor, the built-in potential is [5]:

$$qV_0 = E_{cp} - E_{cn} \quad (I.1)$$

Hence, the concentration of holes in the n -region of the pn-junction can be written as:

$$p_n = p_p \exp\left(\frac{-qV_0}{k_B T}\right) \quad (I.2)$$

The concentration of holes in a p -type semiconductor p_p , approximately equals the acceptor concentration:

$$p_p = N_A \quad (I.3)$$

And the concentration of electrons in the p -region of the pn-junction can be written as:

$$n_p = n_n \exp\left(\frac{-qV_0}{k_B T}\right) \quad (I.4)$$

The concentration of free electrons in an n -type semiconductor n_n , approximately equals the concentration of donor atoms:

$$n_n = N_D \quad (I.5)$$

For obvious reasons, both p_n and n_p are called *minority carriers*. In both cases, the product of the concentrations of free electrons and holes equals the square of the intrinsic carrier concentration:

$$n_n p_n = p_p n_p = n_i^2 \quad (I.6)$$

I.3.1 Electrical transport properties

The electron and hole are charge carriers that moves inside the semiconductor and lead to electrical currents. The process by which these charged particles move is called transport. There are two basic transport mechanisms in a semiconductor are *drift* and *diffusion*.

I.3.1.1 Drift

Drift is charged particle motion in response to an electric field, which accelerates the positively charged holes in the direction of the electric field and the negatively charged electrons in the opposite direction. The resulting motion of electrons and holes can be described by average drift velocities V_{dn} and V_{dp} for electrons and holes, respectively. In the case of low electric fields, the average drift velocities are directly proportional to the electric field ξ as expressed by:

Chapter I: Overview of The Principles of solar cells

$$V_{dn} = -\mu_n \xi \quad (I.7a)$$

$$V_{dp} = \mu_p \xi \quad (I.7b)$$

The proportionality factor is called mobility μ , it is a central parameter that characterizes electrons and holes transport due to drift. Although the electrons move in the opposite direction to the electric field because the charge of an electron is negative the resulting electron drift current is in the same direction as the electric field [7]. The electron and hole drift current densities are then given as:

$$J_{n,drift} = -qnV_{dn} = qn\mu_n \xi \quad (I.8a)$$

$$J_{p,drift} = qpV_{dp} = qp\mu_p \xi \quad (I.8b)$$

Combining Eqs (I.8a) and (I.8b) leads to the total drift current:

$$J_{drift} = q(n\mu_n + p\mu_p)\xi \quad (I.9)$$

Mobility is a measure of how easily the charged particles can move through a semiconductor material.

As mentioned earlier, the motion of charged carriers is frequently disturbed by collisions, When the number of collisions increases, the mobility decreases. Increasing the temperature increases the collision rate of charged carriers with the vibrating lattice atoms, which results in a lower mobility. Increasing the doping concentration of donors or acceptors leads to more frequent collisions with the ionized dopant atoms, which also results in a lower mobility [7].

I.3.1.2 Diffusion

Diffusion is a process whereby particles tend to spread out from regions of high particle concentration into regions of low particle concentration as a result of random thermal motion. The driving force of diffusion is a *gradient* in the particle concentration. Currents resulting from diffusion are proportional to the gradient in particle concentration. For electrons and holes, they are given by:

$$J_{n,diff} = qD_n \nabla n \quad (I.10a)$$

$$J_{p,diff} = qD_p \nabla p \quad (I.10b)$$

Combining Eqs. (I.10a) and (I.10b) leads to the total diffusion current:

$$J_{diff} = q(D_n \nabla n + D_p \nabla p) \quad (I.11)$$

The proportionality constants, D_n and D_p are called the electron and hole *diffusion coefficients*, respectively.

Chapter I: Overview of The Principles of solar cells

The diffusion coefficients of electrons and holes are linked with the mobilities of the corresponding charge carriers by the *Einstein relationship* that is given by:

$$\frac{D_n}{\mu_n} = \frac{D_p}{\mu_p} = \frac{k_B T}{q} \quad (\text{I.12})$$

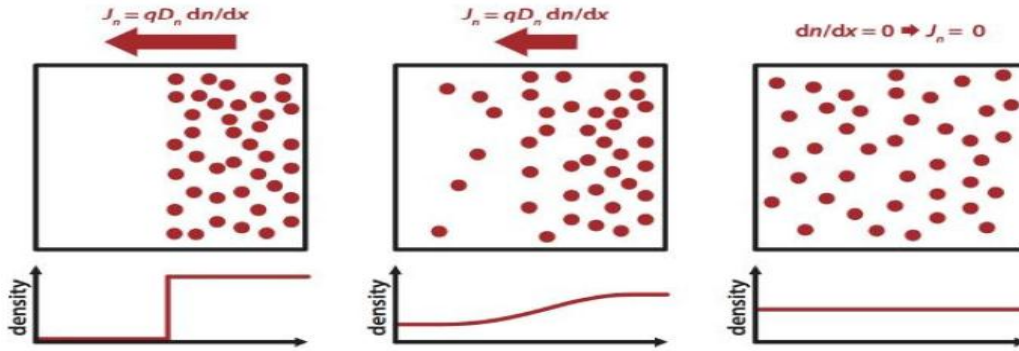


Figure I.1: Visualization of electron diffusion [7].

Figure I.1 visualizes the diffusion process as well as the resulting directions of particle fluxes and current. Combining Eqs (I.9) and (I.11) leads to the total current:

$$J = J_{drift} + J_{diff} \quad (\text{I.13})$$

$$J = q(p\mu_p + n\mu_n)\xi + q(D_n \nabla n + D_p \nabla p) \quad (\text{I.14})$$

I.3.2 Electrical conductivity

The drift current density, given by Eq (I.9), may be written as:

$$J_{drf} = e(\mu_n n + \mu_p p)E = \sigma E \quad (\text{I.15})$$

where σ is the *conductivity* of the semiconductor material, the conductivity is given in units of $(\Omega \cdot \text{cm})^{-1}$ and is a function of the electron and hole concentrations and mobilities [8]. The reciprocal of conductivity is *resistivity*, which is denoted by ρ and is given in units of ohm.cm, we can write the formula for resistivity as:

$$\rho = \frac{1}{\sigma} = \frac{1}{e(\mu_n n + \mu_p p)} \quad (\text{I.16})$$

Hence, equation of conductivity that is given by

$$\sigma = e(\mu_n n + \mu_p p) \quad (\text{I.17}) [8].$$

I.3.3 Carrier generation and recombination

Generation and recombination processes that happen from bandgap to bandgap are also called *direct* generation and recombination, they are much more likely to happen in direct bandgap materials, these processes are most usually *radiative*, which means that a photon is absorbed when an electron-hole pair is created, and a photon is emitted if electron-hole pairs recombine directly.

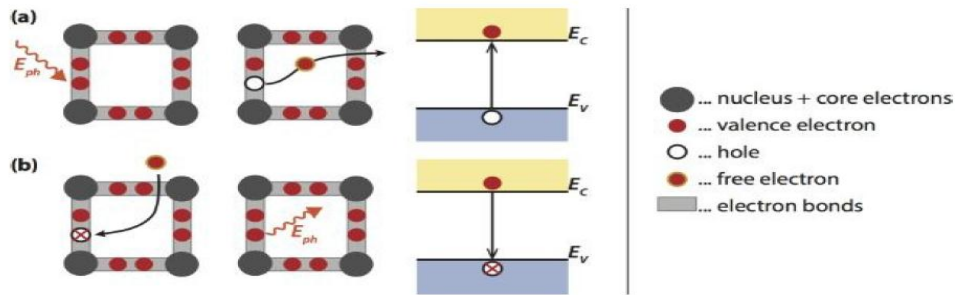


Figure I.2 : Visualization of bandgap-to-bandgap (a) generation, and (b) recombination processes using the bonding model and the energy band diagram [7].

I.3.3.1 Generation

When light penetrates into a material it will be (partially) absorbed as it propagates through the material. If the photon energy is higher than the bandgap energy of the semiconductor, it is sufficient to break bonds and to excite a valence electron into the conduction band, leaving a hole behind in the valance band; hence electron-hole pairs are created. This process is called *photogeneration* (Figure I.2(a)) [7].

The *photon flux* $\phi_{ph,\lambda(x)}$, decreases exponentially with the distance x travelled through the absorber:

$$\phi_{ph,\lambda(x)} = \phi_{ph,\lambda}^0 e^{-\alpha(\lambda)x} \quad (\text{I.18})$$

where $\phi_{ph,\lambda}^0$ is the incident photon flux and $\alpha(\lambda)$ is the absorption coefficient, the photon flux is defined as the number of photons per unit area, unit time and unit wavelength, it is related to the spectral irradiance $I_{e\lambda}$ of the solar radiation via:

$$\phi_{ph,\lambda}^0 = I_{e\lambda} \frac{\lambda}{hc} \quad (\text{I.19})$$

The spectral generation rate $G_{L,\lambda}(x)$, which is the number of electron-hole pairs generated at a depth x in the film per second unit volume and unit wavelength, by photons of wavelength λ , is calculated according to:

$$G_{L,\lambda}(x) = \eta_g \phi_{ph,\lambda}^0 \alpha(\lambda) e^{-\alpha(\lambda)x} \quad (\text{I.20})$$

Where we assume zero reflection. η_g is the generation quantum efficiency, usually assumed equal to unity, this assumption means that every photon generates one and only one electron-hole pair. The optical generation rate $G_L(x)$ is calculated from the spectral generation rate by integrating over the desired wavelength range:

$$G_L(x) = \int_{\lambda_1}^{\lambda_2} G_{L,\lambda}(x) d\lambda \quad (\text{I.21})$$

It has the unit $[G_L] = cm^{-3}s^{-1}$, the optical generation rate is related to the absorption profile $A(x)$ in the film via [7]:

$$G_L(x) = \eta_g A(x) \quad (\text{I.22})$$

$$\text{Where: } A(x) = \int_{\lambda_1}^{\lambda_2} \phi_{ph,\lambda}^0 \alpha(\lambda) e^{-\alpha(\lambda)x} d\lambda \quad (\text{I.23})$$

I.3.3.2 Recombination

I.3.3.2.1 Direct recombination

We will now discuss direct recombination which mainly occurs in direct bandgap semiconductors. Let us first look at the situation at *thermal equilibrium*, if the temperature is higher than 0 K, the crystal lattice is vibrating, this vibrational energy will be sufficient to break bonds from time to time, which leads to the generation of electron-hole pairs at a generation rate G_{th} , where the “*th*” stands for *thermal*, as we are in thermal equilibrium, the expression ($np = n_i^2$ (1.25)) must be valid [7]. Hence, recombination takes place at the same rate as generation:

$$R_{th} = G_{th} \quad (\text{I.26})$$

We may assume that the direct recombination rate is proportional to the concentration of electrons in the conduction band and to the concentration of the available holes in the valence band:

$$R^* = \beta np \quad (\text{I.27})$$

Where β is a proportionality factor, for the thermal recombination we have:

$$R_{th} = \beta n_0 p_0 \quad (\text{I.28})$$

We now look at a situation where the semiconductor is illuminated such that a constant generation rate G_L is present throughout the volume of the semiconductor, in this situation excess electrons and holes are created, as the electron and hole concentrations increase, the recombination rate will also increase according to Eq.(I.27). At some point, the generation and

Chapter I: Overview of The Principles of solar cells

recombination rates will be the same, such that n and p do not change any more, This situation is called the *steady state* situation [7]. The total recombination and generation rates are given by:

$$R^* = \beta np = \beta(n_0 + \Delta n)(p_0 + \Delta p) \quad (\text{I.29})$$

$$G = G_{th} + G_L \quad (\text{I.30})$$

Where n_0 and p_0 are the equilibrium concentrations, Δn and Δp are the excess carrier concentrations that are given by:

$$\Delta n = n - n_0 \quad (\text{I.31a})$$

$$\Delta p = p - p_0 \quad (\text{I.31b})$$

In steady state R^* and G are equal, hence:

$$G_L = R^* - G_{th} = R_d \quad (\text{I.32})$$

Where R_d denotes the *net* radiative recombination rate. By substituting Eqs (I.27) and (I.28) into Eq (I.32), we obtain:

$$G_L = R_d = \beta(np - n_0p_0) \quad (\text{I.33})$$

We now assume the semiconductor to be n -type and under *low-level injection*, which means that $\Delta n \ll n$ and $p \ll n$, under these assumptions the recombination rate becomes:

$$R_d \approx \beta n_0(p - p_0) = \frac{p - p_0}{\tau_{pd}} \quad (\text{I.34})$$

Where:

$$\tau_{pd} = \frac{1}{\beta n_0} \quad (\text{I.35})$$

Is the *lifetime of the minority holes* in the n -type semiconductor. Clearly, if no excess carriers are present $R_d = 0$, the excess carrier concentration is given as the product of the generation rate and the lifetime:

$$p - p_0 = G_L \tau_{pd} \quad (\text{I.36})$$

To understand the meaning of the *lifetime*, we consider a situation where the light and generation at the rate G_L is suddenly shut off, without loss of generality we may assume that the light is shut off at the instant $t = 0$. As there is no longer any generation, the excess carrier concentration will change according to the differential equation:

$$\frac{dp}{dt} = -\frac{p(t) - p_0}{\tau_{pd}} \quad (\text{I.37})$$

If we solve this equation with the boundary condition $p(t = 0) = p_0 + G_L \tau_{pd}$, we find:

$$p(t) = p_0 + G_L \tau_{pd} \exp\left(-\frac{t}{\tau_{pd}}\right) \quad (\text{I.38})$$

Therefore, see that the minority carrier lifetime is the time constant at which an excess carrier concentration decays exponentially, if external generation is no longer taking place [7].

For a p -type semiconductor at low-level injection ($\Delta p \ll p$ and $n \ll p$) we find similar expressions:

$$R_d \approx \beta p_0 (n - n_0) = \frac{n - n_0}{\tau_{nd}} \quad (\text{I.39})$$

Where the lifetime of the electrons is given by:

$$\tau_{nd} = \frac{1}{\beta p_0} \quad (\text{I.40})$$

The distance over which the minority carriers diffuse is defined as:

For electrons in a p -type material:

$$L_n = \sqrt{D_n \tau_n} \quad (\text{I.41a})$$

For holes in n -type material:

$$L_p = \sqrt{D_p \tau_p} \quad (\text{I.41b})$$

where D_n and D_p are the diffusion coefficients, L_n and L_p are called the *minority carrier diffusion lengths* [7].

I.3.3.2 Shockley–Read–Hall recombination

In the *Shockley–Read–Hall* (SRH) recombination process, which is illustrated in Figure I.4(a), the recombination of electrons and holes does not occur directly from bandgap o bandgap, it is facilitated by an *impurity atom* or *lattice defects*, their concentration is usually small compared to the acceptor or donor concentrations. These recombination centers introduce allowed energy levels (E_T) within the forbidden gap, so-called *trap states*, an electron can be *trapped* at such a defect and consequently recombines with a hole that is attracted by the trapped electron, though this process seems to be less likely than the direct thermal recombination, it is the dominant recombination-generation process in semiconductors at most operational conditions. The process is typically non-radiative and the excess energy is dissipated into the lattice in the form of heat. The name is a to William B. Shockley, William T. Read and Robert N. Hall, who published the theory of this recombination mechanism in 1952 [7].

General expressions for the free electron and hole concentrations n and p , respectively, both under equilibrium and non-equilibrium conditions as:

Chapter I: Overview of The Principles of solar cells

$$n = N_c \exp\left(\frac{E_{Fn} - E_c}{k_B T}\right) \quad (\text{I.42a})$$

$$p = N_v \exp\left(\frac{E_v - E_{Fp}}{k_B T}\right) \quad (\text{I.42b})$$

This leads to the definition of the quasi-Fermi levels for electrons and holes, E_{Fn} and E_{Fp} , which determine the carrier concentrations under non-equilibrium conditions, note that in thermal equilibrium $E_{Fn} = E_{Fp} = E_F$ [7]. Where E_c (E_v) is the conduction (valence) band edge and N_c (N_v) the effective density of states in the conduction (valence) band, respectively.

According to the Fermi–Dirac statistics the occupation function in thermal equilibrium is given by:

$$f(E_T) = \frac{1}{1 + \exp\left(\frac{E_T - E_F}{k_B T}\right)} \quad (\text{I.43})$$

Where E_T is the trap energy; Hence, the *Shockley–Read–Hall* (SRH) recombination equation is:

$$R_{SRH} = v_{th} \sigma N_T \frac{np - n_i^2}{n + p + 2n_i \cosh\left(\frac{E_T - E_{Fi}}{k_B T}\right)} \quad (\text{I.44})$$

We now look at an n -type semiconductor at low injection rate, the concentration of excess electrons is small compared to the total electron concentration $n \approx n_0$, where n_0 is the electron concentration under thermal equilibrium. Further, we may assume $n \gg p$, by applying these assumptions to Eq (I.44) we obtain:

$$R_{SRH} = v_{th} \sigma N_T \frac{p - p_0}{1 + \frac{2n_i}{n_0} \cosh\left(\frac{E_T - E_{Fi}}{k_B T}\right)} = c_p N_T (p - p_0) = \frac{p - p_0}{\tau_{p,SRH}} \quad (\text{I.45})$$

Where c_p is called the *hole capture coefficient*, $\tau_{p,SRH}$ is the lifetime of holes in an n -type semiconductor.

In a similar manner, can derive for a p -type semiconductor at a low injection rate:

$$R_{SRH} = v_{th} \sigma N_T \frac{n - n_0}{1 + \frac{2n_i}{p_0} \cosh\left(\frac{E_T - E_{Fi}}{k_B T}\right)} = c_n N_T (n - n_0) = \frac{n - n_0}{\tau_{n,SRH}} \quad (\text{I.46})$$

With the electron capture coefficient c_n and the electron lifetime $\tau_{n,SRH}$.

We see that the lifetime is related to the capture coefficients via:

$$\tau_{p,SRH} = \frac{1}{c_p N_T} \quad (\text{I.47a})$$

$$\tau_{n,SRH} = \frac{1}{c_n N_T} \quad (\text{I.47b})$$

The lifetime of the minority carriers due to Shockley–Read–Hall recombination therefore is indirectly proportional to the trap density N_T ; Hence, for a good semiconductor device it is crucial to keep N_T low [7].

I.3.3.2.3 Auger recombination

We already mentioned that direct recombination is not possible or at least very limited for indirect semiconductors, because both transfer in energy and momentum must occur for an electron in the conduction band to recombine with a hole in the valence band. In indirect semiconductors, *Auger recombination* becomes important, in comparison to direct and SRH recombination, which involve two particles, an electron and a hole, Auger recombination is a three particle process, in Auger recombination, momentum and energy of the recombining hole and electron is conserved by transferring energy and momentum an another electron (or hole), if the third particle is an electron, it is excited into higher levels in the electronic band, this excited electron relaxes again, transferring its energy to vibrational energy of the lattice, or *phonon modes* and finally heat. Similarly, if the third particle is a hole, it is excited into deeper levels of the valence band, from where it rises back to the valence band edge by transferring its energy to phonon modes. The Auger recombination rate R_{Aug} strongly depends on the charge carrier densities for the electrons n and holes p :

$$R_{Aug} = C_n n^2 p + C_p p^2 n \quad (I.48)$$

respectively, where C_n and C_p are the proportionality constants that are strongly dependent on the temperature [7].

I.3.3.2.4 Surface recombination

All the recombination mechanisms that we discussed so far are *bulk recombination* mechanisms, which can happen inside the bulk of a semiconductor. For example, impurities can cause trap states within the semiconductor bandgap leading to Shockley–Read–Hall recombination. However, in semiconductor devices, not only bulk recombination is important, but also surface recombination as we see in Figure I.3 (a), at a semiconductor material surface many valence electrons on the surface cannot find a partner to create a covalent bond with, the result is a so-called *dangling bond*, which is a defect, due to these defects many surface trap states are created within the band gap, as illustrated in Figure I.3 (b):

Chapter I: Overview of The Principles of solar cells

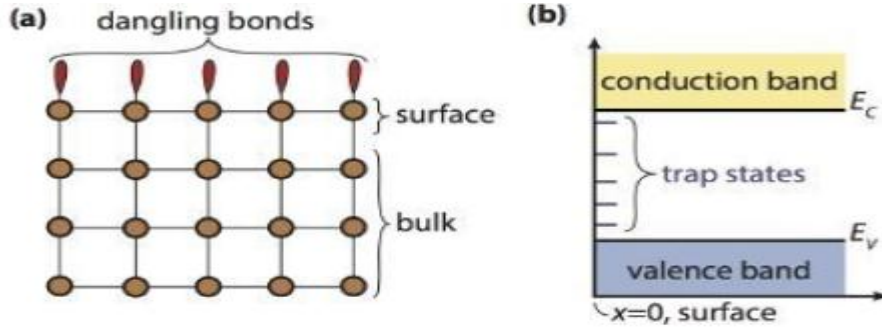


Figure I.3: (a) Dangling bonds (surface defects) on a semiconductor surface. (b) The trap states within the bandgap created by the surface defects [7].

The *surface recombination rate* R_s for an n -type semiconductor can be approximated with:

$$R_s \approx v_{th} \sigma_p N_{sT} (p_s - p_0) \quad (\text{I.49})$$

Where v_{th} is the thermal velocity in cm/s, N_{sT} is the surface trap density in cm^{-2} , and σ_p is the capture cross-section for holes in cm^2 , p_s is the hole concentration at the surface and p_0 is the equilibrium hole concentration in the n -type semiconductor. For a p -type semiconductor, we have to replace σ_p by σ_n , p_s by n_s , and p_0 by n_0 [7]. Note that the product $v_{th} \sigma N_{sT}$ has the unit of a velocity, it is called the *surface recombination velocity*:

$$S_r = v_{th} \sigma N_{sT} \quad (\text{I.50})$$

With σ_p or σ_n for an n - or p -type semiconductor, respectively.

A low surface recombination velocity means that little recombination takes place, while a (Theoretical) value of $S_r = \infty$ would mean that every minority carrier coming to the proximity of the surface recombines [7].

For high quality solar cells, it is crucial to have a low surface recombination velocity S_r , which can be achieved in two different ways:

First, S_r can be made low by reducing the trap density N_{sT} , in semiconductor technology N_{sT} can be reduced with so-called *passivation*, this means that the defect density is reduced by depositing a thin layer of a suitable material onto the semiconductor surface because of this layer the valence electrons on the surface can form covalent bonds such that N_{sT} is reduced.

Secondly, the excess minority carrier concentration at the surface (p_s or n_s) can be reduced, for example by high doping of the region just underneath the surface in order to create a barrier, because of this barrier, the minority carrier concentration is reduced and hence the recombination rate R_s [7].

I.3.3.2.5 Trap-state recombination

The impurities in a semiconductor create states in the energy gap, the gap states are effective intermediate media for a two-step recombination process; see Figure I.4 (a).

Clearly, the higher the concentration of impurities, the more the gap states, and thus the shorter the electron–hole pair lifetime [5].

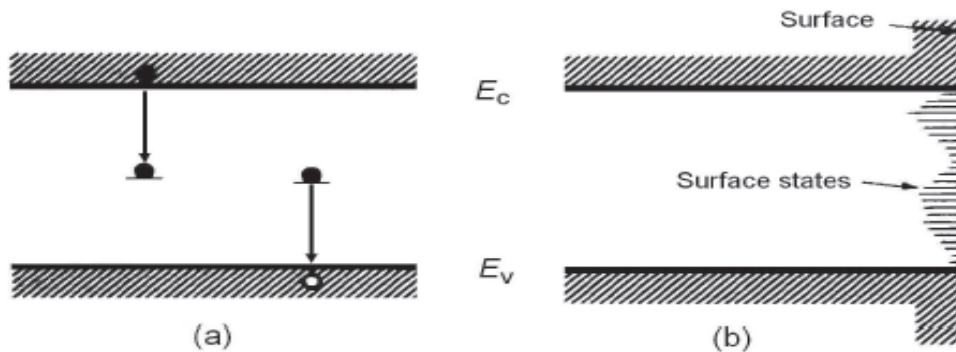


Figure I.4: Two-step recombination processes.

The electron–hole pair can recombine and transfer the energy E_g into either a free electron near the conduction band edge E_c (a). Or free hole near the valance band edge E_v (b) then the excited electron or hole quickly loses its excess energy to the lattice as phonons [5].

I.4 Equivalent circuit of solar cell

The solar cell can be seen as a current generator, the current is produced by injection from light. To better analyze the electrical behavior of solar cell, the equivalent electrical model based on electrical components is been created. The behavior of these components is well known, this equivalent circuit describes the static behavior of the solar cell. This circuit is composed of a current source, a p - n junction diode and a shunt resistor (R_{SH}) in parallel along with a parasitic series resistor (R_s) [9].

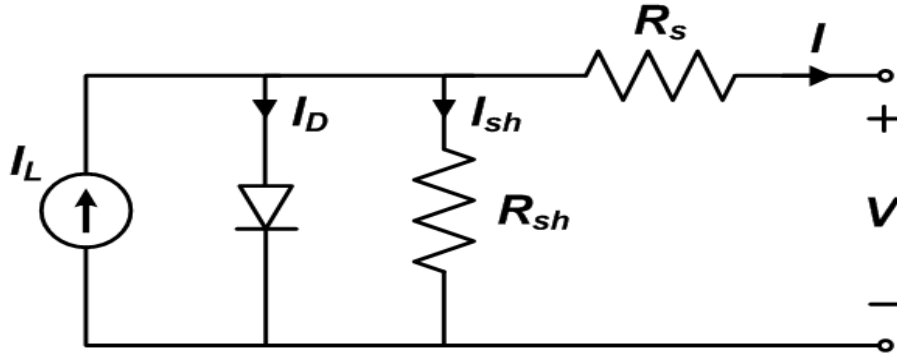


Figure I.5: Equivalent-circuit model for Solar cells [10].

Figure I.5 shows an example of an equivalent circuit of a solar cell with one diode, R_s is the total Ohmic resistance of the solar cell, which is essentially the bulk resistance caused by the fact that a solar cell is not a perfect conductor. For more efficient cells; a smaller R_s value is required, R_{SH} accounts for recombination currents and leakage currents from one terminal to the other due to poor insulation. In this case larger R_{SH} is required for more efficient cell, this means that the recombination currents and leakage currents are reduced, from the equivalent circuit it is evident that the current produced by the solar cell is equal to:

$$I = I_{ph} - I_D - I_{SH} \quad (I.51)$$

Where, I , I_{ph} , I_D and I_{SH} are output current, photogenerated current, diode current, and shunt current respectively [10].

By the Shockley diode equation, the current diverted through the diode is:

$$I_D = I_0 \left\{ \exp \left(\frac{q(V + IR_s)}{\eta kT} \right) - 1 \right\} \quad (I.52)$$

Where I_0 , n , q , k , T are reverse saturation current, diode ideality factor (1 for an ideal diode), elementary charge, Boltzmann's constant and absolute temperature respectively at 25°C, kT/q is approximated to 0.0259 V [9].

By Ohm's law, the current diverted through the shunt resistor is [9] :

$$I_{SH} = \frac{V + IR_s}{R_{SH}} \quad (I.53)$$

Substituting these into the first equation produces the characteristic equation of a solar cell, which relates solar cell parameters to the output current and voltage:

$$I = I_L - I_0 \left\{ \exp \left[\frac{q(V + IR_s)}{\eta kT} \right] - 1 \right\} - \frac{V + IR_s}{R_{SH}} \quad (I.54)$$

The [-1] term in the above equation can usually be neglected since the exponential term is usually $\gg 1$ [11].

I.5 PV Electrical characteristics of solar cell

PV cells are usually characterized with four performances: short circuit current I_{sc} , open circuit voltage V_{oc} , Fill factor FF , and conversion efficiency η . These parameters can be represented using Figure (I.6)

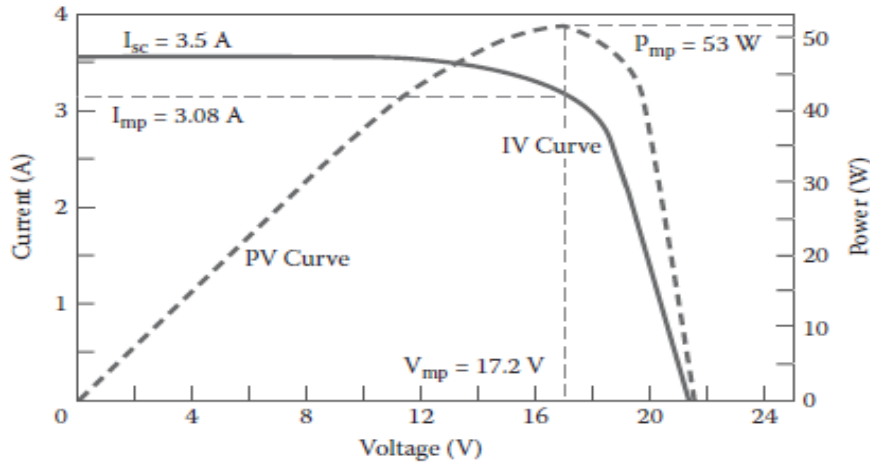


Figure I.6 : Typical I-V and power curves for a PV module operating at 1000 W/m^2 [12].

I.5.1 Short circuit current I_{sc}

The short circuit current is current that flows across the external circuit when the cell is in the form of a short circuit or in other words when the voltage across the solar cell is zero ($V=0$), which is equal to the photogenerated current as:

$$I_{sc} = I_{ph} \quad (I.55)$$

The short-circuit current is dependent on the incident photons flux density [7].

I.5.2 Open circuit voltage V_{oc}

The open-circuit voltage is the maximum voltage that a solar cell can provide, when the current is not flowing through the external circuit ($I_{sc}=0$):

$$V_{oc} = \frac{k_B T}{q} \ln \left(\frac{J_{ph}}{J_s} + 1 \right) \approx \frac{k_B T}{q} \ln \left(\frac{J_{ph}}{J_s} \right) \quad (I.56)$$

Where the approximation is justified because of $J_{ph} \gg J_s$ [12].

Chapter I: Overview of The Principles of solar cells

I.5.3 Fill factor

The fill factor is the ratio between the maximum power point (mpp) ($P_{max} = J_{mpp}V_{mpp}$) generated by a solar cell and the product of V_{oc} with J_{sc} [7]:

$$FF = \frac{J_{mpp}V_{mpp}}{J_{sc}V_{oc}} \quad (I.57).$$

I.5.4 Efficiency

The conversion efficiency is the most important property of a solar cell, it is defined as the ratio between the generated maximum power P_{max} , generated a solar cell and the incident power P_{in} , where the incident light is described by the **AM1.5** spectrum and has an irradiance of $I_{in} = 1000 \text{ W/m}^2$ [7]:

$$\eta = \frac{P_{max}}{I_{in}} = \frac{J_{mpp}V_{mpp}}{I_{in}} = \frac{J_{sc}V_{oc}FF}{I_{in}} \quad (I.58).$$

I.5.5 External quantum efficiency

The external quantum efficiency EQE (λ) is the fraction of photons incident on the solar cell that create electron-hole pairs in the absorber which are successfully collected. It is wavelength dependent and is usually measured by illuminating the solar cell with monochromatic light of wavelength λ and measuring the photocurrent I_{ph} through the solar cell. The external quantum efficiency is then determined as:

$$EQE(\lambda) = \frac{I_{ph}(\lambda)}{q\psi_{ph,\lambda}} \quad (I.59)$$

Where q is the elementary charge and $\psi_{ph,\lambda}$ is the spectral photon flow incident on the solar cell [7].

I.6 Types of solar cells and application

Solar cells are typically named after the semiconducting material they are made of, these materials must have certain characteristics in order to absorb sunlight, some cells are designed to handle sunlight that reaches the Earth's surface, while others are optimized for use in space, solar cells can be made of only one single layer of light-absorbing material (single-junction) or

Chapter I: Overview of The Principles of solar cells

use multiple physical configurations (multi-junctions) to take advantage of various absorption and charge separation mechanisms.

Solar cells can be classified into first, second and third generation cells. The first-generation cells also called conventional, traditional or wafer-based cells are made of crystalline silicon, the commercially predominant PV technology, that includes materials such as polysilicon and monocrystalline silicon. Second generation cells are thin film solar cells, that include amorphous silicon, CdTe, CIGS and Cuprous oxide (Cu₂O) cells and are commercially significant in utility-scale photovoltaic power stations, building integrated photovoltaics or in small stand-alone power system. A variety of substrates (flexible or rigid, metal or insulator) can be used for deposition of different layers (contact, buffer, absorber, reflector, etc.) using different techniques (PVD, CVD, ECD, plasma-based, hybrid, etc.). Such versatility allows tailoring and engineering of the layers in order to improve device performance. The benefits of this type of solar device are they less expensive to produce than traditional silicon solar cells as they require a decreased amount of materials for construction.

The basic structure of a thin film solar cell consists of the four major parts: Back contact, p-type layer, n-type layer, and a top contact. In contrast, it is a technology that contains a significant amount of defects and impurities, which is a great challenge for researchers. The third generation of solar cells includes a number of thin-film technologies often described as emerging photovoltaics most of them have not yet been commercialized and are still in the research or development phase, many use organic materials such as polymer and dye-sensitized solar cells. Despite the fact that their efficiencies had been low and the stability of the absorber material was often too short for commercial applications, there is a lot of research invested into these technologies as they promise to achieve the goal of producing low-cost and high-efficient solar cells [13].

I.7 Reasons for low efficiency and improvements

This section identifies the major sources of loss in the solar cell conversion efficiency process and the corresponding approaches to mitigating the losses thereby improving the efficiency.

Simply put, the efficiency is a measure of how much electricity can be extracted from a solar cell and clearly, it would be desirable for a solar cell to have a high efficiency in order to be cost effective [14]. The difference between the theoretical and experimental efficiencies is

Chapter I: Overview of The Principles of solar cells

due to losses. A number of factors will cause real efficiencies to be lower than maximum theoretical efficiency; are presented:

I.7.1 Series and shunt resistance losses

They are two types of electric resistance that reduce efficiency in a PV device, these resistances are called parasitic resistance in series (R_s) and shunt resistance (R_{sh}). To produce a cell that is as efficient as possible the series resistance would ideally be as small as possible and it is preferable that the parallel resistance is infinitely large. The small series resistance allows current to flow through the device and the large shunt resistance prevents current from flowing around the edges of the device. The series resistances come from resistances of the cell material to the current flow for examples at the junctions between the p-type and n-type materials and at the connection with the pn-materials and their contacts. The shunt resistances arise from leakages in the device, the lower the shunt resistance is the more the device allows current to flow around the edges between the contacts, avoiding the pn-junction entirely. Increase in the series resistance and decrease in the parallel resistance reduce the fill factor, which in turn reduces the efficiency. Clearly some loss in efficiency is inevitable during manufacturing to avoid this problem we can use techniques such as surface passivation [15].

I.7.2 Non-absorption

The efficiency of a solar cell is strongly dependent on the material bandgap (E_g), as photons with energy below the bandgap ($E < E_g$) do not get absorbed as shown in figure I.7 (a). For a single-junction device under a fixed spectrum, there is an optimum bandgap where the efficiency reaches a maximum. Hence, non-absorption of sunlight exerts a significant impact on the solar cell efficiency. When the Photons with energies much greater than the bandgap ($E > E_g$) are strongly absorbed by the device with the excess energy above the bandgap lost as heat this process is called Thermalization [16] as illustrated in Figure I.7 (b).

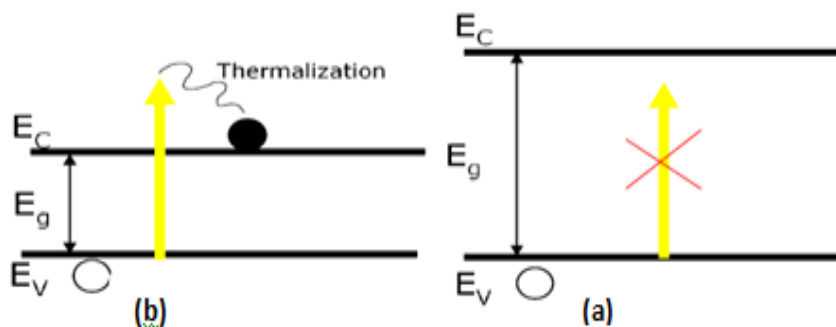


Figure I.7: Comparison of energy losses from narrow bandgap materials (left) and wide bandgap materials (right) [17].

Problem is exceeded by layering two cells and creating a tandem cell. This would minimize the losses that are present in all solar cells because the layering strategy will allow wider energy photons to be absorbed first and then the below bandgap photons to be transmitted to the cell below thus limiting the loss [17].

I.7.3 Recombination

Recombination commonly occurs at grain boundaries, which is a problem for polycrystalline materials used in solar cells, particularly for thin film photovoltaics, if the charge carriers recombine before reaching the cell contacts, the absorbed energy gets lost as a photon (radiative) or a phonon (non-radiative) or as kinetic energy to another free carrier (Auger). Recombination may occur in the bulk material or at the surface. Techniques such as surface passivation and the use of back-surface field are often employed to reduce recombination [15].

I.7.4 Reflection

Reducing the optical losses is a key to achieving high efficiency solar cells. The reflection on the solar cells without antireflection coatings is very high, according to the equation [18]:

$$R = \left(\frac{n_1 - n_0}{n_1 + n_0} \right)^2 \quad (\text{I.60})$$

I.7.4.1 Double layers antireflection coating

It is not sufficiently effective to have a single layer coating for solar cells because the single layer coating only can effectively reduce the reflection in a narrow wavelength range.

In other words, the single layer just can realize the minimization of one wavelength. Two or more anti-reflection coating layers are generally required to get better transmittance. An alternative is a graded-index coating which the refractive indices increase from small to large from the air. Therefore, double layers antireflection coatings (DLARC) which contain low and high refractive indices are necessary to get further reflectivity decrease.

In addition, a rear reflector is often used to increase absorption by reflecting the light into the cell for potential reabsorption. We can design several layers from anti-reflection coating [18], as illustrated in Figure I.8.

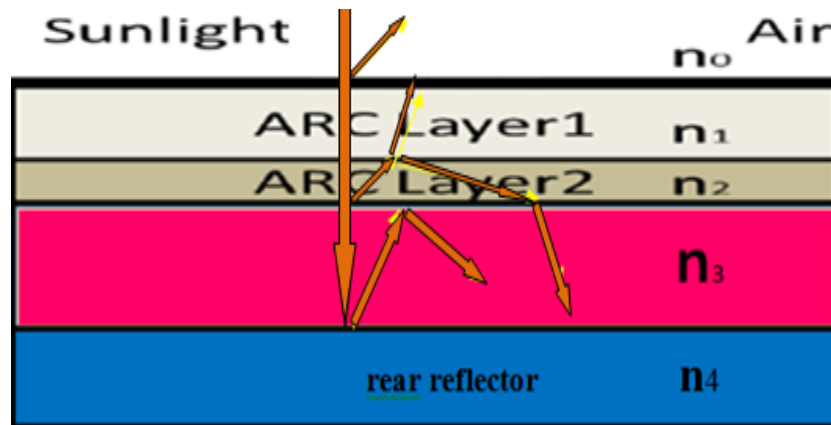


Figure I.8: The structure of ARC layers on semiconductor material and rear reflector.

I.7.4.2 Textured interfaces

The last approach that we discuss for realizing anti-reflective coating is to use textured interfaces. In this case, which is also called the geometrical limit, it is a technique to reduce the reflectance loss is to a pattern of cones and pyramids. This texturing helps to enhance the coupling of light into the layer. In principle, the light should be reflected back and forth inside the absorber until everything is absorbed. However, at every internal reflection part of the light is transmitted out of the film. If the light could travel through the layer at an angle greater than the critical angles of the front and back interfaces of the absorber, it could stay there until everything is absorbed without any loss [19].

The influence of the microstructure surface on the solar cell properties is mainly due to pathway of light propagation in the solar cells. Both refraction and reflection can happen there as shown in Figure I.9(a). This means that the pyramid shape structure of cell caused the increase the path of light in the cell that could allowed the photons to absorb more effectively. Therefore, this solar cell has high efficiency compared to a flat interface of the same materials.

Chapter I: Overview of The Principles of solar cells

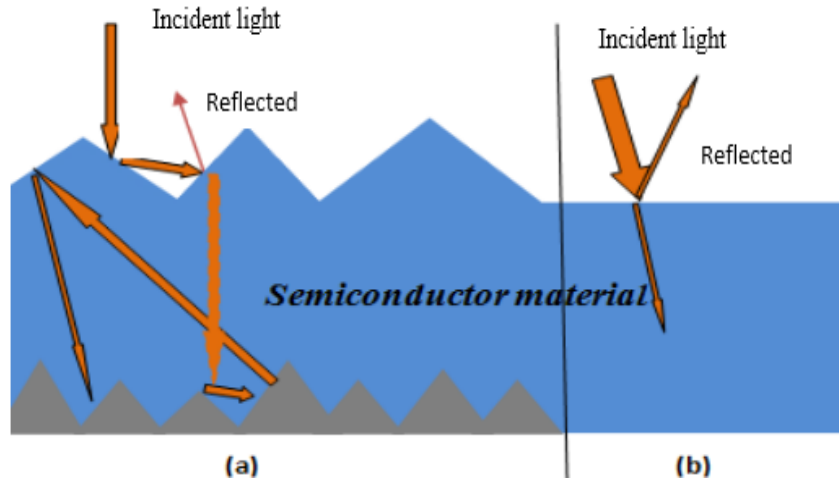
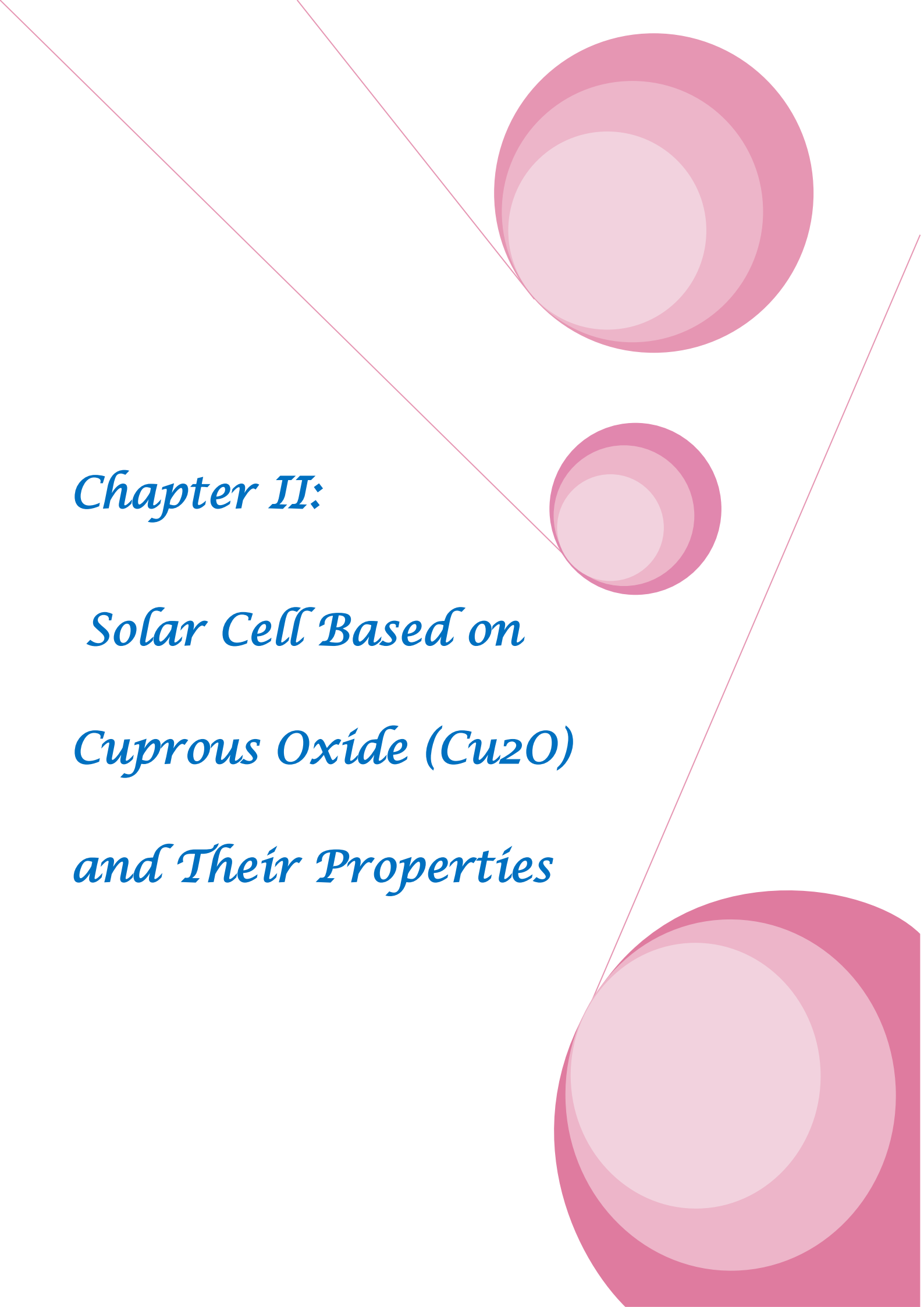


Figure I.9: Textured interfaces (a) compared to a flat interface (b).

I.8 Conclusion

This chapter describes some basics of solar cell that collects energy of radiations and convert it into electricity in the process called photovoltaic effect, starting with the source of energy that is the sun and its principle of operation to external parameters and types of solar cells.

The objective of this chapter is the boot to study the absorber layer of heterojunction solar cell, which is a thin film Photovoltaic made from cuprous oxide (Cu_2O).



Chapter II:

*Solar Cell Based on
Cuprous Oxide (Cu₂O)
and Their Properties*

Chapter II: Solar Cell Based on Cuprous Oxide (Cu_2O) And Their Properties

II.1 Introduction

Cuprous oxide thin film (Cu_2O) is promising photovoltaic semiconductor oxide material with p-type conductivity without doping; this oxide attract attention due to its properties such as low cost, high optical absorption and direct band gap energy.

Modern thin film solar cells usually are created on the basis of heterojunctions thin-film such as n- ZnO /p- Cu_2O (as in the present case) attract more attention of researchers for low-cost photovoltaic applications, abundant, non-toxic and relatively stable.

II.2 Cuprous Oxide Thin Film (Cu_2O)

II.2.1 History cuprous oxide material (Cu_2O)

In August 1925, document 1.640.335 was filed at the US patent office as a patent granted to L. O. Grondahl for a unidirectional current-carrying device based on a Cu_2O -metal contact [1]. It marked the beginning of current semiconductor electronics long before the Ge and Si era started. From 1926, L. O. Grondahl and P. H. Geiger worked on a copper- Cu_2O -solar cell [2]. In spite of the historical importance; Cu_2O as a naturally p-type conducting semiconductor material never gained great interest [20].

Currently, there is renewed interest especially on Cu_2O with respect to solar-cell applications. There is a lot of directions for improvement. Up to now there is difficulty in using successful n-type doping of Cu_2O and hence homojunction diodes are still under consideration; this is why, so far, the focus has been on heterojunction solar cells devices in combination with several the n-type transparent conducting window layers as ZnO.

II.2.2 Cuprous Oxide material (Cu_2O)

Cu_2O forms a simple cubic Bravais lattice; which each oxygen is at the center of a tetrahedron of copper atoms linearly coordinated with two oxide ions as seen in figure II.1.

Chapter II: Solar Cell Based on Cuprous Oxide (Cu₂O) And Their Properties

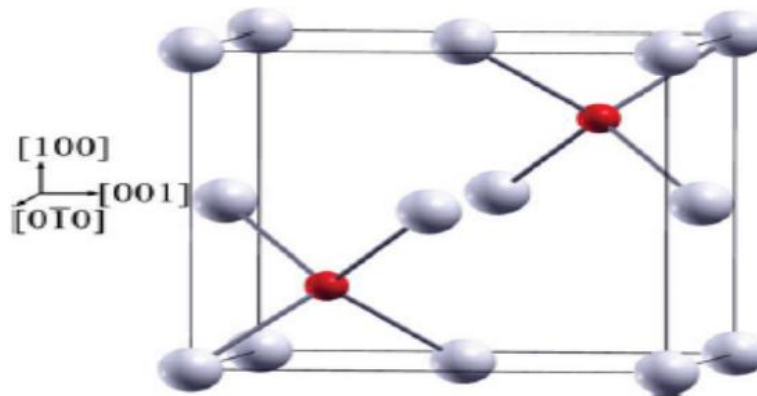


Figure II.1: Unit cell of bulk Cu₂O; small red and larger white spheres denote O and Cu atoms, respectively [21].

The results of the Cu₂O crystallographic properties are given in Table II.1.

Table II.1: Crystallographic properties of Cu₂O [20].

lattice constant	$4.2696 \pm 0.0010 \text{ \AA}$
space group	$Pn\bar{3}m (224)$
bond length Cu–O	1.849 \AA
separation O–O	3.68 \AA
separation Cu–Cu	3.012 \AA
cell volume	$(77.833 \pm 0.055) \times 10^{-24} \text{ cm}^3$
formula weight	143.14 g/mol
density	$5.749\text{--}6.140 \text{ g/cm}^3$
melting point	$1235 \text{ }^\circ\text{C}$

Cu₂O thin films find diverse applications in oxygen and humidity sensors, electrochromic devices [22], and photovoltaic devices such as thin film solar cells. However, defects at the cuprous oxide heterojunction and film quality are still major constraining factors for achieving high power conversion efficiency.

Chapter II: Solar Cell Based on Cuprous Oxide (Cu_2O) And Their Properties

II.2.3 Cuprous oxide (Cu_2O) Doping

II.2.3.1 P-Type

The nature of Cu_2O was described as: "copper oxide is a defect semiconductor ... the main impurity centers, acceptors in this case, are probably vacant ion lattice sites "; so, the cuprous oxide naturally is p type semiconductor. Copper vacancies are widely believed to act as shallow acceptors. P-type conductivity can also be increased by doping such as nitrogen N, it is a non-toxic, low-cost and abundant material which can be active as an acceptor in Cu_2O with acceptor energy level of 0.14eV above VB, if incorporated into the oxygen lattice site. Nitrogen-doping can reduce electrical resistivity of the film down to $1.8 \times 10^{-1} \Omega\text{cm}$ by increasing the hole concentration at (1.7 at.%) [23]; it is about $4.29 \times 10^{20} \text{cm}^{-3}$.

II.2.3.2 N-type

Since the cuprous oxide naturally is p-type semiconductor, i.e. that intrinsic defects are not the source of n-type conductivity in undoped Cu_2O thin films. Hence, that the n-type conductivity stems from an inversion layer formed during electro-deposition or from some external impurity (e.g., Cl doping).

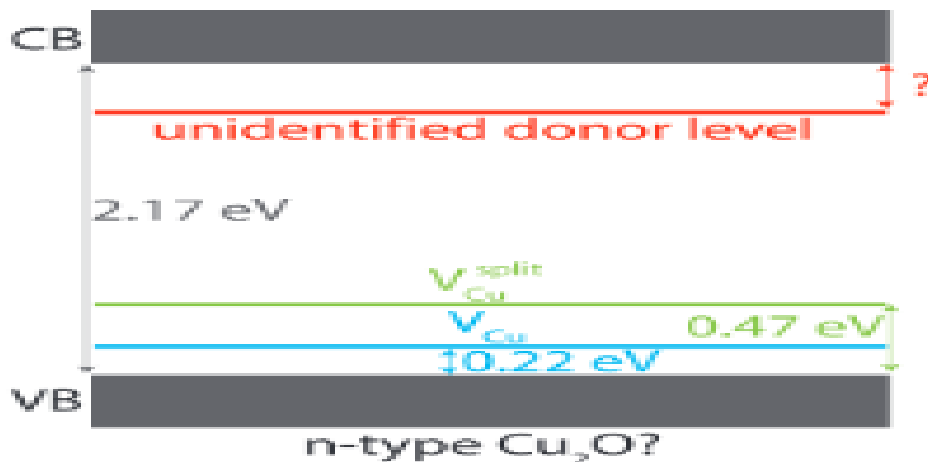


Figure II.2: Cause of that cuprous oxide of p-type not n-type is acceptor levels [24].

Chapter II: Solar Cell Based on Cuprous Oxide (Cu₂O) And Their Properties

II.2.4 Defects and interface states in Cu₂O

In reality, solar cell performances normally are not as good as theoretical prediction for the ideal cases as there always exist impurities; defects and interface states in the device.

II.2.4.1 Defects in Cu₂O

Defects introduce deep level recombination centers causing Shockley-Read Hall (SRH) recombination which deteriorates the cell; performance significantly. For further understanding, Through what has been experimentally stated in [25, 26]; we assume the defects have a donor-like or acceptor-like nature with a Gaussian distribution ($\sigma = 0.15$) as follows:

$$Nt(E) = \frac{Nt_0}{\sqrt{2\pi\sigma^2}} e^{-\frac{(E-E_0)^2}{2\sigma^2}} \quad (\text{II.1})$$

where $Nt(E)$ is the distribution of defects at an energy level E , Nt_0 is the maximum defect density at the central energy level E_0 and σ is the distribution constant. These defects introduce hole states above the valence-band maximum (VBM), due to the oxidation of Cu(I) to Cu (II). In Cu_2O hole states (acceptor levels) have been reported in experiments in the range 0.12–0.70 eV above the VBM. Deep level transient spectroscopy (DLTS) has shown the presence of hole traps 0.45–0.55 eV above the VBM, attributed to structural anomalies, a hole trap at 0.45 eV above the VBM, as identified previously, was attributed to copper vacancy, V_{Cu} , and a new trap level at 0.25 eV was tentatively assigned to a Cu divacancy, and found that a “simple” copper vacancy, V_{Cu} , in which one Cu is removed leaving two three-coordinate oxygens, is less stable than a “split” vacancy geometry, V_{split} Cu, where one remaining Cu moves toward the vacancy site, to achieve tetrahedral coordination they found V_{Cu} to be the most favored defect, and hence suggested it as the most likely source of p-type charge carriers.

For effect of defects in the Absorber-layer were found to have a significant effect on the performance of cells, such as acceptor-like and donor-like defects. All the performance parameters decrease rapidly with increase in defect density for both the acceptor-like and donor-like defects, even at a very low density of $10^{14} \sim 10^{15} \text{ cm}^{-3}$ [26]. The reason is that the A-layer does play a big role in absorbing the solar spectrum. These defects and impurities will change the doping concentration, hence affect the cell performance severely.

The existence of defects in a semiconductor is expected to impede the flow of charge carriers and hence the mobility. It is therefore expected that hole mobility would be lower for

Chapter II: Solar Cell Based on Cuprous Oxide (Cu_2O) And Their Properties

the unannealed samples because of the presence of defects resulting from high-temperature oxidation and quenching. These crystal defects are minimized after the annealing process, resulting in higher values of hole mobility in Cu_2O for the annealed samples [27].

II.2.4.2 Interface states ISt in Cu_2O

The interface state density could be very high due to the large lattice mismatch between the two materials used to form heterostructure cells which will cause serious problems for the devices such as recombination and tunneling. The interface states have similar properties as ‘defects’ in the semiconductor layers and behave as donor-like or acceptor-like defects. We assume the interface states are acceptor-like states with a Gaussian distribution with different energy levels of E_{IST} above E_V of the A-layer. The cell performance initially decreases very slowly with increase in ISt density and then suddenly drops for each performance parameter as the ISt density increases further; showing a stepwise change, as a result of some previous studies [26].

II.2.5 Electrical and optical properties

II.2.5.1 Electrical properties

Cuprous oxide is a semiconductor with a band gap of 2.1 eV as shown by experimental Studies, some electrical properties such as specific resistance that from van der Pauw measurements as a function of the oxygen flow for the series of sputtered copper-oxide samples, within the different copper oxide phases the specific resistance decreases with increasing oxygen flow whereas an increasing resistance indicates a phase change and carriers concentration as a function of the oxygen flow of the three copper-oxide compounds of the series of sputtered copper oxide samples determined from Hall measurements; the carrier concentration increases with increasing oxygen flow and reaches saturation before dropping sharply at each phase change are shown in Figure II.3; was reported by Mayer and others. For Cu_2O the carrier densities start around $10^{15}cm^{-3}$ and increase up to $10^{19}cm^{-3}$, for Cu_4O_3 a similar trend is observed, for CuO the lowest carrier densities are around $10^{17}cm^{-3}$; which increase up to $10^{20}cm^{-3}$. This strongly suggests that tuning the stoichiometry around the correct stoichiometric composition of the three compounds (oxygen poor to oxygen rich) allows the electrical conductivity and hole density to be increased, most likely due to the creation of copper vacancies.

Chapter II: Solar Cell Based on Cuprous Oxide (Cu_2O) And Their Properties

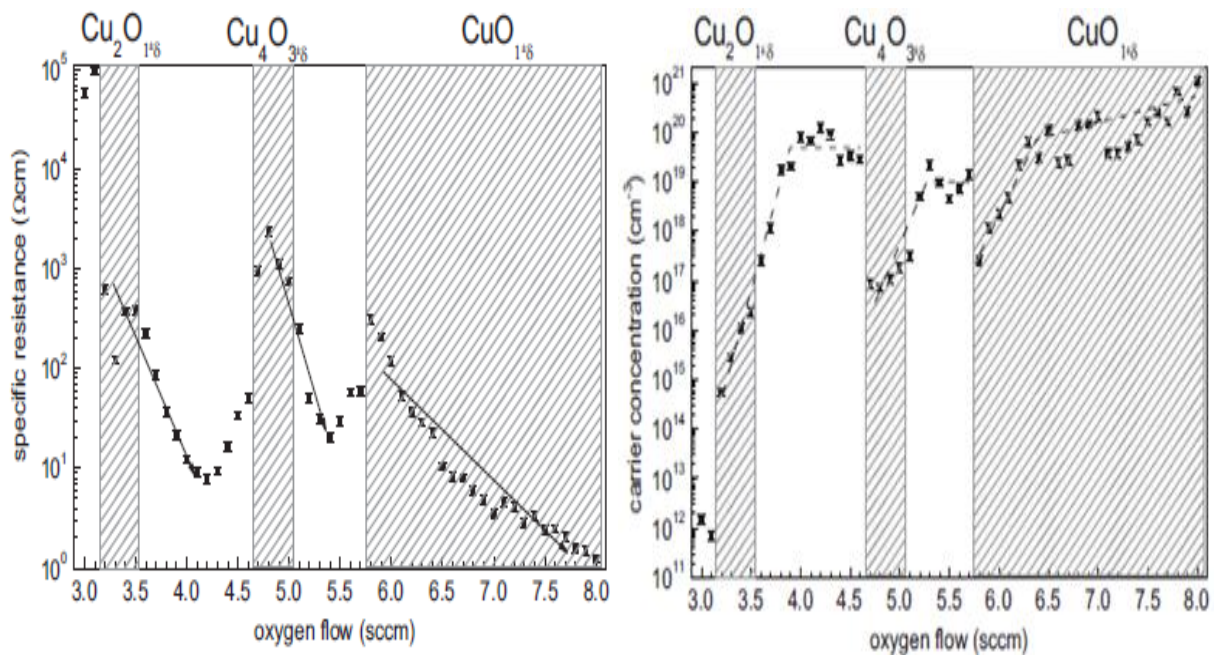


Figure II.3: Carrier concentrations and Specific resistance as a function of the oxygen flow [20].

II.2.5.2 Optical properties

The optical properties of Cu_2O depend on deposition conditions for each method for example electro-deposited method. We observe from the curves as shown in Figure II.4; that the transmittance changes with the pH values and also the final transmittance of the sample cannot be considered as transmittance of only Cu_2O because some amount of light transmitted through the Cu_2O layer is reflected at the interface between the Cu_2O and the ITO and absorbed in the ITO/glass substrate.

About the energy band gap; we observe that the energy band-gaps of 2.101eV, 2.064eV and 2.061eV were obtained at solution pH of 9.0, 11.0 and 12.0, respectively. Also The dependence of the energy band gap of Cu_2O on the deposition voltage; it was found that the energy band-gap slightly decreased as the potential increased [28]. Cuprous oxide (Cu_2O) is a well-known p-type semiconductor with a band gap depending on the deposition conditions. Cu_2O thin films have high optical transmittance at wavelengths above 600nm with a slightly yellowish appearance [22], the absorption coefficient of Cu_2O is relatively high ($\sim 10^5 \text{cm}^{-1}$) [1].

Chapter II: Solar Cell Based on Cuprous Oxide (Cu_2O) And Their Properties

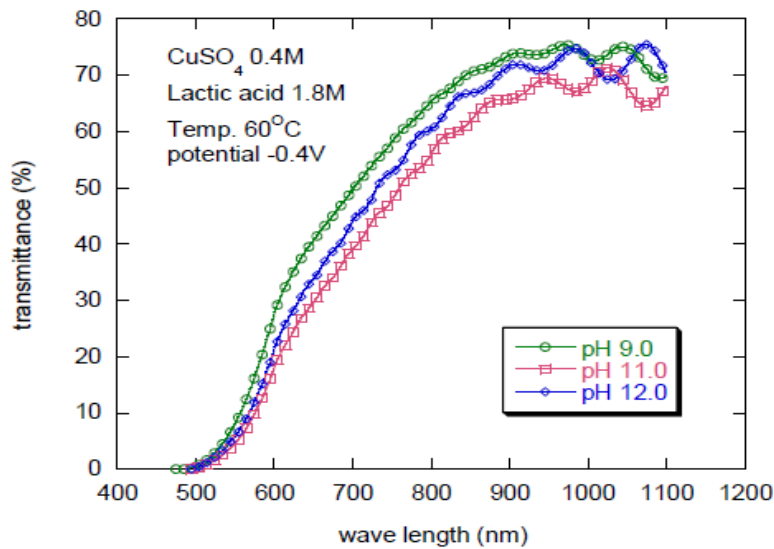


Figure II.4: Transmittance of Cu_2O deposited at different pH values.

II.3 Methods of manufacturing cuprous oxide material

The most important methods for the production of Cu_2O are by thermal oxidation, electro-deposition, sputtering and others.

II.3.1 Thermal Oxidation

This is by far the most widely used method of producing Cu_2O for the fabrication of solar cells. The procedure involves the oxidation of high purity copper at an elevated temperature (1000 – 1,500 °C) for times ranging from few hours to few minutes depending on the thickness of the starting material (for total oxidation) and the desired thickness of Cu_2O (for partial oxidation) [2].

The oxidation process can be carried out either in pure oxygen or in laboratory air. Cu_2O has been identified to be stable at limited ranges of temperatures and oxygen pressure. It has been indicated that during oxidation, Cu_2O is formed first and after a sufficiently long oxidation time, CuO is formed. However, at temperatures below 1000 °C and at atmospheric pressure; mixed oxides of Cu_2O and CuO are formed as observed from the X-ray diffraction (XRD) results. It has been suggested that the probable reactions that could account for the presence of CuO in layers oxidized below 1000°C are:



Chapter II: Solar Cell Based on Cuprous Oxide (Cu_2O) And Their Properties

The unwanted CuO can be removed using an etching solution containing $FeCl_3$, HCl and $NaCl$ [27]. The oxidation process is followed by annealing the sample at $500\text{ }^\circ C$ and then stopping the process by quenching in cold water. This process leads to good quality polycrystalline Cu_2O with the bulk resistivity in the range of $10^2 - 10^4 \Omega cm$ [2].

II.3.2 Electro-deposition

Another method of producing thin films of Cu_2O is by electro-deposition. Thin films of Cu_2O can be electrodeposited by cathodic reduction of an alkaline cupric lactate solution, either on metallic substrates or on transparent conducting glass slides coated with highly conducting semiconductors. The properties of the electrodeposited films of Cu_2O are largely similar to those prepared by thermal oxidation. The grain sizes of the electrodeposited ranges from 0.1 to $10\mu m$. The major problem is the high resistivity ($10^4 - 10^6 \Omega cm$) of the electrodeposited Cu_2O film [2].

II.3.3 Sputtering

Cathode sputtering is essentially one of the methods used for the preparation of thin films. The method requires very low pressure in the working space and therefore makes use of vacuum technique. The material to be sputtered is used as a cathode in the system in which a glow discharge is established in a gas at a pressure of $10^{-1} - 10^{-2}$ torr and a voltage of a few kilovolts. The substance on which the film is to be deposited is placed on the anode of the system. The positive ions of the gas created by the discharge are accelerated towards the cathode (target). Under the bombardment of the ions the material is removed from the cathode. The liberated components condense on surrounding areas and consequently on the substrates placed on the anode. Reactive sputtering is used in the production of Cu_2O . A chemical reaction that occurs with the cathode material (Cu in this case) by the active gas (oxygen) either added to the working gas or as the working gas itself. The resistivity of the deposited Cu_2O film can be controlled over a wide range by simply varying the oxygen pressure. Cu_2O films of resistivity as low as $25 \Omega cm$ have been reproducibly obtained by this technique [29].

II.4 Homojunction and heterojunction solar cells

II.4.1 Homojunction solar cells

Homojunction Cu_2O solar cells are less advanced than the heterojunction solar cells and this is due to less understanding and development of n-type Cu_2O . As Cu_2O is an inherently p-

Chapter II: Solar Cell Based on Cuprous Oxide (Cu_2O) And Their Properties

type semiconductor. A more-detailed study of the Cu_2O p-n junction revealed highly resistive n-type Cu_2O by electrochemical deposition in the range of 2.5×10^7 to $8.0 \times 10^8 \Omega\text{cm}$, leading to a low efficiency of $\sim 0.1\%$ for a solar cell built on the Cu_2O p-n junction. Therefore, doping in both n-type and p-type Cu_2O is required to improve the efficiency. Some doping attempts in Cu_2O were reported in the past such as Cl and N as p-type dopants [30]. It was also reported that Cl can be used as an n-type dopant in Cu_2O by co-precipitation during electrodeposition.

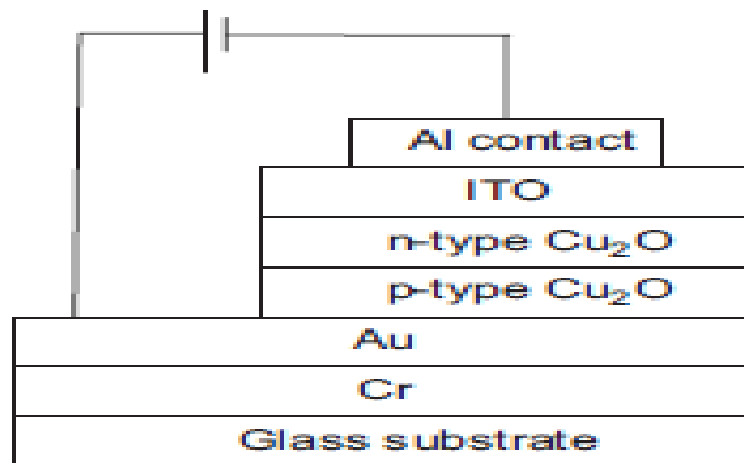


Figure II.5: Schematic of the p-n homojunction Cu_2O solar cell [28].

II.4.2 Heterojunction solar cells

As in our current study, the heterojunction (HJ) structure of the cell consists of two basic layers of two different materials; one of these layers of an HJ obviously must be an absorber, the other may be an absorber, too or it may be a window layer; i.e. a wider-gap semiconductor that contributes little to light absorption but is used to create the heterojunction and to support carrier transport. Window materials collect holes or electrons, function as majority carrier transport layers. The interface they form with the absorber is also used for exciton dissociation in cells where absorption is by exciton formation.

Since cuprous oxide is naturally p-type, the other layer should be type n, it is called the transparent conducting metal oxides, this was achieved due to the interest they had on metal oxides being generally stable compounds and the assumption that they are not likely to react with Cu_2O , to form PN heterojunction. Cu_2O based solar cells have been fabricated with p-n heterojunctions such as n-CdO/p- Cu_2O , n-ITO/p- Cu_2O , n- Ga_2O_3 /p- Cu_2O and n-ZnO/p- Cu_2O (as in the present case) as shown in Figure II.6. They are fabricated by depositing n-type

Chapter II: Solar Cell Based on Cuprous Oxide (Cu_2O) And Their Properties

semiconductor of suitable band gap on Cu_2O . Methods like vacuum deposition, sputtering and electrodeposition have been used for the deposition [2].

Combining p-type absorber layers and n-type window layers, one inherently faces the problems of lattice mismatch of band alignment and band offsets and of low interface quality due to defects.

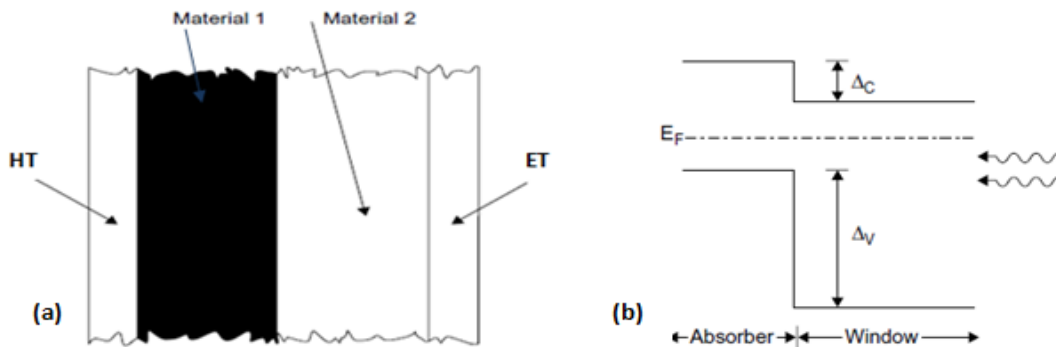


Figure II.6: (a) This cross-section is structure of heterojunction cell; shows material 1 and material 2. The anode is the left-side contact (ET) and the cathode is the right-side contact (HT), (b) band diagram of heterojunction cell from p-n absorber-window structure with light entering [31].

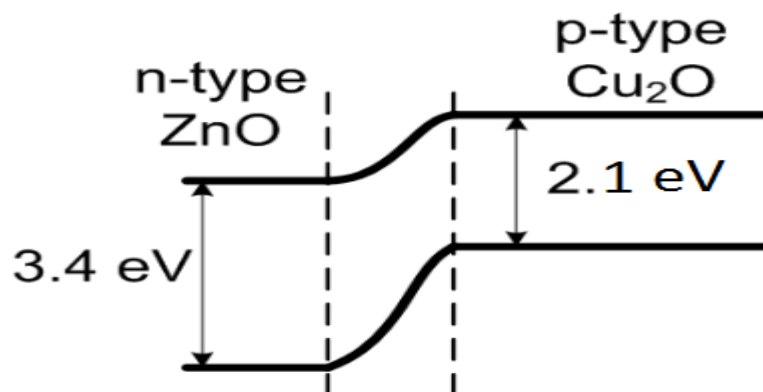


Figure II.7: Band diagram of a Cu_2O/ZnO heterojunction.

II.5 ZnO as a solar cell material

ZnO based thin films have attracted a great interest nowadays in semiconductor materials field because it is inexpensive and environmental friendly as compared to Indium Tin Oxide (ITO); high transparency in the visible and near ultraviolet spectral region, large band gap and

Chapter II: Solar Cell Based on Cuprous Oxide (Cu₂O) And Their Properties

high exciton binding energy of 60meV and also its suitability for Transparent Conductive Oxide (TCO's) devices, it is common in such thin films to dope ZnO with aluminum at the Zn sites, creating AZO.

ZnO is a good n-type semiconductor with a hexagonal crystal structure and is useful as an n-type semiconductor in inorganic thin film solar cells with an energy gap of around 3.37eV . ZnO has been used to fabricate many crucial devices such as heterojunction devices window, light emitting devices and photo detectors. ZnO has drawn the attention of researchers on its unique properties such as high electrochemical stability, resistivity control, and good transparency in the visible range with a wide band gap and the absence of toxicity and abundance in nature [3].

To evaluate and improve the buffer layer; we should study the effect of the main parameters of the ZnO buffer layer such as layer thickness, doping ...etc.

II.6 Effect of some parameters on solar cell properties

II.6.1 Effect thickness of Cu_2O and ZnO layers

II.6.1.1 Electrical properties

It is observed through experiments and results described in Figure II.8, that the device for thinner absorber of $2.2\mu\text{m}$ experiences significant shunt leakage current. It is believed that absorber thickness of $3.3\mu\text{m}$ is at least required in our current conditions to minimize the physical shunting of the device but the series resistance under light (RSL) of the devices also slightly increases from 35 to $57\Omega\cdot\text{cm}^2$ as compared to the device with $2.2\mu\text{m}$ Cu_2O . When the thickness of the absorber further increases to $4.5\mu\text{m}$, it limits the fluent collection of the light-generated carriers, the series resistance (RSL) of the devices also increases. Thus, decreasing J_{sc} . The increase in RSL is consistent with the increased film thickness of Cu_2O such increase in RSL is attributed to the intrinsic nature of Cu_2O absorber.

Chapter II: Solar Cell Based on Cuprous Oxide (Cu_2O) And Their Properties

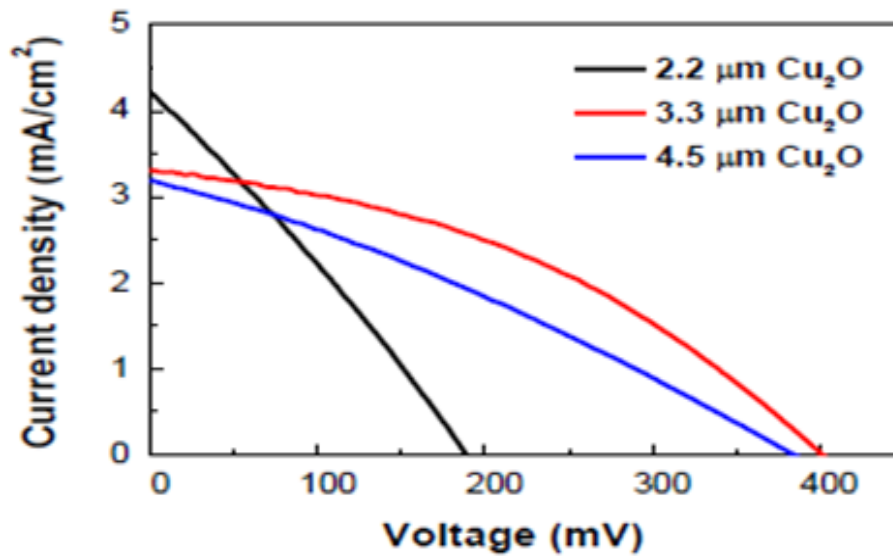


Figure II.8: J - V characteristics of the $\text{Cu}_2\text{O}/\text{ZnO}$ TFSCs for various thicknesses (2.2-4.5 μm) of the absorber under light [33].

II.6.1.2 Optical properties

From the transmission spectrum of ZnO. All the ZnO samples show an excellent transparency within the visible light region with the transmission rate above 80%. From the observation there was no significant effect of thickness on the transmission. For Cu_2O samples, the transmission percentage is less than ZnO sample, Cu_2O is physically dark and therefore the fabricated thin film is less transparent compared to ZnO thin film [3].

II.6.2 Doping effect of Cu_2O material

It is known that the impurities in semiconductors play a fundamental role even a very small concentration of impurities can alter significantly the properties of the semiconductor. Doped material is an important goal to achieve for several reasons. A p-type doped material with higher controlled, conductivity allows to build solar cells with smaller R_s and therefore with a better Fill factor (FF) and a better J_{sc} . Moreover, lowering the Fermi level, an increase in the V_{oc} can be obtained. Doping of Cu_2O has been attempted using several elements that have given a clear conductivity increase: Silicon, nitrogen, fluorine and chlorine. After Cl-doping (by Fan Ye, Jun-Jie Zeng and others 2017) for example, the hole concentration p increases while the resistivity decreases, since:

$$\rho^{-1} = e\mu p \quad (\text{II.3})$$

Chapter II: Solar Cell Based on Cuprous Oxide (Cu₂O) And Their Properties

Where e is the amount of electron charge [34].

The results of the Hall effect measurements are listed in Table II.2. All the samples are of p-type, in agreement with those doped with Cl by radio-frequency sputtering or thermal oxidation. A comparison of the undoped and those containing no impurities (Prepared at the diffusion temperatures of 1123K and 1223K) shows that the resistivity is reduced and the hole concentration is increased.

Table II.2: The resistivity ρ , mobility μ and carrier concentration p of the samples [34].

Temp. (K)	ρ ($\Omega \times \text{cm}$)	μ ($\text{cm}^2/(\text{V} \times \text{S})$)	p (cm^{-3})
undoped	240.1	19.7	1.3×10^{15}
823	190.9	16.5	2.0×10^{15}
973	305.1	19.0	1.1×10^{15}
1123	11.6	28.5	1.9×10^{16}
1223	18.2	18.1	1.9×10^{16}

The obtained absorption spectra of the samples are present in Figure II.9. For a direct band gap semiconductor, the relation between the absorption coefficient α and the optical band gap E_g is:

$$(\alpha h\nu)^2 = A(h\nu - E_g) \quad (\text{II.4})$$

Where A is a constant, h is the plank constant and ν is the frequency of the photon.

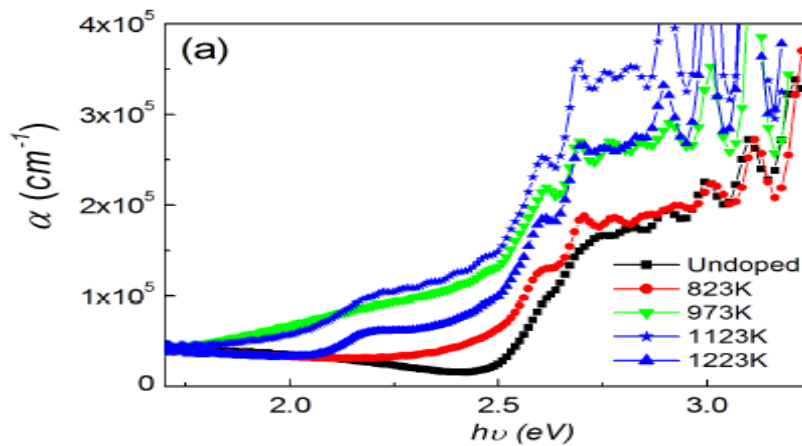


Figure II.9: The absorption spectra of the samples.

Chapter II: Solar Cell Based on Cuprous Oxide (Cu₂O) And Their Properties

The optical band gaps for the undoped and those prepared at the diffusion temperatures of 823K, 973K, 1123K and 1223K are 2.53eV, 2.49eV, 2.47eV, 2.43eV and 2.47eV, respectively. The optical band gaps of our samples are larger than that of F-doped Cu₂O thin films prepared with electrodeposition. Our F-doped samples have smaller optical band gaps than our undoped one and this is in accordance with those electrodeposited samples, F-doped Cu₂O thin films without impurity phase such as CuO or Cu can be obtained at the diffusion temperatures of 1123K or 1223K. Higher diffusion temperature favors larger grain size. All the samples are of p-type. F-doped Cu₂O samples have smaller lattice constant, smaller resistivity, smaller band gaps, larger Urbach tails and larger hole concentrations than undoped samples [34].

II.6.3 Effect of passivation types

Passivation is a process to improve the performance of solar cells to reduce their surface recombination by hydrogen treatment either from the passivation layer itself or during annealing under a hydrogen atmosphere, cyanide treatment and other elements for polycrystalline nitrogen-doped Cu₂O thin films, is called chemical passivation. It was found that the optical and electrical properties of polycrystalline nitrogen-doped Cu₂O thin films were improved by each treatment through several studies. Such improvements may be caused by a passivation of the non-radiative recombination centers and donor-like defects by making chemical bonds of Cu–H or Cu–CN; it was also found that the cyanide passivation has a higher thermal stability than that of the hydrogen passivation, possibly due to a strong chemical bond between Cu and CN than Cu and H [35].

There is also other type of passivation where the tunneling layers have traditionally been used in metal-insulator-semiconductor solar cells for inversion layer emitters. The tunnel oxide is a core element of this contact as it has to reduce the minority carrier recombination but simultaneously must not hamper the majority carrier flow. This process occurs when an effort barrier is formed in the valence and conduction bands of the semiconductor; this barrier prevents the passage of minority carriers while, the majority carriers cross it by tunnel effect, that increases their concentration near the contact, and decreases minority concentration, therefore decreases recombination rate [36].

And another process of passivation as well, is called field effect passivation or the term back surface field (BSF) that refers to a low high (pp⁺ or nn⁺) unipolar junction that is formed between the base region of the solar cell and a highly doped, alloyed or diffused region of the

Chapter II: Solar Cell Based on Cuprous Oxide (Cu_2O) And Their Properties

same polarity formed near its back surface. There has been a widespread belief that this creates an electric field that repels minority carriers away from the surface, saving them from recombining.

The recombination current prefactor J_{0p+} is plotted in Figure II.10 as a function of the total dopant dose in the p^+ region. In general, J_{0p+} decreases as the dopant dose increases, reaching the lowest values for the highest width explored here: $10\mu\text{m}$. The path to reduce J_{0p+} is, therefore, to increase the dose, primarily by increasing the width of the p^+ region, but by increasing the dopant concentration as well.

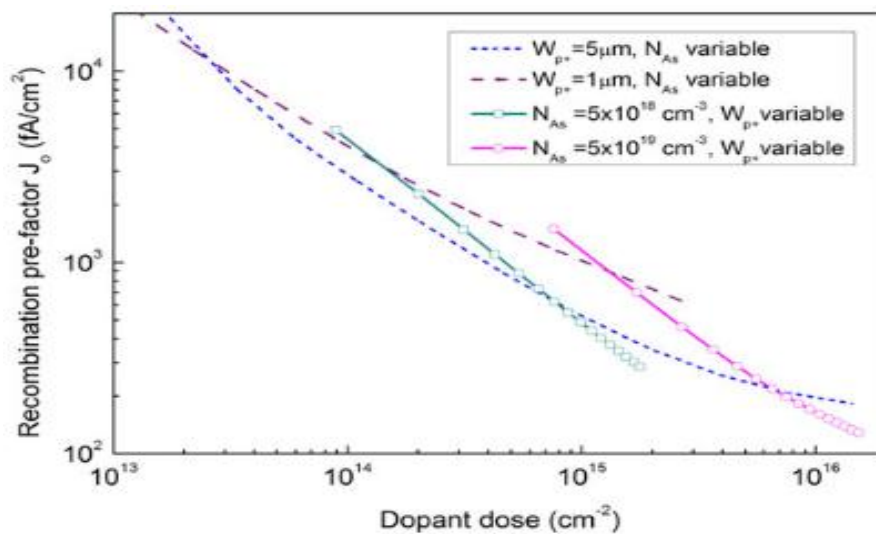


Figure II.10: Recombination current prefactor J_{0p+} as a function of the total dopant dose for Gaussian p^+ back surface regions with a varying depth or a varying surface dopant concentration [37].

II.7 Literature review of Cu_2O based heterojunction solar cells

Many Cu_2O based heterojunction solar cells were manufactured in order to achieve the best performance. A summary of notable attempts and the achieved conversion efficiencies and their electrical properties are listed in Table II.3.

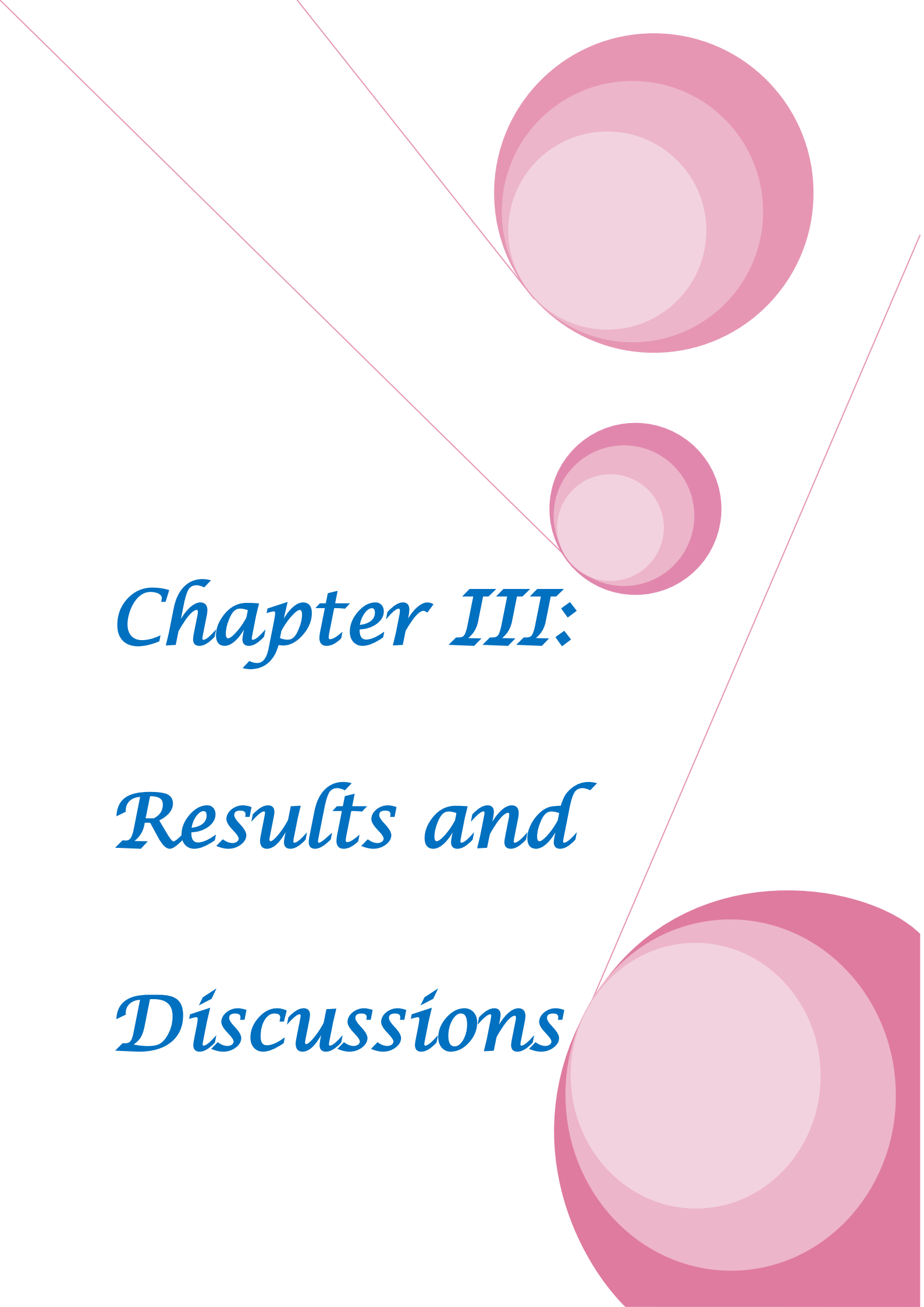
Chapter II: Solar Cell Based on Cuprous Oxide (Cu_2O) And Their Properties

Table II.3: Literature review of Cu_2O solar cells.

Type of junction	Deposition Method	Voc (V)	Jsc ($mAcm^{-2}$)	FF (%)	Eff (%)	Ref
p-Cu ₂ O/n-ZnO/NESA (2004)	Electrodeposition	0.19	2.08	29.5	0.117	[38]
Cu ₂ O/GaN (2012)	RF-sputtering	0.85	2.10	78.0	0.14	[20]
Cu ₂ O/ $Al_xGa_{1-x}O$	PLD pulsed laser déposition				6.10	[1]
Ti/p-CuO/n-Cu ₂ O/Au	Electrochemical	0.19	6.40		0.52	[1]
Cu ₂ O/ZnO : Al (2004)	PLD	0.40	7.10	40.0	1.20	[39]
IGZO/ZnO/Cu ₂ O : Na (2017)	DC magnetron	0.68		42.0	1.68	[40]
ZnO: Al/ZnO/Cu ₂ O Takiguchi Model (2015)		0.64	13.07	52.9	4.48	[41]
MgF ₂ /Al-ZnO/ Zn _{0.38} Ge _{0.62} -O/Cu ₂ O: Na	Thermally oxidizing	1.25	11.50	70.0	8.10	[42]
AZO/p-Cu ₂ O (2019)	Sputtering				3.21	[43]
AZO/Ga ₂ O ₃ /Cu ₂ O (2013)	Thermally oxidizing				5.38	[44]

II.8 Conclusion

After looking for the most important properties of cuprous oxide Cu_2O thin films in this chapter, it has become possible to investigate the most relevant properties in order to get the best cuprous oxide based solar cells and optimize their conversion efficiency.

A decorative graphic on the right side of the page. It features three overlapping circles of varying sizes, all in shades of pink. The largest circle is at the top, a medium one in the middle, and the largest one at the bottom right. Two thin, light pink lines originate from the top left and extend towards the circles, one passing through the top circle and the other through the middle one.

Chapter III:

Results and

Discussions

III.1 Introduction

In this chapter, the results obtained will be presented and then interpreted and discussed. Since this thesis uses Silvaco Atlas to optimize solar cell performance, we will introduce Silvaco TCAD definition and some of its features in the first section.

III.2 Silvaco TCAD

SILVACO TCAD is the abbreviation of Silicon Valley Corporation Technology Computer Aided Design. It is a software package used to simulate semiconductor devices. It predicts the electrical behavior of a device, which can be modeled in one dimension (1D), two dimensions (2D) or three dimensions (3D). The software consists of several integrated tools that work together to achieve the desired results. The interactive tools or modules are Deckbuild, Devedit, Tonyplot, Maskviews...etc. And the main simulators which are Atlas and Athena gathered under one environment called DECKBUILD. These tools give the user the ability to simulate the production process to manufacture a semiconductor device and test its characteristics. There are many models, numerical methods, and types of material built into the program, giving a wide range of functionality to the user. This allows the modeling of anything from simple devices to complex circuits.

III.2.1 Numerical Methods

To simulate the device, there are three techniques depending on the equations, decoupled Gummel, fully-coupled Newton, and Block. The Gummel method solves each unknown while keeping the other variables constant. It continues to do this until a stable solution is found. The Newton method solves the total system of equations together to find a solution. The Block method solves the equations using a combination of the Newton and Gummel methods in special cases.

III.2.2 Tools

The Tools are a suite of applications that provide users with a comfortable environment within which all TCAD simulations can be performed, such as:

- ✓ **Maskviews:** Drawing tool for masks (Layouts).
- ✓ **Devedit:** Structure editing tool, we can create new structures or even modify current structures, we can define meshes or refine current meshes.

Chapter III: Results and Discussions

- ✓ **TonyPlot:** Is a tool to visualize and plot simulation results and the structure of the device that being studied as Figures III.1 and III.2:

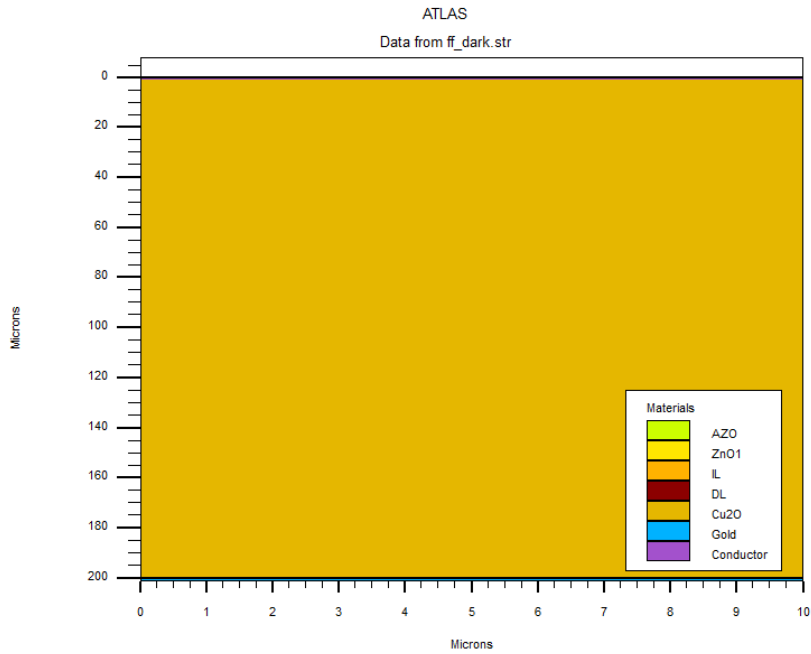


Figure III.1: Schematic diagram of studied device from TonyPlot.

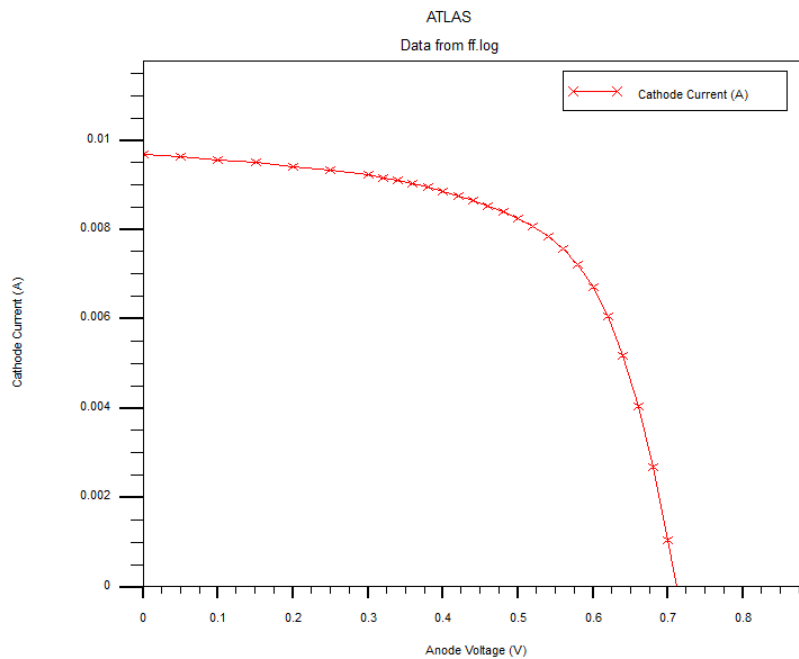


Figure III.2: Curve I-V of the studied device from TonyPlot.

Chapter III: Results and Discussions

- ✓ **DeckBuild:** is the main program that runs the simulation and calls the associated programs as needed. And it is the environment of Atlas and Athena. Where DeckBuild consists of two windows, editor window and output window, as shown in Figure III.3.

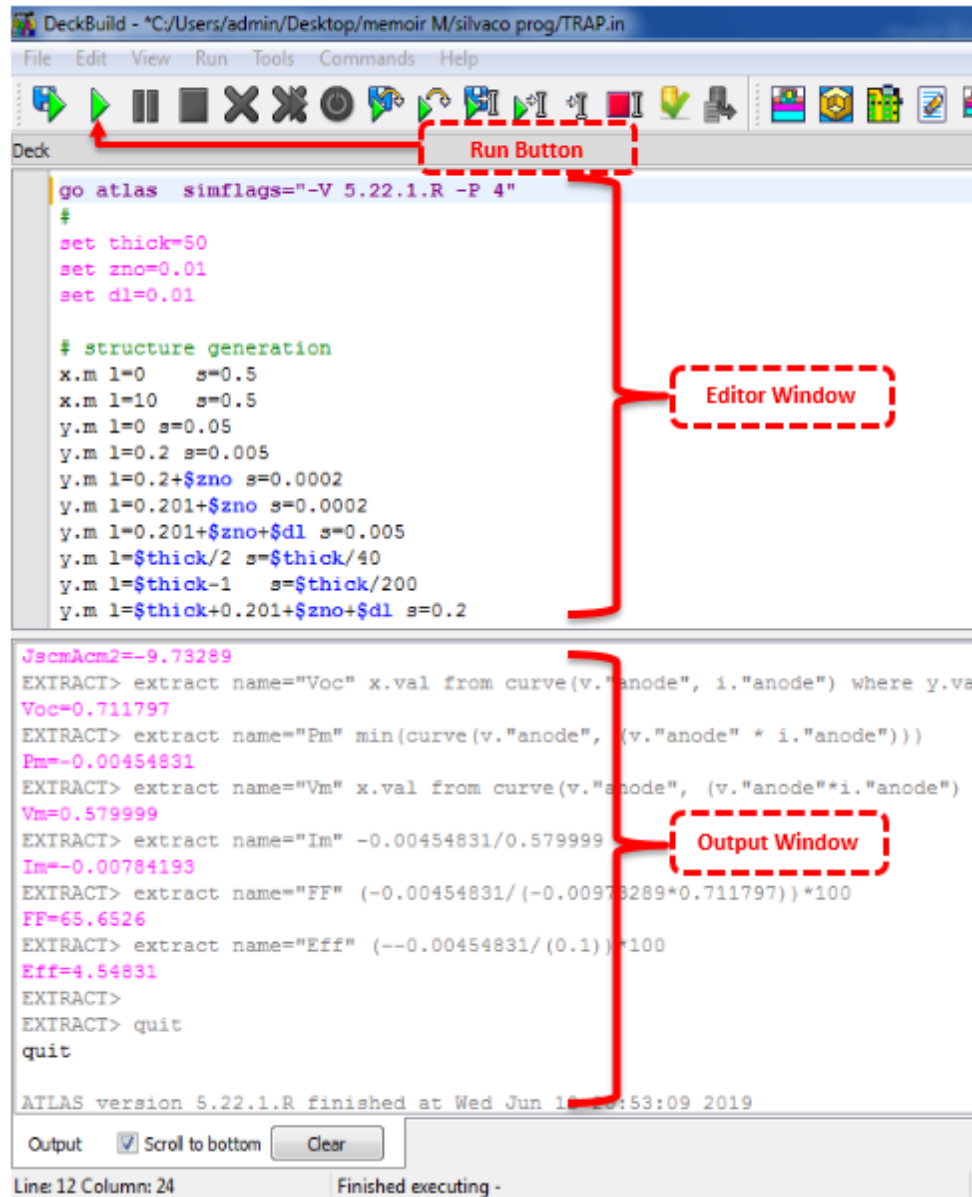


Figure III.3: DeckBuild window interface.

- **Athena:** Simulator of technological processes which makes it possible to simulate the different steps performed and thus to obtain the structure of the device (constituent layers, dimensions, geometry) with the doping profiles.
- **Atlas:** Is a semiconductor device simulator based on physical principles. It predicts the electrical behavior associated with the physical structure under specified conditions. Atlas achieves this by partitioning the device specified by a grid. Atlas then applies a

set of equations, based on Maxwell's laws, to the mesh to simulate the transport of charge carriers across the structure. Atlas is based on several statements which is Mesh, Region, Electrode, Doping, Material, Defects, Models, Beam, Solve, Extract. Each of them consists of parameters.

III.2.3 Statements

To run Atlas simulator simply type: *go Atlas*

This runs the Atlas program within Deckbuild and is usually the first command unless running one of the other programs, such as Athena, first. Once Atlas is initiated, Atlas has a specific order in which the statements must be placed, the next step is to set the parameters of the device. Otherwise the program may not function correctly, even if it does run, it is possible that certain parameters may not be used, which causes inaccurate results[45]. Generally, the format is:

STATEMENT **PARAMETER = <VALUE>**

III.2.3.1 Mesh

The first thing that needs to be specified is the mesh on which the device will be constructed. A grid is a series of horizontal and vertical lines on the axes. For accurate calculations, where multiple equations are resolved at each intersection point of the lines, the division of mesh is uniform or nonuniform. As shown in Figure III.4. By use the statement *Mesh* as:

mesh

x.m l=0 s=0.5

x.m l=10 s=0.5

y.m l=0 s=0.05

y.m l=0.2 s=0.005

y.m l=0.2+\$zno s=0.0002

y.m l=0.201+\$zno s=0.0002

y.m l=0.201+\$zno+\$dl s=0.005

y.m l=\$thick+0.201+\$zno+\$dl s=0.002

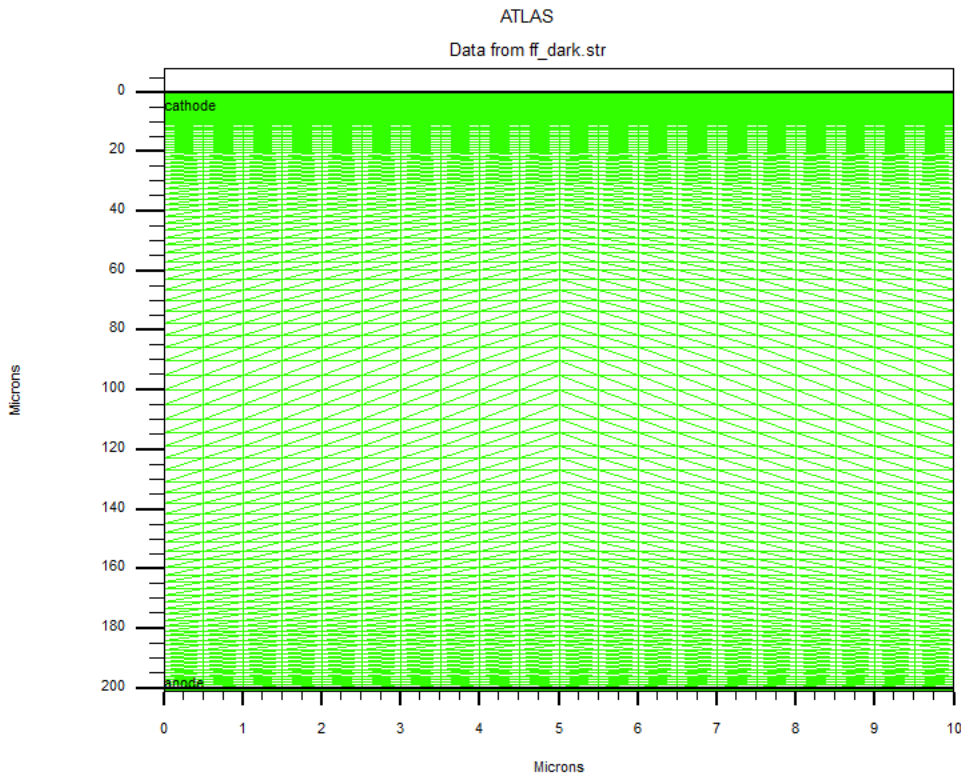


Figure III.4: Mesh of the studied device structure.

III.2.3.2 Region

After defining the mesh, it is necessary to define the regions. From Figure III.5, the code that defines the regions is identified. There are seven defined regions. The boundaries of each region are explicitly identified in the axes, then give the material name as a reference by use the statement *Region*. There are two cases as follows:

The first case, when the material is not defined in Silvaco's Library:

```
region num=1 y.min=0 y.max=0.2 name=AZO user.material=AZO
```

The second case, when the material is defined in Silvaco:

```
region num=7 mat=Gold y.min=7.652 y.max=8.652 name=Gold
```

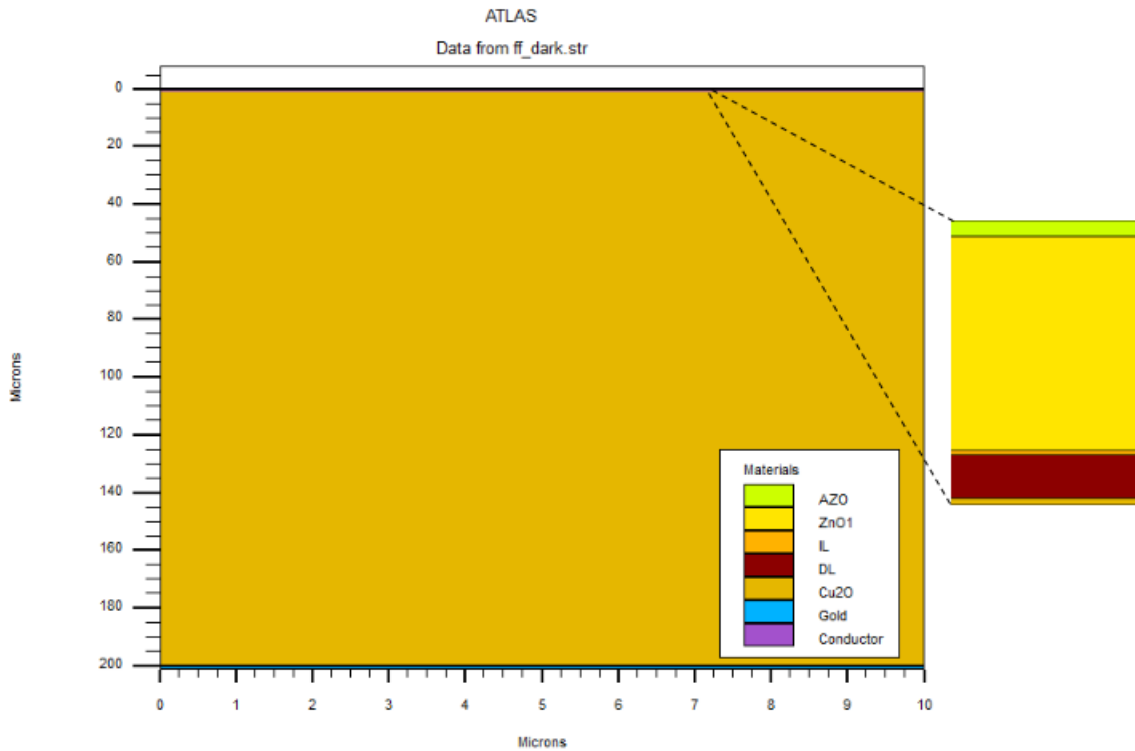


Figure III.5: Regions with defined materials of the simulated structure.

III.2.3.3 Electrode

To define the electrodes of the device, their position and size need to be entered. Additional information about their materials and work functions can be supplied if needed. There must be at least one electrode (that touches the semiconductor material) defined for the program to run. Typically, in this simulation the only electrodes defined are the anode and the cathode, as shown in Figure III.6. By use the statement *Electrode* as:

```

elec num=1 name=cathode top
elec      num=2      name=anode      y.min=$thick+0.201+$zno+$dl+$pp
y.max=$thick+1.201+$zno+$dl+$pp mat=Gold
    
```

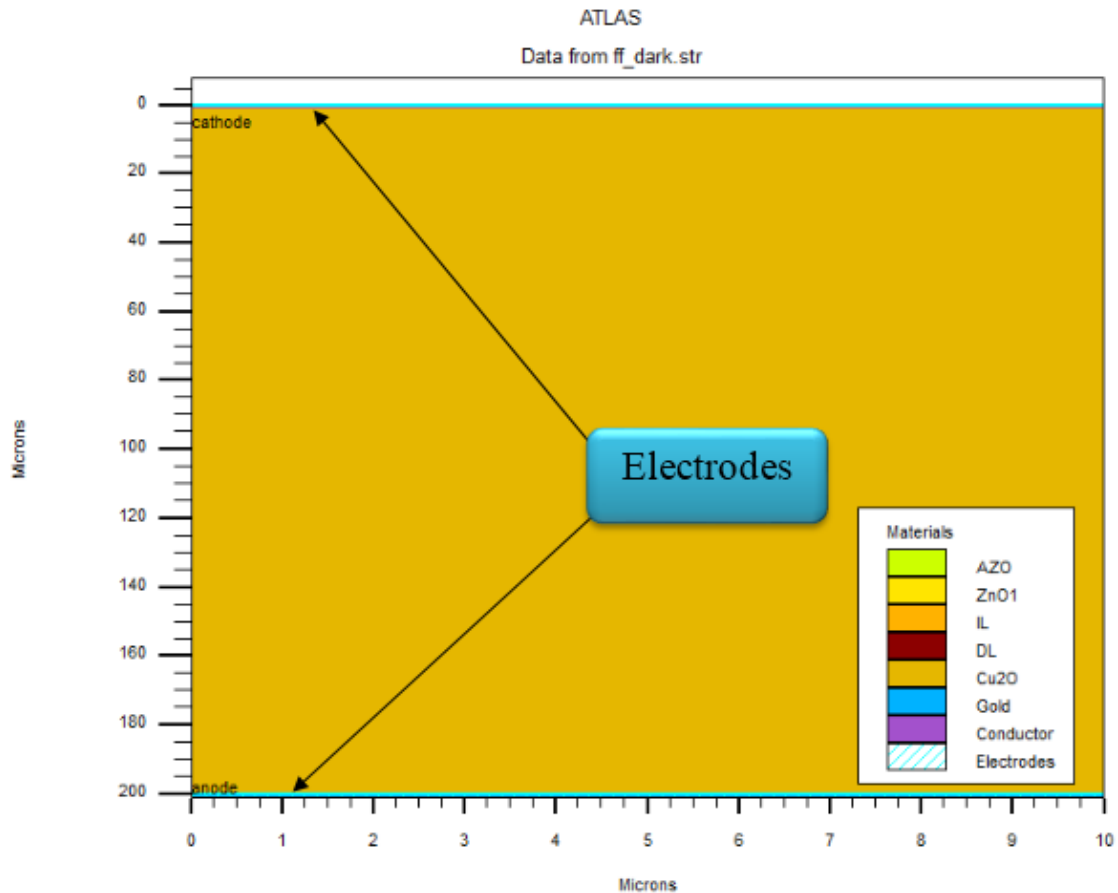


Figure III.6: Electrodes of the simulated structure.

III.2.3.4 Material

Materials used throughout the simulation can be selected from Silvaco library that includes a number of common elements and compounds with their most important parameters. However, even the used material is not defined in Silvaco's library we can add new materials, in that purpose Silvaco has the ability to define all the required parameters for simulation, such as bandgap, mobility, life time of carriers ...etc. By using the statement *Material:*

```
Material      material=Cu2O  EG300=2.1  MUN=200  MUP=100  affinity=3.2
permittivity=7.6  NC300=2.43e19  NV300=1.34e19  index. File= Cu2O.nk
```

```
user. Group= semiconductor user. Default=zno
```

III.2.3.5 Doping

The doping parameters such as concentration, type and distribution can be determined by Atlas using the statement *doping* as follow:

```
#doping AZO
```

```
doping region=1 uniform n. type conc= $1 \times 10^{21}$ 
```

```
#doping Cu2O
```

```
doping region=5 uniform n. type conc= $6 \times 10^{15}$ 
```

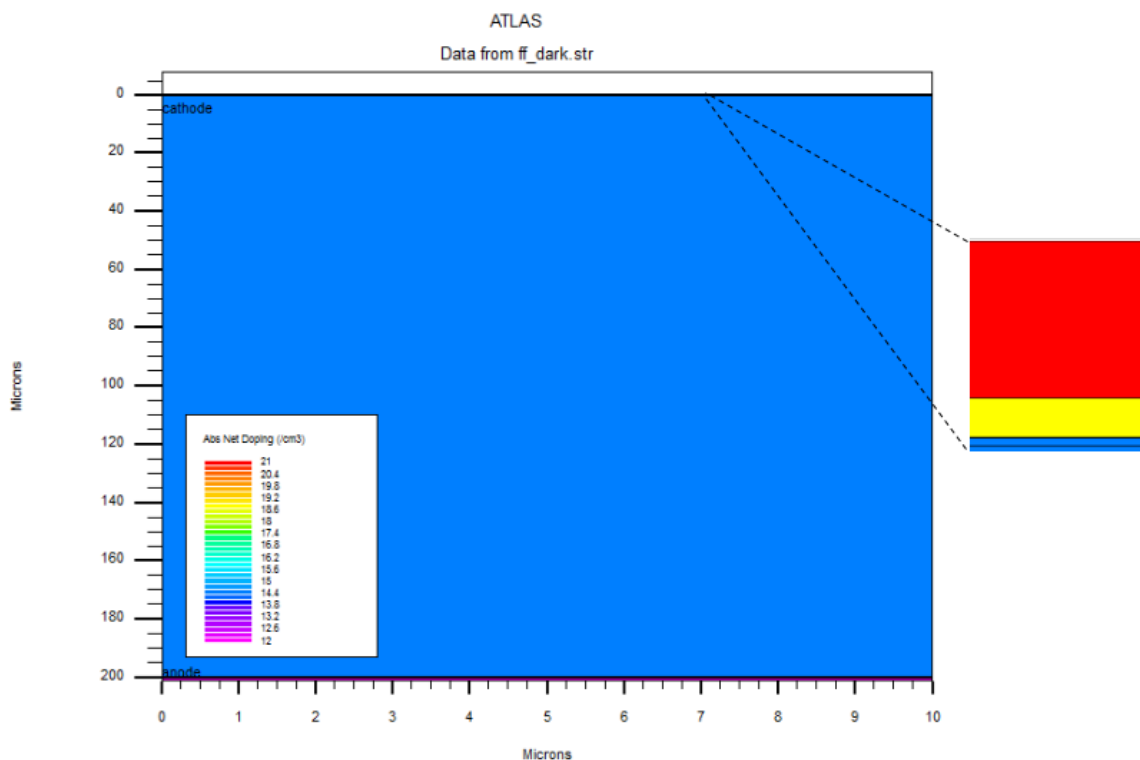


Figure III.7: Doping concentration is specific by colors of simulated structure.

III.2.3.6 Defects

For exact and correct results, the device must be close to reality. Therefore, the types and quantity of defects must be determined. As follows:

```
#DEFECTS Cu2O
```

```
DEFECTS mat=Cu2O NGD=0.7E14 EGD=1.05 WGD=0.1 SIGGDE=5e-13  
SIGGDH=1e-15 NGA=0 NTA=0 NTD=0 EGA=0 WTA=0 WTD=0 WGA=0 SIGTAE=0  
SIGTAH=0 SIGTDE=0 SIGTDH=0 SIGGAE=0 SIGGAH=0
```

III.2.3.7 Models

More than seventy models can be used to achieve better description of a full range of physical phenomena and to make the device close to reality. Each model is accompanied by a full set of its parameters. The physical models fall into several categories such of which: mobility, recombination, carrier statistics, impact ionization, and tunneling. The syntax of the model statement is as follows:

```
models BGN SRH temp=300.
```

III.2.3.8 Beam

To simulate solar cells, it is necessary to determine the light source. Silvaco offers the ability to use a number of light sources and adjust their location, orientation and intensity. The spectrum of the light can be described in all the necessary detail. Polarization and reflectivity are also among the simulator's features. which can be done using for example:

```
beam num=1 x.orig=5 y.orig=-10 angle=90 am1.5 wavel.num=200
```

III.2.3.9 Solve

The *solve initial* statement performs a solution at the initial point. Then open a log file by statement *log* to save the results calculated by Atlas. Finally, the *solve* statement is used to start calculating and get the final solutions by defining the starting bias point, the step and the final point.

III.2.3.10 Extract

Deckbuild allows extracting electrical quantities such as current short circuit (J_{sc}), open circuit voltage (Voc), efficiency (η) ... etc. from simulation results and are stored in a file called *Results.Final*. by written the statement: *Extract* for example:

```
extract name="Jsc" y.val from curve (v."anode", i."anode") where x.val=0.0
```

III.3 Description of simulated structure of heterojunction solar cell based on Cuprous oxide (Cu₂O)

In this work, we optimize the performance of heterojunction solar cell based on cuprous oxide (Cu₂O), in order to increase their conversion efficiency, by studying some effects such as (doping, thickness, passivation... etc.), by simulation using the Silvaco's atlas program. This cell was simulated last year depending on Takiguchi model [46], where its structure is based on Cu₂O as an absorber layer and ZnO as a buffer layer (AZO/n-ZnO/p-Cu₂O), it gave an efficiency of 4.24% at ZnO thickness of 0.05μm, Cu₂O thickness of 200μm, doping concentration in ZnO layer of $1 \times 10^{19} \text{cm}^{-3}$ and doping concentration in Cu₂O layer of $2.5 \times 10^{14} \text{cm}^{-3}$, as shows in Figure III.8:

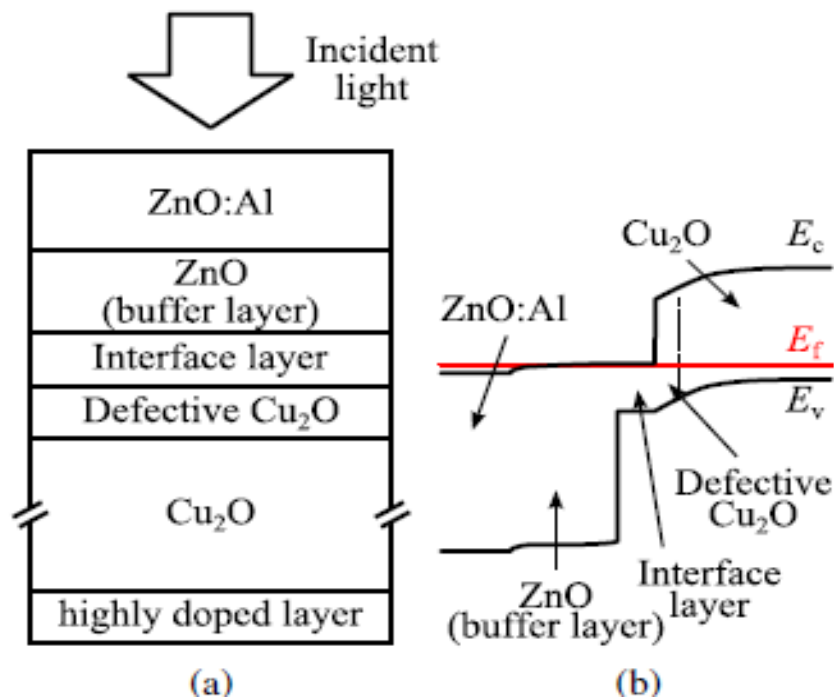


Figure III.8: (a) Structure and (b) band diagram of simulated structure [41].

To develop a more reliable simulation model, an interface layer (IL) and a defective Cu₂O layer (DL) have been introduced based on the Takiguchi model. The χ of the IL was the same as that of the buffer layer and the position of the valence band maximum of the IL was the same as that of the Cu₂O absorber. The defective Cu₂O layer was inserted between the IL and the Cu₂O absorber layer, it has the same properties of the absorbent layer Cu₂O except for the Defect density. Figure III.1 illustrates the schematic structure of the solar cell that is simulated by Silvaco program, it consists of a transparent conductive layer (AZO), Zinc oxide buffer layer

Chapter III: Results and Discussions

(ZnO), interface layer (IL), defect layer (DL), cuprous oxide adsorbent layer (Cu₂O), and a layer of gold as a conductive layer, their properties are shown in Table III.1:

Table III.1: Properties of the used materials for the simulation.

Parameters	AZO	ZnO	IL	DL	Cu ₂ O
Thickness (μm)	0.2	Variable	0.001	0.01	Variable
Bandgap (eV)	3.35	3.35	0.9	2.1	2.1
Electron affinity (eV)	4.4	4.4	4.4	3.2	3.2
Dielectric constant	9	9	7.6	7.6	7.6
Effective density of states of conduction band minimum (cm ⁻³)	2.2 × 10 ¹⁸	2.2 × 10 ¹⁸	2.43 × 10 ¹⁹	2.43 × 10 ¹⁹	2.43 × 10 ¹⁹
Effective density of states of valence band maximum (cm ⁻³)	1.8 × 10 ¹⁹	1.8 × 10 ¹⁹	1.34 × 10 ¹⁹	1.34 × 10 ¹⁹	1.34 × 10 ¹⁹
Electron mobility [cm ² =(V·s)]	10	10	200	200	200
Hole mobility [cm ² =(V·s)]	5	5	100	100	100
Donor concentration (cm ⁻³)	1 × 10 ²¹	Variable	0	0	0
Acceptor concentration (cm ⁻³)	0	0	Variable	Variable	Variable
Defect type	D-like, Gaussian	D-like, Gaussian	Trap	D-like, Gaussian	D-like, Gaussian
Defect distribution	Gaussian	Gaussian	Banded	Gaussian	Gaussian
Defect density (cm ⁻³)	1 × 10 ¹⁸	5 × 10 ¹⁷	0.8 × 10 ¹³	1.1 × 10 ¹⁷	0.7 × 10 ¹⁴
Defect level (eV)	Midgap	Midgap	0.75E _g /0.25E _g	Midgap	Midgap
Defect distribution width (eV)	0.1	0.1	-	0.1	0.1
Capture cross section of electrons (cm ²)	1 × 10 ⁻¹²	1 × 10 ⁻¹²	1 × 10 ⁻¹³	1 × 10 ⁻¹³	1 × 10 ⁻¹³
Capture cross section of holes (cm ²)	1 × 10 ⁻¹⁵	1 × 10 ⁻¹⁵	1 × 10 ⁻¹³	1 × 10 ⁻¹⁵	1 × 10 ⁻¹⁵

All simulation steps for the device studied are presented in Section III.2. The structure and regions of the cell that simulated in 2 dimensional (2D), was illustrated in Figure 4 using

Tonyplot. The Cuprous oxide material are not known by the program so it should be defined as new material by use the statement *Material* with its own parameters inserted. Each region is uniformly doped (Figure III.7), then the device is exposed to 1 sun illumination with propagation angle is 90° , with AM1.5. To perform more reliable simulation, some physical models must be used:

- ✓ BGN: Specifies bandgap narrowing model, in the presence of heavy doping, as the doping level increases, a decrease in the bandgap separation occurs, where the conduction band is lowered by approximately the same amount as the valence band is raised. In Atlas this is simulated by a spatially varying intrinsic concentration n_{ie} defined according to Eq. III.1 [45]:

$$n_{ie}^2 = n_i^2 \exp\left(\frac{\Delta Eg}{kT}\right) \quad \text{(III.1)}$$

ΔEg is the variation in bandgap. (ref atlas).

- ✓ SRH: Specifies Shockley-Read-Hall recombination, according to Eq. (I.46).
- ✓ Temp: Specifies the temperature in Kelvin.

III.4 Results and discussions

In this section, we will present the simulation results of cuprous oxide heterojunction cell structure (AZO/ZnO/Cu₂O).

Starting by changing the thickness of the ZnO layer, which is the window layer so it affects the amount of light reaching the absorbent layer (Cu₂O).

III.4.1 Thickness effect of the ZnO layer

The first simulation was done to study the effect of the ZnO layer thickness on the electrical characteristics of the solar cell. The results were as follows:

Chapter III: Results and Discussions

Table III.2: ZnO Thickness effect on the output parameters of Cu₂O based heterojunction solar cell.

ZnO Thickness (μm)	Eff (%)	FF (%)	Voc (V)	Jsc (mA/cm^2)
0.10	4.167	61.614	0.710	9.514
0.05	4.247	61.585	0.711	9.691
0.045	4.248	61.578	0.711	9.700
0.042	4.250	61.572	0.711	9.704
0.041	4.253	61.568	0.711	9.706
0.04	4.252	61.567	0.711	9.707
0.03	4.250	61.544	0.711	9.711
0.01	4.240	61.477	0.712	9.681

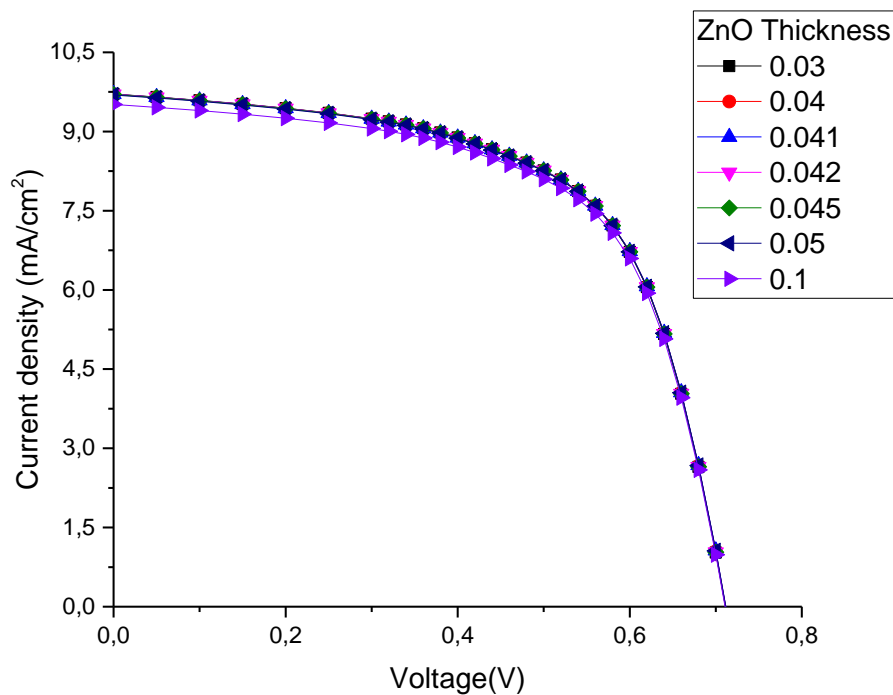


Figure III.9: The effect of ZnO thickness on the J-V characteristics.

Figure III.10 shows the conversion efficiency (η), fill factor (FF), open circuit voltage (V_{oc}), and short circuit current (J_{sc}) as functions of the ZnO film thickness with changing the thickness from 0.01 to 0.1 μm [47]. An increase in both J_{sc} and η until of 0.041 μm and a slight continuous increase in FF with increasing thickness of the layer was observed, this can be attributed to that more photons will be absorbed. Then we observe a decrease in both J_{sc} and η

with any other increase in thickness, which can be attributed to the short lifetime of minority carriers in the ZnO thin film. And also because of the values of transmittance decrease as thickness increase. On the other hand, it is clear that V_{oc} is not affected by thickness. Thus, the optimum ZnO thickness is at about $0.041\mu\text{m}$. The changes observed in the electrical characteristics are small due to the small contribution of the ZnO layer, which acts as a window layer.

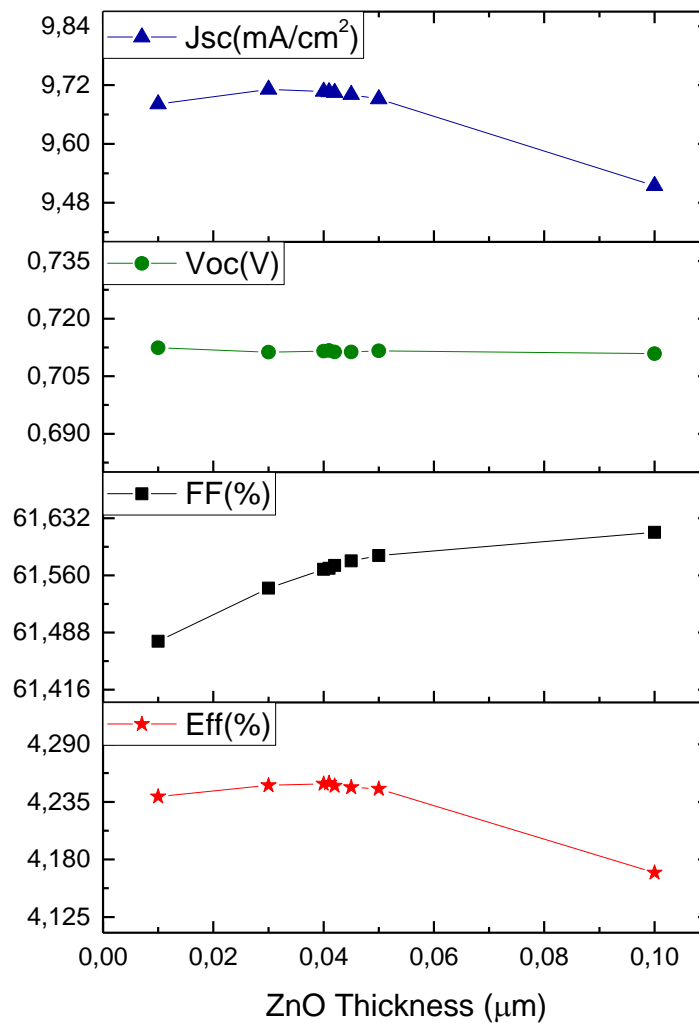


Figure III.10: η , V_{oc} , J_{sc} and FF as functions of the ZnO thin-film layer thickness.

III.4.2 Thickness effect of the Cu₂O layer

To study the effect of the absorption layer thickness (Cu₂O) on the electrical properties, Cu₂O thickness can be changed from 1 to 250 μm as reported in [41]. When the value of ZnO thickness was fixed at the optimum value of 0.041 μm. The results were as follows:

Table III.3: Cu₂O Thickness effect on the output parameters of Cu₂O based heterojunction solar cell, when the ZnO layer has a thickness of 0.041 μm.

Cu ₂ O Thickness (μm)	Eff (%)	FF (%)	Voc (V)	Jsc (mA/cm ²)
250	4.159	60.316	0.711	9.688
200	4.253	61.568	0.711	9.706
100	4.456	64.310	0.711	9.740
10	4.640	66.844	0.710	9.770
7	4.646	66.957	0.710	9.766
6.6	4.646	66.977	0.710	9.763
6.5	4.646	66.982	0.710	9.763
1	4.017	68.517	0.705	8.305

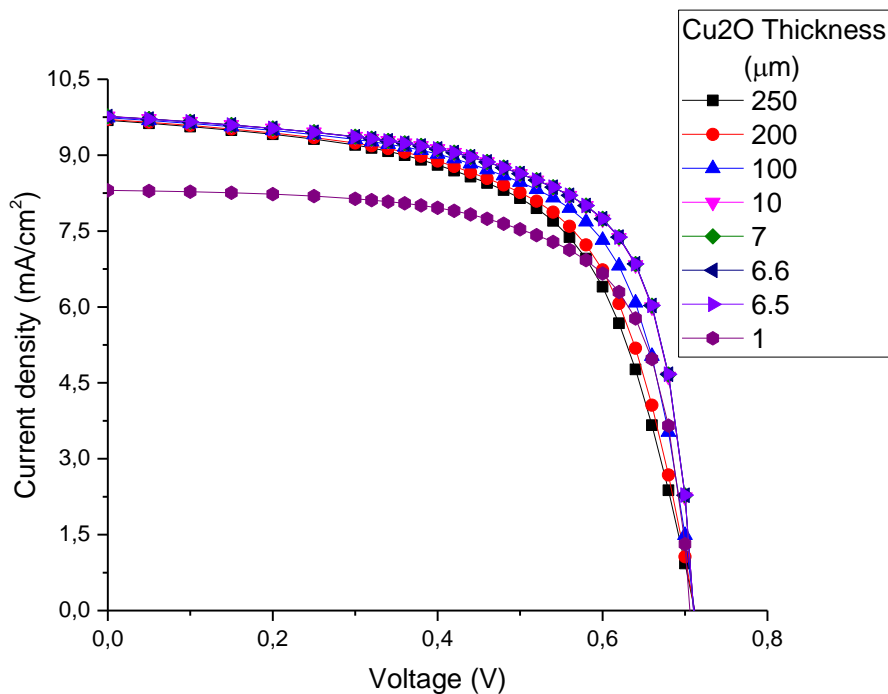


Figure III.11: The effect of Cu₂O thickness on the J-V characteristics.

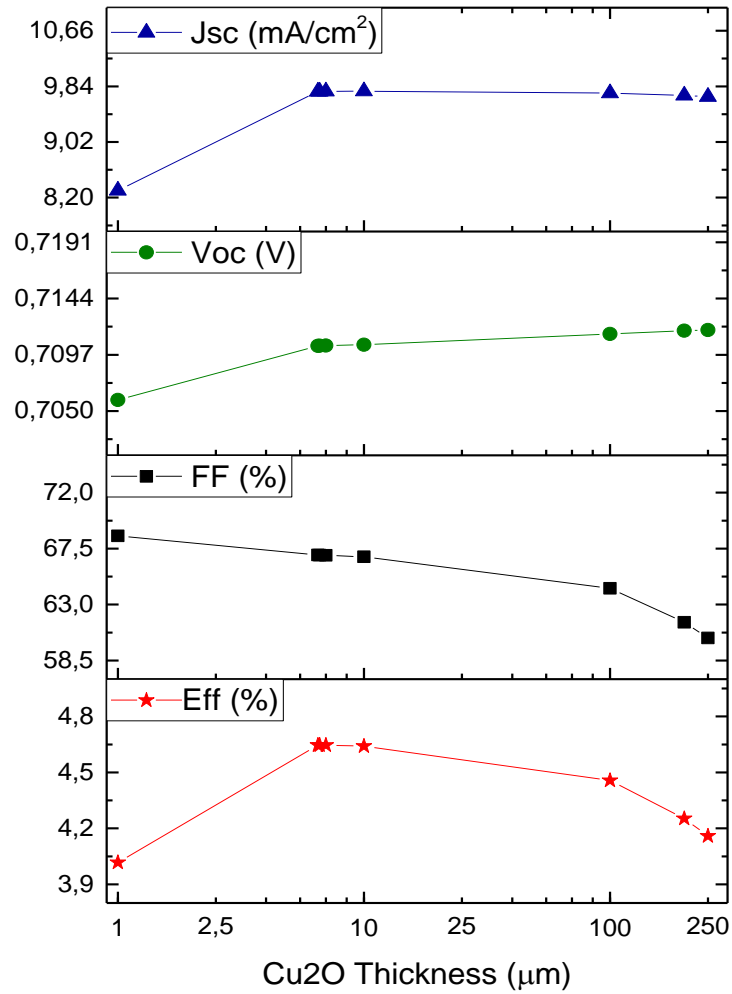


Figure III.12: η , V_{oc} , J_{sc} and FF as functions of the Cu_2O thin-film layer thickness.

In Figures III.11 and III.12 we observe an increase in J_{sc} with increasing of Cu_2O thickness which acts as an absorber layer, and results more light absorption, which increases the generated charge carriers. This has a direct effect on efficiency (η) which increased affected by the gain from J_{sc} . Contrariwise the FF decreases with increasing Cu_2O thickness, that could be due to the increase of layer thickness compared to majority carrier's diffusion length and also increase the structural defects, that leads to an increase of the resistivity. We can also observe that V_{oc} takes same J_{sc} behavior, which can be explained by [48]:

$$V_{oc} \approx V_T \ln\left(\frac{J_{sc}}{J_s}\right) \quad (III.2)$$

However, if the thickness increased more, the charge carriers will be far away from the junction (That maximum distance that can be traveled to be collected should be smaller or equal

to the diffusion length), and we observe both FF and η decreases with increasing thickness at large values, this can be attributed to short the majority carrier transport length (Diffusion length) at about 430nm[49]. But, reaching very small thicknesses can affect light absorption, the photocurrent decreases because the longer wavelength photons will not be absorbed. Therefore, the conversion efficiency decreases as the thickness is reduced. Thus, the optimum Cu₂O thickness at about 6.6 μ m.

III.4.3 Doping effect of the ZnO layer

The relationship between the doping concentration of the ZnO layer and the electrical characteristics of the solar cell are shown in Figures III.13 and III.14. The doping concentration was changed from $1 \times 10^{17} \text{cm}^{-3}$ to $1 \times 10^{21} \text{cm}^{-3}$ depending on what was reported in [50]. Both thickness of the ZnO and Cu₂O were fixed at their best values 0.041 μ m and 6.6 μ m, respectively.

Table III.4: Doping concentration effect of ZnO layer on the output parameters of Cu₂O based heterojunction solar cell.

ZnO Doping (cm^{-3})	Eff (%)	FF (%)	Voc (V)	Jsc (mA/cm^2)
1×10^{17}	4.148	65.830	0.647	9.731
1×10^{18}	4.409	66.631	0.678	9.754
1×10^{19}	4.646	66.982	0.710	9.763
1×10^{20}	4.802	66.804	0.737	9.744
3×10^{20}	4.823	66.774	0.745	9.692
1×10^{21}	4.790	66.564	0.750	9.583

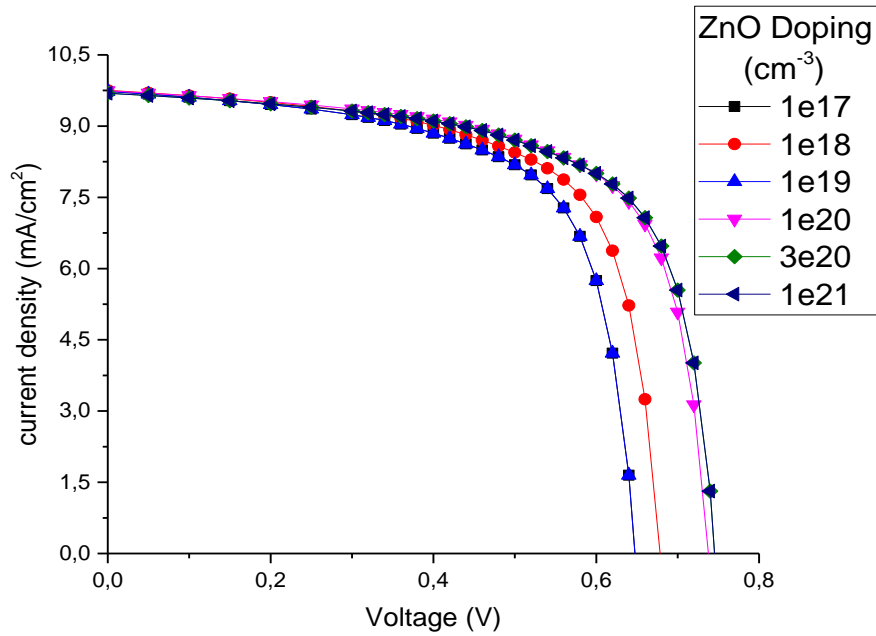


Figure III.13: The effect of ZnO doping concentration on the J-V characteristics.

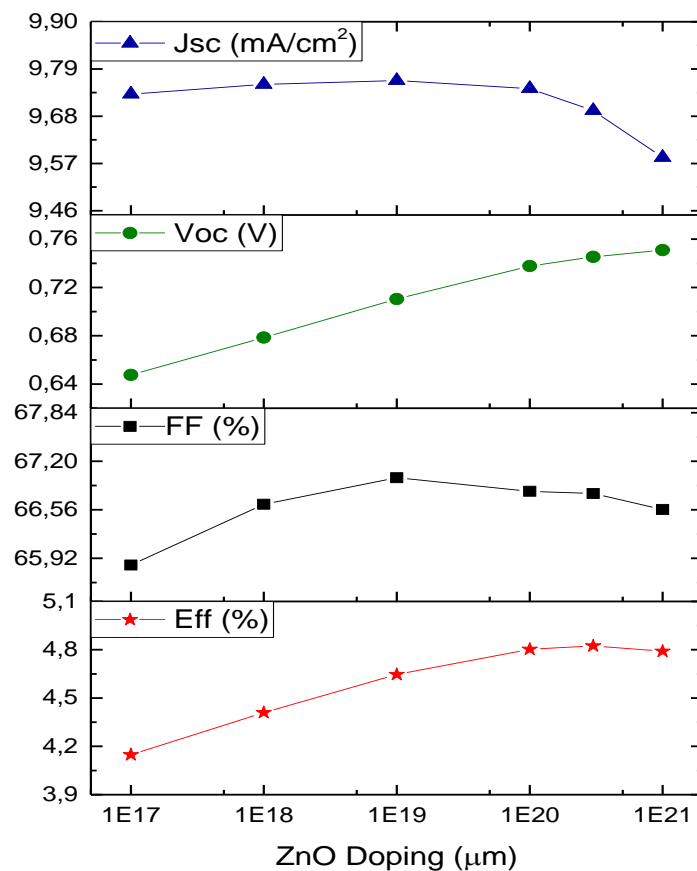


Figure III.14: η , V_{oc} , J_{sc} and FF as functions of doping concentration of the ZnO layer.

Chapter III: Results and Discussions

We observe from the Figure III.14 continuous increase in V_{oc} and η with increased doping concentration. This increase can be due to the increase in the major carriers, and can be explained that by the relationship:

$$V_{oc} = \frac{nkT}{q} \ln(J_{sc}) - \frac{nkT}{q} \ln\left(qN_cN_v \left(\frac{1}{N_A} \sqrt{\frac{D_n}{\tau_n}} + \frac{1}{N_D} \sqrt{\frac{D_p}{\tau_p}}\right) e^{-E_g/kT}\right) \quad (III.3)$$

Acquired by [51]:

$$V_{oc} = \frac{nkT}{q} \ln\left(\frac{J_{sc}}{J_0} + 1\right) \quad (III.4)$$

$$J_0 = qN_cN_v \left(\frac{1}{N_A} \sqrt{\frac{D_n}{\tau_n}} + \frac{1}{N_D} \sqrt{\frac{D_p}{\tau_p}}\right) e^{-E_g/kT} \quad (III.5)$$

In addition, the highly doped ZnO layer creates a small depletion width in the ZnO, and a large one in the absorber layer. Hence, the photogenerated carriers increase. FF decrease when doping concentration is higher than $1 \times 10^{19} \text{cm}^{-3}$. J_{sc} also decreases with increasing doping at large values, this can be attributed to the recombination rate as shown in Figures III.15 and III.16. When the doping concentration of the ZnO layer is $1 \times 10^{17} \text{cm}^{-3}$, the photocurrent (J_{ph}) is higher due to the difference between the doping concentration of the ZnO and AZO layers near the AZO layer; where the diffusion of electrons from AZO to ZnO occurs, resulting in lower holes in ZnO layer, hence the recombination rate decrease. While, when the doping concentration of the ZnO layer is $1 \times 10^{21} \text{cm}^{-3}$, we observe a great recombination rate, because there is no diffusion of the electrons and therefore the stability of the holes concentration, which leads to reduced photocurrent, which in turn leads to a decrease in efficiency η . As shown in Figure III.14. From the above we conclude that the optimum concentration of doping amount in ZnO buffer layer about $3 \times 10^{20} \text{cm}^{-3}$.

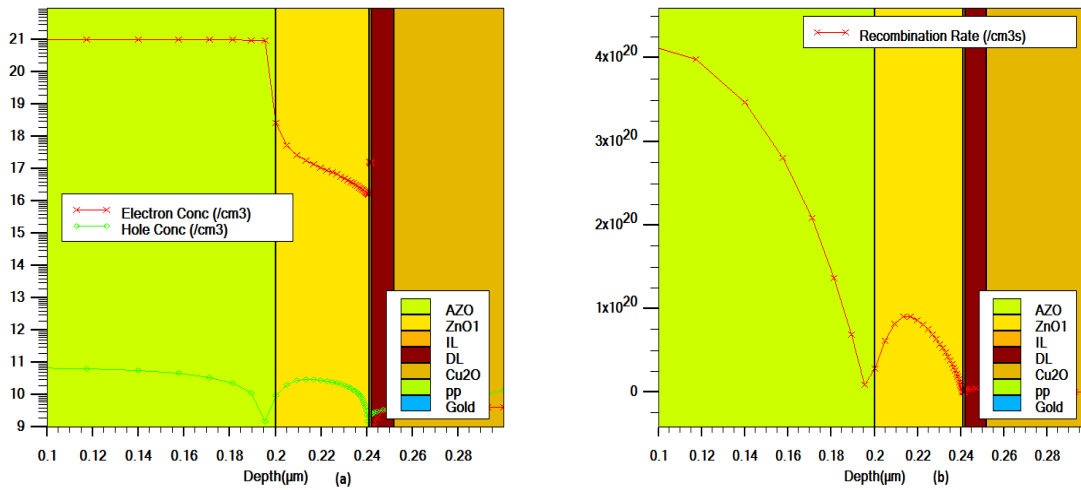


Figure III.15: (a) The electrons and holes concentration distribution, and (b) the recombination rate as function of structure depth for doping concentration in the ZnO layer at $1 \times 10^{17} \text{ cm}^{-3}$.

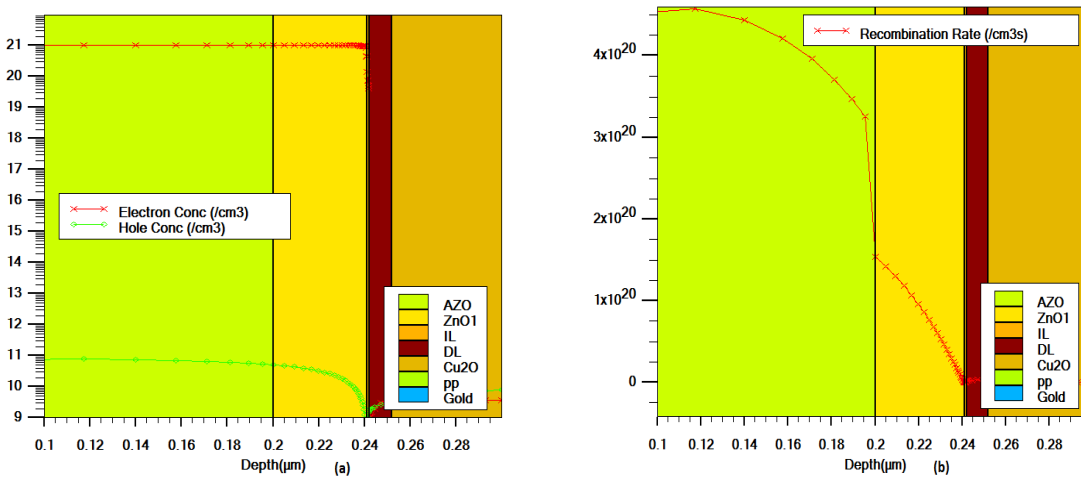


Figure III.16: (a) The electrons and holes concentration distribution, and (b) the recombination rate as function of structure depth for doping concentration in the ZnO layer at $1 \times 10^{21} \text{ cm}^{-3}$.

III.4.4 Doping effect of the Cu2O layer

Varying the doping concentration of Cu2O layer from 1×10^{14} to $1 \times 10^{17} \text{ cm}^{-3}$ depending on what is reported in [52], to study their effects on the electrical characteristics of cell. When the ZnO and Cu2O layers have thickness of $0.041 \mu\text{m}$, $6.6 \mu\text{m}$ respectively and doping concentration of the ZnO layer of $3 \times 10^{20} \text{ cm}^{-3}$.

Chapter III: Results and Discussions

Table III.5: Doping concentration effect of Cu₂O layer on the output parameters of Cu₂O heterojunction cell.

Cu ₂ O Doping (cm ⁻³)	Eff (%)	FF (%)	V _{oc} (V)	J _{sc} (mA/cm ²)
1×10 ¹⁴	4.804	63.357	0.743	10.198
1×10 ¹⁵	4.945	72.874	0.749	9.053
6×10 ¹⁵	5.015	78.374	0.753	8.487
1×10 ¹⁶	5.012	79.348	0.754	8.372
5×10 ¹⁶	4.991	81.528	0.754	8.110
1×10 ¹⁷	4.982	82.222	0.754	8.032

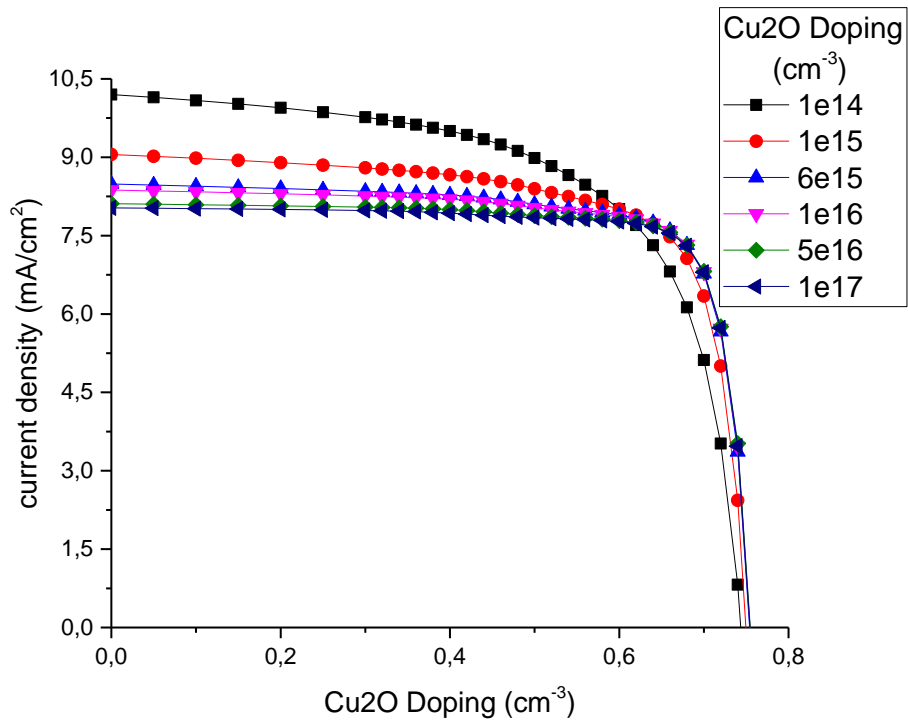


Figure III.17: The effect of Cu₂O doping concentration on the J-V characteristics.

The concentration of doping significantly affects the open circuit voltage V_{oc} of solar cells, which increases with doping concentration increase, through the following relationship:

$$V_{oc} = \frac{nkt}{q} \ln(J_{sc}) - \frac{nkt}{q} \ln\left(qN_cN_v \left(\frac{1}{N_A} \sqrt{\frac{D_n}{\tau_n}} + \frac{1}{N_D} \sqrt{\frac{D_p}{\tau_p}}\right) e^{-E_g/kT}\right) \quad (\text{III.6})$$

Chapter III: Results and Discussions

It's clear that the relation between the open circuit voltage and the doping concentration is logarithmic relation which leads to a saturation in the increase of V_{oc} . On the other hand, a J_{sc} decrease with the doping concentration increase was observed, this can be due to the depletion width in the Cu₂O that will decrease, hence, the absorption of photons decreases.

The efficiency changes can be explained by combining these two effects (J_{sc} and V_{oc}). Where the increase of V_{oc} with increasing doping dominates at first, which leads to an increase in efficiency. After the value of $5 \times 10^{16} \text{ cm}^{-3}$, the V_{oc} will be stabilized at a fixed value, in this case the decrease of J_{sc} will dominate the efficiency, hence it will decrease. Finally, the optimum doping concentration amounts to about $6 \times 10^{15} \text{ cm}^{-3}$.

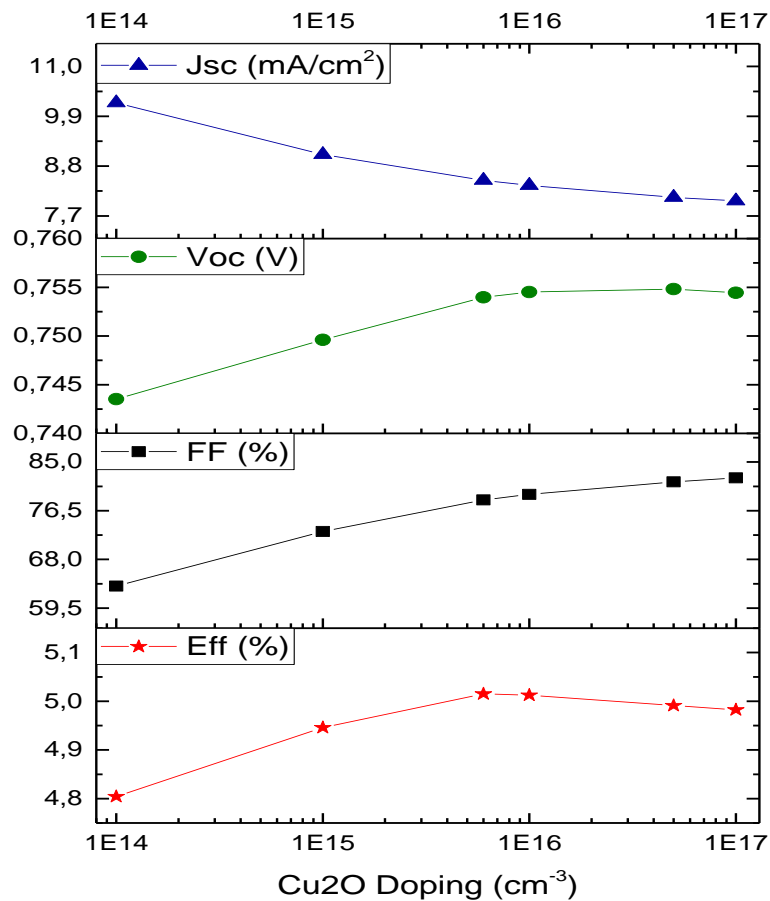


Figure III.18: η , V_{oc} , J_{sc} and FF as functions of the doping concentration of the Cu₂O layer.

III.4.5 Passivation effect on the solar cell characteristics

To study effects of the passivation on the cell, was inserting a heavily doped layer (p^+) which is create a back-surface field (BSF). The degree to which the improvement is made depends greatly on the two parameters of the p^+ layer: The thickness and the doping concentration.

III.4.5.1 Doping and thickness effect of the p^+ layer

Doping concentration effect of the p^+ layer on the electrical characteristics of the solar cell are shown in Figure III.19. The doping concentration was changed from $6 \times 10^{15} \text{cm}^{-3}$ to $4 \times 10^{20} \text{cm}^{-3}$ [54]. When the thickness of p^+ layer was fixed at $0.4 \mu\text{m}$. And when the ZnO and Cu₂O layers have thickness of $0.041 \mu\text{m}$ and $6.6 \mu\text{m}$, respectively and doping concentration of both the ZnO and Cu₂O layers of $3 \times 10^{20} \text{cm}^{-3}$ and $6 \times 10^{15} \text{cm}^{-3}$, respectively. The results were as follows:

Table III.6: Doping concentration effect of the p^+ layer on the output parameters of Cu₂O based heterojunction solar cell.

P⁺ Doping (cm⁻³)	Eff (%)	FF (%)	Voc (V)	Jsc (mA/cm²)
6×10^{15} (Without BSF)	5.015	78.372	0.753	8.487
1×10^{16}	5.015	78.372	0.753	8.488
1×10^{17}	5.016	78.370	0.753	8.489
1×10^{18}	5.016	78.370	0.753	8.490
1×10^{19}	5.016	78.370	0.753	8.490
1×10^{20}	5.016	78.367	0.753	8.490
4×10^{20}	5.017	78.369	0.753	8.490

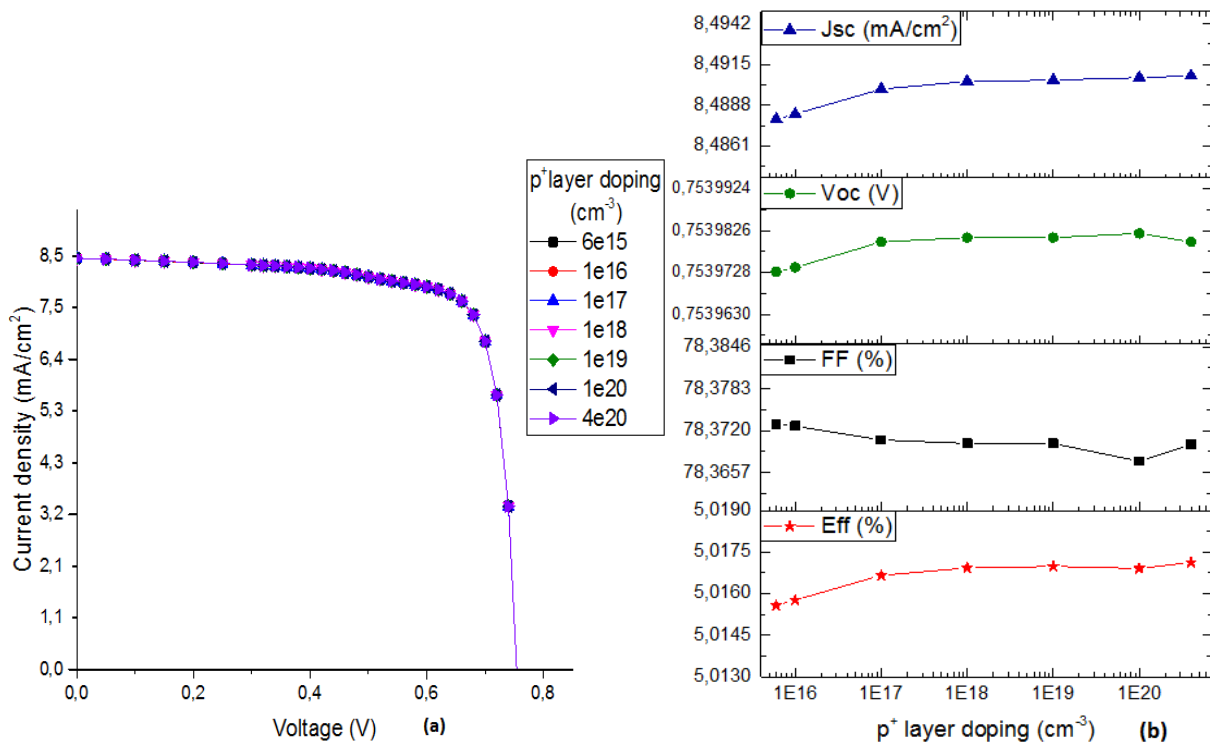


Figure III.19: (a) Effect of the doping concentration of the p⁺ layer on the J-V characteristics and (b) η , Voc, Jsc and FF output parameters.

Thickness effect of the p⁺ layer on the electrical characteristics of the solar cell are shown in Figure III.20. The thickness was changed from 0.1 μm to 1 μm [55]. When the doping concentration of p⁺ layer was fixed at $4 \times 10^{20} \text{cm}^{-3}$. The results were as follows:

Table III.7: Thickness effect of p⁺ layer on the output parameters of Cu₂O based heterojunction solar cell.

P ⁺ Thickness (μm)	Eff (%)	FF (%)	Voc (V)	Jsc (mA/cm ²)
0.1	5.01693	78.362	0.753	8.491
0.2	5.01706	78.355	0.753	8.492
0.3	5.01703	78.386	0.753	8.488
0.4	5.01713	78.369	0.753	8.490
0.6	5.01716	78.385	0.753	8.489
0.8	5.01710	78.374	0.753	8.490
1	5.01713	78.372	0.753	8.490

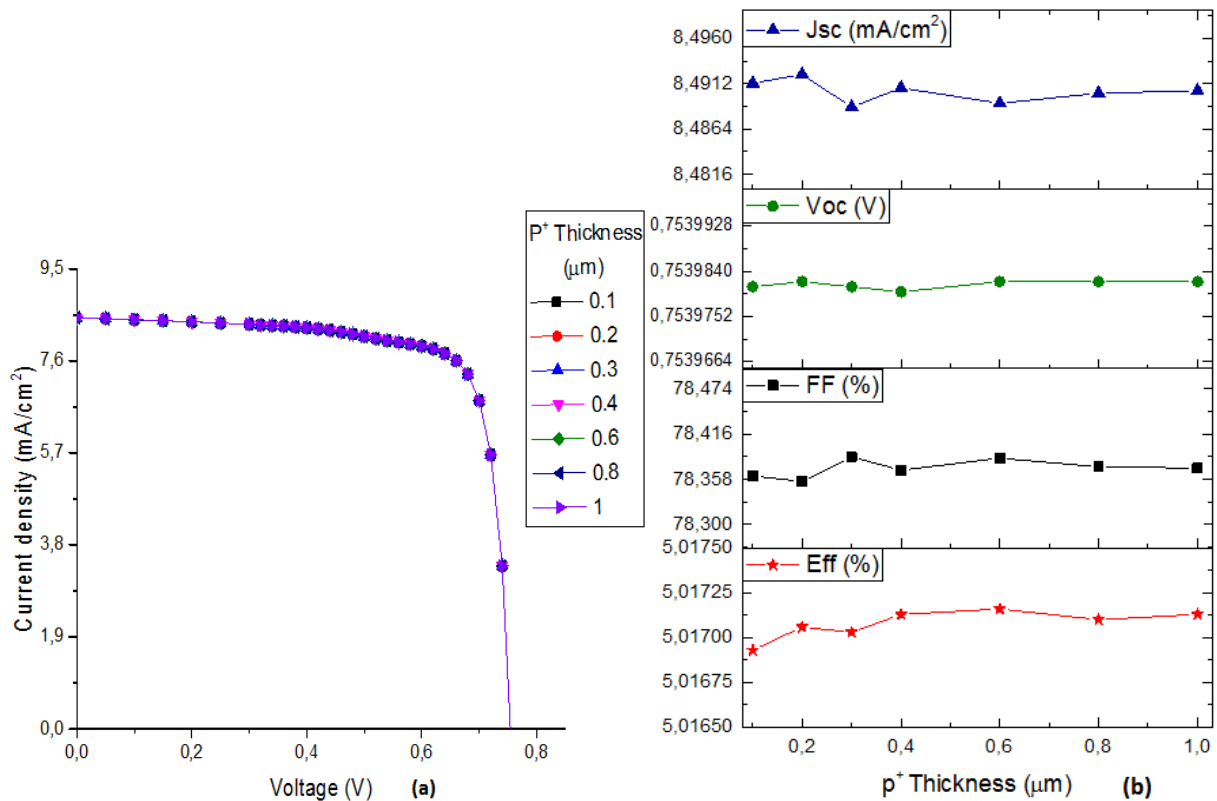


Figure III.20: (a) Thickness effect of the p⁺ layer on the J-V characteristics and (b) η , V_{oc} , J_{sc} and FF output parameters.

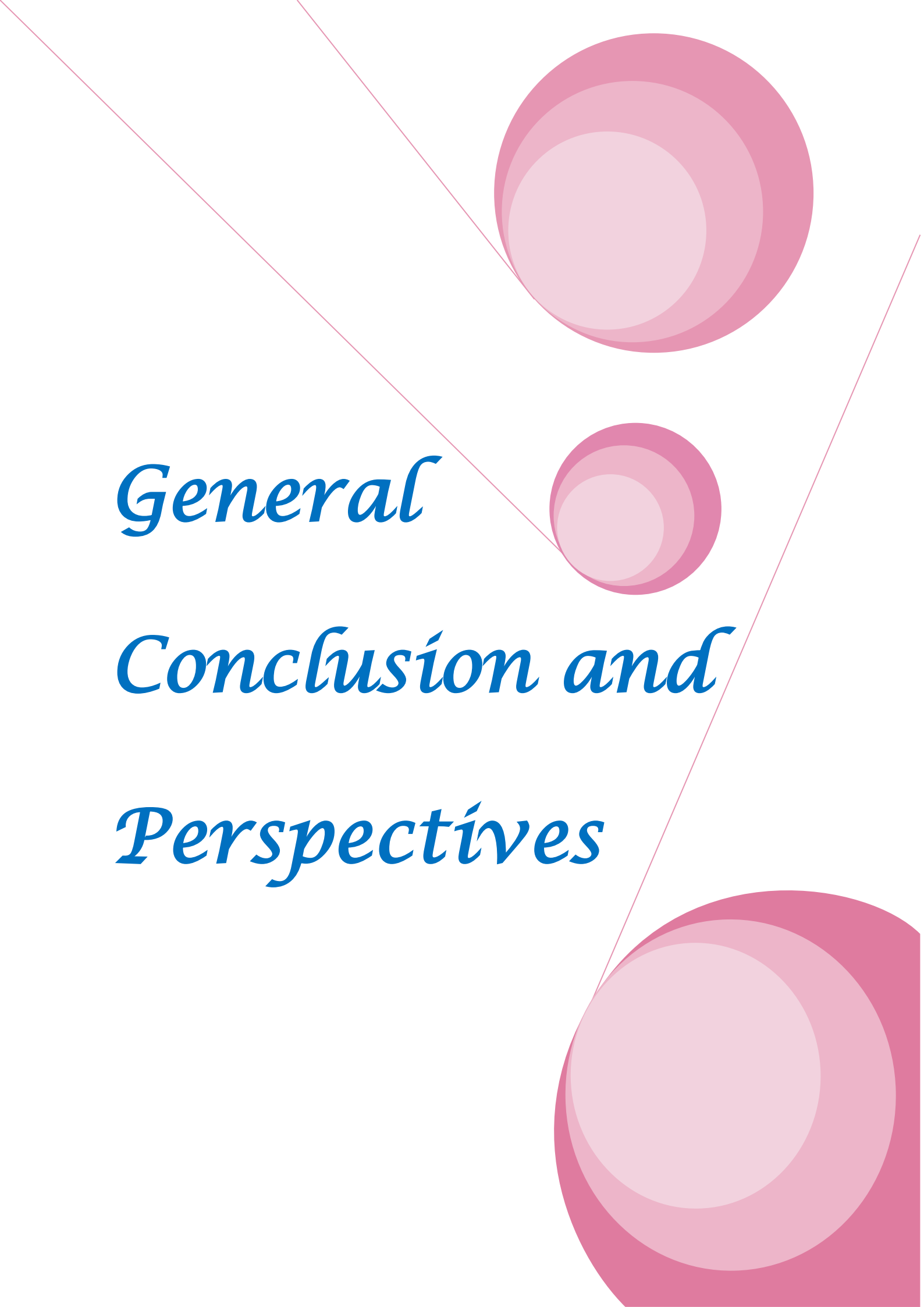
It is clear through Figures III.19 and III.20 that the p⁺ layer has a small effect on the output parameters of the solar cell which can be neglected. Where, the optimum conversion efficiency was found at **5.01716%**. This can be attributed to that this cell have a good ohmic contact, therefore, no matter how much thickness and doping concentration of this layer will have no effect. This behavior has been observed, before in a thesis entitled Simulation of passivated area effect on silicon solar cell [56].

III.5 Conclusion

In our study we used the Silvaco TCAD software to simulate the behavior of ZnO/Cu₂O solar cell. We presented in part one of this chapter, the principal operations of Silvaco Atlas software and the main Tools which can help us to understand and use this simulator. In part two, description of simulated structure of heterojunction solar cell based on Cuprous oxide (Cu₂O). While part three, was about studying the influence of the several parameters on the Cuprous oxide (Cu₂O) heterojunction solar cell performances and interpretation of the results obtained using Atlas simulator. The results show that the output parameters of solar cell can be improved as follow: The optimum value of the ZnO layer thickness is 0.041μm, where the output

Chapter III: Results and Discussions

parameters of the cell are $J_{sc} = 9.706 \text{ mA/cm}^2$, $V_{oc} = 0.711 \text{ V}$, $FF = 61.568\%$ and $\eta = 4.253\%$. these values can be improved more by studying the Cu_2O absorbent layer thickness, where the best results were found to be at $6.6 \mu\text{m}$, in this case we got the values of $J_{sc} = 9.763 \text{ mA/cm}^2$, $V_{oc} = 0.710 \text{ V}$, $FF = 66.977\%$ and $\eta = 4.646\%$. Another parameter had a great effect on the output parameters, which is the doping concentration of both sides. We started first by changing the ZnO doping concentration where the best results were found at $3 \times 10^{20} \text{ cm}^{-3}$, at this concentration the output parameters of the cell are $J_{sc} = 9.692 \text{ mA/cm}^2$, $V_{oc} = 0.745 \text{ V}$, $FF = 66.774\%$ and $\eta = 4.823\%$. and the optimum parameters for this cell were found by studying the doping concentration of the Cu_2O layer where reached to the values of the Cu_2O layer where the output parameters reached to the values of $J_{sc} = 8.487 \text{ mA/cm}^2$, $V_{oc} = 0.753 \text{ V}$, $FF = 78.374\%$ and $\eta = 5.015\%$ at $6 \times 10^{15} \text{ cm}^{-3}$. Finally, we observed that the presence of the heavily doped layer does not strongly effect on output parameters, where: when its doping concentration and thickness at $4 \times 10^{20} \text{ cm}^{-3}$, and $0.6 \mu\text{m}$, we found $\eta = 5.017\%$ and 5.017% , respectively.

The background features a decorative graphic consisting of three overlapping pink circles of varying sizes, arranged vertically. Two thin, light pink lines intersect at the top left and extend diagonally across the page, framing the central text.

General

Conclusion and

Perspectives

General conclusion and perspectives

Cuprous oxide (Cu₂O) based solar cells are modern thin film solar cells usually created as heterojunctions such as n-ZnO/p-Cu₂O as in our study, and have attracted more attention of researchers for low-cost photovoltaic applications, because they are abundant, non-toxic and relatively stable.

The objective of the present work was to improve the performances of heterojunction solar cell AZO/n-ZnO/p-Cu₂O by changing several parameters using Silvaco Atlas software, which is a simulation software that calculates the electrical output parameters of the studied solar cell. The idea was about changing thickness, doping concentration of layers and inserting a highly doped layer as a passivation layer in order to improve the solar cell performance. One of the benefits of this work is the exploitation of the results obtained through the optimization by simulation without material loss and time, i.e. as an application to our work.

The thesis was organized in three chapters. The first one was dedicated to the principles of solar cells which presented in details. In the second one, describes solar cells on the basis of cuprous oxide absorber layer (Cu₂O), and their structure, optical and electrical properties, their methods of manufacturing, definition of ZnO as a solar cell material, effect of some parameters on ZnO/Cu₂O heterojunction solar cell characteristics, finally, literature review of the Cu₂O based heterojunction solar cells. While in the third chapter, the most important elements were presented in this work, starting with general concepts about Silvaco TCAD software with the simulation steps of the studied device, description of simulated structure of heterojunction solar cell based on Cuprous oxide (Cu₂O) with the model adopted in our study, finally, all the results were presented in the form of curves and tables with their discussions, where the optimum parameters obtained in this work are: First, at thickness of the ZnO layer of **0.041μm**, conversion efficiency was determined of **4.253%**, showing that their effects are most likely negligible, because it as a window layer. At Cu₂O thickness of **6.6μm**, we obtained a conversion efficiency of **4.646%**, showing significant effect, because it is an absorbent layer. At doping concentration of the ZnO layer of $3 \times 10^{20} \text{cm}^{-3}$, conversion efficiency was determined of **4.823%**, and at doping concentration of Cu₂O layer of $6 \times 10^{15} \text{cm}^{-3}$, we obtained a conversion efficiency of **5.015%**. Thus, these changes have clear effects on the conversion efficiency of solar cell. While, the presence of the heavily doped layer does not strongly effect on output parameters, where: At its doping concentration and thickness at $4 \times 10^{20} \text{cm}^{-3}$, and **0.6μm**, we found $\eta = 5.017\%$ and **5.017%**, respectively.

In conclusion, we are confident that the Cuprous oxide (Cu_2O) heterojunction solar cells have the ability to achieve high efficiency because they have high theoretical efficiency. The data collected in this effort raises many questions for future research. The data reveals many interesting electronic and optical properties of Cuprous oxide. Efforts could be made to better understand thus, improve better. Where we can offer further enhancements. For example, we can change band gap (E_g) and investigate its effect, because Cu_2O has a non-fixed band gap value. Also, we can insert others types of passivation such as chemical passivation and passivation of a metal contact with a tunneling layer; to reduce the recombination surface.

Bibliography

1. Wong, T., et al., Current status and future prospects of copper oxide heterojunction solar cells. *Materials*, 2016. 9(4): p. 271.
2. Abdu, Y. and A. Musa, Copper (I) oxide (Cu₂O) based solar cells-a review. *Bayero Journal of Pure and Applied Sciences*, 2009. 2(2): p. 8-12.
3. Saafie Salleh, F.P.C., FABRICATION AND CHARACTERIZATION OF Cu₂O/ZnO THIN FILMS FOR pn HETEROJUNCTION DEVICES. *BORNEO SCIENCE*, 2016.
4. Nordseth, et al., Metal Oxide Thin-Film Heterojunctions for Photovoltaic Applications. *Materials*, 2018. 11(12): p. 2593.
5. Chen, C.J., *Physics of Solar Energy* 2011: Wiley.
6. van de Krol, R. and M. Grätzel, *Photoelectrochemical Hydrogen Production* 2011: Springer US.
7. Smets, A., et al., *Solar Energy: The Physics and Engineering of Photovoltaic Conversion, Technologies and Systems* 2016: UIT Cambridge.
8. Neamen, D., *Semiconductor Physics And Devices* 2003: McGraw-Hill Education.
9. SHAHRESTANI, S.M., *ELECTRO DEPOSITION OF CUPROUS OXIDE FOR THIN FILM SOLAR CELL APPLICATIONS*, 2013, MONTRÉAL.
10. Sharma, N., F. Ansari, and P.K. Panday, Modeling and Simulation of Photovoltaic Cell Using Matlab/Simulink. *International Journal of Scientific and Research Publications*, 2013. 3(7).
11. Shukla, A., M. Khare, and K. Shukla, Modeling and Simulation of Solar PV Module on MATLAB/Simulink. 2015.
12. Foster, R., M. Ghassemi, and A. Cota, *Solar energy: renewable energy and the environment* 2009: CRC Press.
13. Askari, M., V. Mirzaei Mahmoud Abadi, and M. Mirhabibi, *Types of Solar Cells and Application*. Vol. 3. 2015. 2015.
14. Jacobsen, E.C., *Analysis of the ZnO/Cu₂O Thin Film Heterojunction for Intermediate Band Solar Cell Applications*, 2015, NTNU.
15. Nelson, J., *The Physics of Solar Cells* 2003: World Scientific Publishing Company.
16. Sharma, P., *Modeling, optimization, and characterization of high concentration photovoltaic systems using multijunction solar cells*, 2017, Ottawa, Canada.

17. MORTENSEN, E.L., INVESTIGATION OF ELECTRODEPOSITED CUPROUS OXIDE THIN FILMS, 2016, New Jersey.
18. Pettit, R.B., C.J. Brinker, and C.S. Ashley, Sol-gel double-layer antireflection coatings for silicon solar cells. *Solar Cells*, 1985. 15(3): p. 267-278.
19. Abdullah, M.F., et al., Research and development efforts on texturization to reduce the optical losses at front surface of silicon solar cell. Vol. 66. 2016. 380-398.
20. Meyer, B.K., et al., Binary copper oxide semiconductors: From materials towards devices. *physica status solidi (b)*, 2012. 249(8): p. 1487-1509.
21. Le, D., S. Stolbov, and T.S. Rahman, Reactivity of the Cu₂O(100) surface: Insights from first principles calculations. *Surface Science*, 2009. 603(10): p. 1637-1645.
22. Palmieri, V., Study of Thin Film Solar Cell based on Copper Oxide Substrate by DCReactive Magnetron SputteringRelatore, 2008, UNIVERSITÀ DEGLI STUDI DI PADOVA.
23. Lee, Y.S., et al., Nitrogen-doped cuprous oxide as a p-type hole-transporting layer in thin-film solar cells. *Journal of Materials Chemistry A*, 2013. 1(48): p. 15416-15422.
24. Scanlon, D.O. and G.W. Watson, Undoped n-type Cu₂O: fact or fiction? *The Journal of Physical Chemistry Letters*, 2010. 1(17): p. 2582-2585.
25. Scanlon, D.O., et al., Acceptor levels in p-type Cu₂O: rationalizing theory and experiment. *Physical Review Letters*, 2009. 103(9): p. 096405.
26. Zhu, L., G. Shao, and J. Luo, Numerical study of metal oxide heterojunction solar cells. *Semiconductor Science and Technology*, 2011. 26(8): p. 085026.
27. Musa, A., T. Akomolafe, and M. Carter, Production of cuprous oxide, a solar cell material, by thermal oxidation and a study of its physical and electrical properties. *Solar Energy Materials and Solar Cells*, 1998. 51(3-4): p. 305-316.
28. Han, K.T., Meng, Electrochemically deposited p-n homojunction cuprous oxide solar cells. *Solar Energy Materials and Solar Cells*, 2009. 93(1): p. 153-157.
29. Drobny, V. and L. Pulfrey, Properties of reactively-sputtered copper oxide thin films. *Thin solid films*, 1979. 61(1): p. 89-98.
30. Han, X., K. Han, and M. Tao, n-Type Cu₂O by electrochemical doping with Cl. *Electrochemical and Solid-State Letters*, 2009. 12(4): p. H89-H91.
31. Fonash, S., *Solar Cell Device Physics* 2012: Elsevier Science.
32. Eom, K., et al., Modified band alignment effect in ZnO/Cu₂O heterojunction solar cells via Cs₂O buffer insertion. *Journal of Physics D: Applied Physics*, 2018. 51(5): p. 055101.

33. Tran, M.H., et al., Cu₂O/ZnO heterojunction thin-film solar cells: the effect of electrodeposition condition and thickness of Cu₂O. *Thin solid films*, 2018. 661: p. 132-136.
34. Ye, F., et al., Doping cuprous oxide with fluorine and its band gap narrowing. *Journal of Alloys and Compounds*, 2017. 721: p. 64-69.
35. Ishizuka, S., et al., Passivation of defects in polycrystalline Cu₂O thin films by hydrogen or cyanide treatment. *Applied surface science*, 2003. 216(1-4): p. 94-97.
36. Moldovan, A., et al. Tunnel oxide passivated carrier-selective contacts based on ultra-thin SiO₂ layers grown by photo-oxidation or wet-chemical oxidation in ozonized water. in *2015 IEEE 42nd Photovoltaic Specialist Conference (PVSC)*. 2015. IEEE.
37. Cuevas, A. and D. Yan, Misconceptions and misnomers in solar cells. *IEEE Journal of Photovoltaics*, 2013. 3(2): p. 916-923.
38. Katayama, J., et al., Performance of Cu₂O/ZnO solar cell prepared by two-step electrodeposition. *Journal of Applied Electrochemistry*, 2004. 34(7): p. 687-692.
39. Tanaka, H., et al., Electrical and optical properties of TCO–Cu₂O heterojunction devices. *Thin solid films*, 2004. 469: p. 80-85.
40. Ke, N.H., et al., The characteristics of IGZO/ZnO/Cu₂O:Na thin film solar cells fabricated by DC magnetron sputtering method. *Journal of Photochemistry and Photobiology A: Chemistry*, 2017. 349: p. 100-107.
41. Takiguchi, Y. and S. Miyajima, Device simulation of cuprous oxide heterojunction solar cells. *Japanese Journal of Applied Physics*, 2015. 54(11): p. 112303.
42. Minami, T., Y. Nishi, and T. Miyata, Efficiency enhancement using a Zn_{1-x}Gex-O thin film as an n-type window layer in Cu₂O-based heterojunction solar cells. *Applied Physics Express*, 2016. 9(5): p. 052301.
43. Miyata, T., et al., Photovoltaic properties of Cu₂O-based heterojunction solar cells using n-type oxide semiconductor nano thin films prepared by low damage magnetron sputtering method. *Journal of Semiconductors*, 2019. 40(3): p. 032701.
44. Minami, T., Y. Nishi, and T. Miyata, High-Efficiency Cu₂O-Based Heterojunction Solar Cells Fabricated Using a Ga₂O₃Thin Film as N-Type Layer. *Applied Physics Express*, 2013. 6(4): p. 044101.
45. Atlas User's Manual, DEVICE SIMULATION SOFTWARE, 2015: Santa Clara, , California, USA.
46. Fateh, M., Simulation Copper Oxide Solar Cells Using Silvaco TCAD, in *Faculty of Exact Sciences and Sciences of Nature and Life* 2018, Med Khider University of Biskra.

47. Minami, T., et al., High-efficiency oxide solar cells with ZnO/Cu₂O heterojunction fabricated on thermally oxidized Cu₂O sheets. *Applied Physics Express*, 2011. 4(6): p. 062301.
48. Andrews, J., N.A. Jelley, and N. Jelley, *Energy Science: Principles, Technologies, and Impacts*2007: OUP Oxford.
49. Liu, Y., et al., Minority carrier transport length of electrodeposited Cu₂O in ZnO/Cu₂O heterojunction solar cells. *Applied physics letters*, 2011. 98(16): p. 162105.
50. Maragliano, C., et al., Quantifying charge carrier concentration in ZnO thin films by Scanning Kelvin Probe Microscopy. *Scientific Reports*, 2014. 4: p. 4203.
51. Soga, T., *Nanostructured Materials for Solar Energy Conversion*2006: Elsevier Science.
52. Minami, T., Y. Nishi, and T. Miyata, Heterojunction solar cell with 6% efficiency based on an n-type aluminum–gallium–oxide thin film and p-type sodium-doped Cu₂O sheet. *Applied Physics Express*, 2015. 8(2): p. 022301.
53. Bhaumik, A., et al., Copper oxide based nanostructures for improved solar cell efficiency. *Thin solid films*, 2014. 572: p. 126-133.
54. Chen, X., et al. Thermoelectric Performance of Hole-Doped Cu₂O. in *APS Meeting Abstracts*. 2013.
55. Marin, A.T., et al., Novel atmospheric growth technique to improve both light absorption and charge collection in ZnO/Cu₂O thin film solar cells. *Advanced Functional Materials*, 2013. 23(27): p. 3413-3419.
56. Djemaa, A., Simulation of passivated area effect on silicon solar cell, in *Faculty of Exact Sciences and Sciences of Nature and Life*2018, Med Khider University of Biskra.